

MASTER OF SCIENCE THESIS

Validation of wind turbine wake models

Using wind farm data and wind tunnel measurements

Douwe J. Renkema

June 11, 2007



Validation of wind turbine wake models

Using wind farm data and wind tunnel measurements

Douwe J. Renkema

June 11, 2007



Abstract

The abstract has yet to be written.

Dear members of the exam committee,

This is the final draft of my thesis report, due next week. As such it may still be a little rough around the edges and surely there will still be errors in it. Don't worry, I will continue working on it this week. I hope you will find time to go through it already, before we will meet on Tuesday, June 19th, at 15:00h.

Comments and suggestions will be happily accepted in the mean time.

Kind regards,

Douwe Renkema June 11, 2007

Acknowledgments

This report is the result of the thesis work that I performed from May 2006 until March 2007 at GE Wind Energy in Salzbergen, Germany. I would like to thank GE Wind Energy for giving me the opportunity to do my thesis work there, especially Henk-Jan Kooijman and Frank Flottemesch for their supervision during my work, it has been a great learning experience.

Furthermore I would like to thank Christian Aalburg, Parag Vyas and especially Clarissa Belloni from GE Global Research Center in Munich for the regular discussions on wakes, and Saskia Honhoff for helping me out with some of the tools. Also many thanks to Carsten Junge, Karsten Hilt, Henri Avila and Carsten Loemker for the fun during my thesis work, and Bart Veldkamp for giving me a place to stay in Enschede.

Also ECN for providing me with the wind tunnel data and Pieter Schaak for the assistance during my short stay there, and Ben Hendriks and Gerard Schepers from ECN for the guidance during my thesis work. Of course also many thanks to Gerard van Bussel from Delft University of Technology.

And last but certainly not least I want to thank my family and Sandra for their patience, their interest and their support, not only during this thesis work, but as well in the years before.

Delft, University of Technology
June 11, 2007

Douwe J. Renkema

Table of Contents

Abstract	iii
Acknowledgments	iv
Nomenclature	xvii
Acronyms	xix
1 Introduction	1
1.1 Goal of this thesis	2
1.2 Outline of the report	2
2 Wake models	5
2.1 Kinematic models	5
2.1.1 Jensen model	6
2.1.2 Larsen model	7
2.1.3 Analytical model by Frandsen	8
2.2 Field models	10
2.2.1 Two-dimensional field models	10
Implementations of the Ainslie model	11
2.2.2 Three-dimensional field models	12
WAKEFARM	12
Elliptic field models	13
2.3 Wake added turbulence models	13
2.3.1 Danish Recommendation	13
2.3.2 Larsen model	14
2.3.3 Frandsen / DIBt model	14
2.3.4 Quarton / TNO models	16

2.3.5	Lange model	16
2.3.6	Model by ForWind	16
2.4	Previous validation results	17
2.5	Introduction to the ENDOW project	17
2.6	Results from ENDOW	18
3	Wind farm measurements and validation	19
3.1	Prettin wind farm	19
3.1.1	Location and layout	19
3.1.2	Flow qualification	21
3.1.3	Analysis of measurement data	21
Turbulence intensity	22	
Power residual	22	
Normalized power	23	
3.1.4	Simulation with WindPRO	24
3.2	Colorado Green wind farm	26
3.2.1	Location and layout	26
3.2.2	Measurement data	27
Turbulence intensity	28	
Power residual	28	
Normalized power	29	
3.2.3	Simulation with WindPRO	30
Jensen models	30	
Ainslie model	31	
Larsen model	32	
Analysis of the results	34	
4	Wind tunnel measurements and validation	37
4.1	TNO wind tunnel	38
4.2	Wind turbine models	38
4.3	Measurement campaigns	40
4.4	Measuring system	40
4.5	Wake measurements behind a single turbine	41
4.6	Validation of the kinematic wake models	42
4.7	Validation of the turbulence models	43
4.7.1	Turbulence intensity using the Larsen/ForWind model	44
4.8	Wake superposition	45
4.8.1	Rotor averaging	45
4.8.2	Wake adding	46
Adding wakes of two turbines	47	
4.8.3	Rotor averaged wind speed	48
4.8.4	Results using superposition models	49
4.9	Wind turbine array	49
4.9.1	Results of the Larsen/ForWind model	51

5 Conclusions and recommendations	55
5.1 WindPRO modeling	55
5.1.1 Conclusions	55
5.1.2 Recommendations	55
5.2 Wind tunnel measurements	56
5.3 Future work	56
Bibliography	57
Appendices	
A About General Electric	63
A.1 GE Wind Energy	63
A.2 GE turbines	64
B Wake tools used at GE	67
C Determination of wake sectors	69
D Larsen model: second order contribution	71
E Near wake length of Vermeulen	73
F EWTW Wieringermeer	75
G Prettin met mast	77
H Sector wise parameters	79
I Single wake calculations: Combining Larsen and ForWind models	81
J Calculating rotor averaged wind speed	87
J.1 Analytical solution to the area	88
K Influence of turbulence intensity input on the new model	91
K.1 Influence on the velocity deficit prediction	91
K.2 Influence on the turbulence intensity prediction	92

List of Figures

2-1 Wake behind a turbine: Jensen model	6
2-2 Wake behind a GE 1.5sl: Larsen model	8
2-3 Wake behind a GE 1.5sl: Frandsen model	9
2-4 Calculated flow field at hub height using the Ainslie model	11
2-5 Correction factors for the Danish Recommendations design turbulence	14
2-6 Turbines taken into account in the Frandsen model	15
2-7 Results od the models used during ENDOW	18
3-1 Location and layout of the Prettin wind farm	20
3-2 Surroundings of the Prettin wind farm	20
3-3 Flow qualifications at Prettin	21
3-4 Turbulence intensity at the met mast	22
3-5 Power residual of Pr4 and Pr5	23
3-6 Normalized power of Pr4 in free stream and wake	24
3-7 Normalized power of Pr4: Simulation with Jensen and Ainslie model	25
3-8 Normalized power of Pr4: Simulation with Larsen model	25
3-9 Colorado Green wind farm location and layout	26
3-10 Terrain at the Colorado Green wind farm	27
3-11 Parts of the Colorado Green wind farm used for analysis	27
3-12 Turbulence intensity at met mast 74	28
3-13 Power residual of turbine 24 (left) and 25 (right)	29
3-14 Normalized power of turbines in first and second part	29
3-15 Normalized power of CG24, CG19 and CG14 using the Jensen model	31
3-16 Normalized power of CG24, CG19 and CG14 using the Ainslie model	32
3-17 Explanation of the wake characteristics	34

3-18 Maximum power loss (left) and energy loss (right) in the wake using the Jensen models	35
3-19 Maximum power loss (left) and energy loss (right) in the wake using the Ainslie model	36
3-20 Maximum power loss (left) and energy loss (right) in the wake Larsen model .	36
4-1 Atmospheric boundary layer wind tunnel of TNO	38
4-2 Wind profile in the TNO tunnel for	39
4-3 Wind turbine model	39
4-4 Thrust curves of ECN's wind turbine models and the GE 1.5 series of turbines	40
4-5 Measurement equipment	41
4-6 Wake behind a single wind turbine, $C_T = 0.91$	41
4-7 Wake behind a single wind turbine, $C_T = 0.56$	42
4-8 Wake velocities at $3D$ behind the rotor	43
4-9 Results of the turbulence models	44
4-10 Turbulence intensities at $3D$ behind the rotor	45
4-11 Wind tunnel set up for the wake adding measurements	47
4-12 Influence of two wakes: separation $2D$	48
4-13 Influence of two wakes: separation $1D$	48
4-14 Calculating the rotor averaged wind speed and its effect on the velocity deficit	49
4-15 Comparison of wake superposition methods	50
4-16 Wind turbine array in the wind tunnel	50
4-17 Normalized velocity through the model wind farm	51
4-18 Added turbulence through the model wind farm	52
4-19 Measured and simulated rotor averaged wind speed at the turbines	53
4-20 Comparison of new tool with measurements	53
4-21 Comparison of new tool with measurements	53
4-22 Comparison of new tool with measurements	54
A-1 Members of the GE family of wind turbines	64
C-1 Determination of wake sectors	69
F-1 Layout of the EWTW test field near Wieringermeer	75
G-1 Schematics of met mast at Prettin wind farm	78
I-1 Measured vs simulated velocity and turbulence: $C_T = 0.91$, $x = D$	81
I-2 Measured vs simulated velocity and turbulence: $C_T = 0.91$, $x = 2D$	82
I-3 Measured vs simulated velocity and turbulence: $C_T = 0.91$, $x = 3D$	82
I-4 Measured vs simulated velocity and turbulence: $C_T = 0.91$, $x = 5D$	82
I-5 Measured vs simulated velocity and turbulence: $C_T = 0.91$, $x = 8D$	83
I-6 Measured vs simulated velocity and turbulence: $C_T = 0.91$, $x = 12D$	83

I-7	Measured vs simulated velocity and turbulence: $C_T = 0.91, x = 20D$	83
I-8	Measured vs simulated velocity and turbulence: $C_T = 0.56, x = D$	84
I-9	Measured vs simulated velocity and turbulence: $C_T = 0.56, x = 2D$	84
I-10	Measured vs simulated velocity and turbulence: $C_T = 0.56, x = 3D$	85
I-11	Measured vs simulated velocity and turbulence: $C_T = 0.56, x = 5D$	85
I-12	Measured vs simulated velocity and turbulence: $C_T = 0.56, x = 8D$	85
I-13	Measured vs simulated velocity and turbulence: $C_T = 0.56, x = 12D$	86
J-1	Method to calculate rotor averaged wind speed	87
K-1	Comparison of new tool with measurements	91
K-2	Comparison of new tool with measurements	92
K-3	Comparison of new tool with measurements	92
K-4	Comparison of new tool with measurements: after 1 st row	93
K-5	Comparison of new tool with measurements: after 3 rd row	93
K-6	Comparison of new tool with measurements: after 5 th row	93

List of Tables

2-1 Parameters for the Quarton and TNO turbulence models	16
3-1 Wind statistics at the met masts	28
4-1 Comparing wind tunnel measurements and full scale experiments	37
4-2 Used offset in (single) wake plots	41
4-3 Generated turbulence using several turbulence models	43
A-1 Characteristics of the GE wind turbines	65
G-1 Sensor heights and types on the Prettin met mast	77
H-1 Relation between wake model parameters	79

Nomenclature

Latin Symbols

ΔU	Velocity deficit
$\overline{u'v'}$	Reynolds stress
A	Rotor disc area
a	Induction factor
A_x	Constant connecting roughness length to turbulence intensity
B	Number of blades
b	Wake width in the Ainslie model
c_1	Non-dimensional mixing length
C_T	Thrust coefficient
D	Rotor diameter
D_{eff}	Effective rotor diameter
H	Hub height
I_a	Ambient turbulence intensity
I'_a	Ambient turbulence intensity for large wind farms
I_d	Design turbulence intensity from the Danish Recommendations
I_T	Maximum center wake turbulence intensity
I_w	Wake added turbulence
I_{eff}	Effective turbulence in a wake
I_{wt}^u	The component of the total turbulence intensity in the wake in the direction of the undisturbed wind
k	Eddy viscosity constant
k	Wake decay constant
k	Wake expansion exponent, Storpark Analytical Model (SAM)
L	Distance between the rotor centers of two turbines
m	Wöhler curve exponent

N	Number of neighboring turbines
P	Power
p_w	Wake probability
$P_{residual}$	Power residual
r	Radial distance from the wake centerline
r_0	'Effective' radius of an expanded rotor disc
R_w	Wake radius
s	Relative distance behind the turbine, $s = \frac{x}{D}$
s_f	Relative turbine spacing between rows
s_i	Relative distance to neighboring turbine i
s_r	Relative turbine spacing within rows
u	Axial component of the flow velocity
u_*	Friction velocity
u_r	Radial velocity in the wake
u_w	Non-uniform wake velocity
U_∞	Undisturbed wind speed
u_{rotor}	Averaged velocity at the rotor
v	Radial component of the flow velocity
x	Distance from rotor plane in free stream direction
x_0	Position of the rotor with respect to the applied coordinate system
x_h	Length of the first part of the near wake by Vermeulen
x_n	Near wake length

Greek Symbols

α	Wake expansion parameter
β	Wake expansion parameter
β_l	Correction factor related to the distance between the wind turbines
β_v	Correction factor related to the mean wind hub velocity
ϵ_1	Wake determination angle
ϵ_2	Wake determination angle
λ	Tip speed ratio
σ	Standard deviation
ε	Eddy viscosity

Subscripts

a	Ambient
c	At the center line of the wake
d	From the downstream turbine
u	From the upstream turbine
w	Wake
met	At the met mast
pc	According to the power curve

Acronyms

BC	Between the columns
CFD	Computational Fluid Dynamics
DEL	Damage Equivalent Load
DIBt	Deutsche Institut fr Bautechnik
DR	Danish Recommendation
ECN	Energy research Centre of the Netherlands
EMD	Energi- og Miljødata
ENDOW	EfficieNt Development of Offshore Windfarms
EWA	European Wind Atlas
EWEC	European Wind Energy Conference
EWTW	ECN Wind turbine Test station Wieringermeer
FLaP	Farm Layout Program
GE	General Electric
GH	Garrad Hassan
HawC	Horizontal axis wind turbine Code
ITO	Inquiry To Order
NASA	National Aeronautics and Space Administration
OWEMES	Offshore Wind Energy in the Mediterranean and other European Seas
RGU	Robert Gordon University

SAM	Storpark Analytical Model
SCADA	Supervisory Control And Data Acquisition
SWP	Sector Wise Parameters
TBONTB	‘To Be Or Not To Be’
TNO	Nederlandse Organisatie voor Toegepast-Natuurwetenschappelijk Onderzoek
UO	University of Oldenburg
UU	University of Uppsala
WAsP	Wind Atlas Analysis and Application Program
WDC	Wake Decay Constant
WRA	Wind Resource Assessment

Chapter 1

Introduction

Though wind energy has been used for centuries, it is only recent that it is used on large scale for electrical energy production. The first wind turbines used for this goal started appearing in the 1980's. They typically used rotor diameters of about 20 meters and could produce between 20 and 60 kW. Nowadays, multi-megawatt turbines are the most sold units and turbines with a rated power of 4 to 6 MW and rotor diameters exceeding 100 meters are being tested.

As air flows through a wind turbine and energy is extracted from it, some of the properties of the flow are changed: the air is decelerated and turbulence intensity is increased¹. The region in the flow behind a turbine where these properties are changed is called the wake of a wind turbine and the effects are referred to as wake effects. As a general rule of thumb, wake effects can be neglected when the turbines are spaced more than 10 rotor diameters from each other. However, as turbines are more and more being grouped together in large wind farms, the spacing between the turbines usually is (much) smaller. This may be because the wind conditions are very favorable at certain parts of a site, but it is often out of cost perspective: tighter spacing means less land or sea area use (especially important for offshore wind farms in extensively used seas such as the North Sea) and less installation cost (think for instance of the cabling).

Because of these smaller spacings the turbines will influence each other through the wake effects: the reduction in wind speed in the wake mainly affects the performance of the downstream wind turbines, while the increased turbulence level affects the loading on the turbines and as such influences the fatigue life. It is thus important to be able to evaluate these wake effects. Within General Electric (GE) Wind Energy two groups are concerned with wake effects. The Validation is mainly responsible for the validation of the used models for loads, design envelope, performance and noise with measurements. The Application Engineering group deals with micrositing, including Wind Resource Assessment (WRA), wind farm layouts, turbine loads, power performance and acoustic analysis during the Inquiry To

¹A third effect of the way the turbine extracts energy from the air is that the air is given a rotation. Wake rotation however will not be considered in this study.

Order (ITO) phase. The main tools GE uses to assess the wake effects are the commercially available software packages Wind Atlas Analysis and Application Program (WAsP) and WindPRO, the in-house developed tool ‘To Be Or Not To Be’ (TBONTB) and FLEX5, see appendix B for a short description of these tools.

In December 2005 WindPRO received an upgrade to version 2.5, one of the new features being the possibility to use different wake models to predict the velocity deficit and the increased turbulence. Only limited validation studies have been published by Energi- og Miljødata (EMD), the creator of WindPRO, and therefore they do not recommend using any of the new models. A more detailed validation of these models is thus requested.

Furthermore a tool is under development at GE that can assist in finding the optimal layout for a wind farm depending on the objective function that is chosen by the user. This can for instance be minimum cost or maximum park efficiency. In any case should be tool check whether all turbines within a proposed layout will remain within their design envelope. The tool should thus at least be capable to calculate the wake losses and turbulence intensity at the proposed positions. As such an optimization tool generally uses a lot of iterations, fast models are required to perform these calculations. Suitable wake models have to be selected and validated to perform these calculations.

1.1 Goal of this thesis

The goal of this thesis work is to validate the wake models included in WindPRO and other wake models that can be used in an optimization tool with measurements performed at operating wind farms and with wind tunnel experiments. Both the prediction of the velocity deficit and the prediction of turbulence intensity should be assessed. Recommendations which model to use within WindPRO should be given.

1.2 Outline of the report

The outline of the report is as follows:

Chapter 2 will give an overview of existing wind turbine wake models for the velocity deficit and the wake added turbulence and shortly discusses previous validation studies.

Chapter 3 will present the validation of the WindPRO wake models with wind farm measurements at the two sites Prettin, Germany and Colorado Green, United States.

Chapter 4 then discusses the validation of several wake models with wind tunnel measurements performed by ECN in the TNO atmospheric wind tunnel. It also focusses on a combination of the Larsen velocity deficit model with a turbulence model introduced by ForWind in order to provide fast calculations of the wake effects including wake shear and realistic turbulence shape.

Chapter 5 concludes this work and will provide recommendations for further study.

Throughout this report the readers are assumed to have basic (wind turbine) aerodynamic knowledge. For a review of aerodynamics, see for instance Anderson [1]. Good material covering wind turbine aerodynamics are that of Manwell et al. [2] and Burton et al. [3].

Chapter 2

Wake models

Wind turbine wakes are generally divided in the near wake, where the influence of the separate rotor blades can be distinguished, and the far wake. Although the naming may imply otherwise, there is a gradual transition from one to the other, not an abrupt one. Different studies suggest different lengths for the near wake, ranging from one to a maximum of several rotor diameters. In recent years quite some research has been done on modeling the near wake. Typical models describing the near wake are the asymptotic acceleration potential method (see Van Bussel [4]), vortex wake models and generalized actuator disc models. While some of these methods have been applied to study the flow through several wind turbines, they are computationally too intensive to use for general wind farm calculations. Because the goal of this study is to clearly focus on wind farm situations, the main focus will be on the far wake models. In this chapter both velocity deficit and wake added turbulence models will be described (including all models available in WindPRO), but it is certainly not exhaustive.

Far wake models can be divided in kinematic wake models (also called explicit models) and field models (or implicit models). Besides these two types of models, in their study Vermeer et al. [5] also mention boundary layer wake models. Because of the similarity between boundary layer models and field models when used for wind farm modeling, this study will not make this distinction. The same was done in Crespo et al. [6]. In the early days of wind farm modeling, the wind farm was seen as distributed roughness elements that disturbed the atmospheric flow, though there also are recent studies following this approach, see for instance Hegberg et al. [7].

2.1 Kinematic models

Kinematic wake models use only the momentum equation to model the velocity deficit of the wake behind a turbine. The wake descriptions do not consider the initial expansion region of the wake. They also do not cover the change in turbulence intensity in the wake behind a turbine, so they have to be coupled with a turbulence model if values of the turbulence intensity in the wakes and throughout the wind farm are desired.

2.1.1 Jensen model

One of the oldest wake models is the model by N.O. Jensen (referred to from now as the Jensen model). It is quite a simple wake model, assuming a linearly expanding wake with a velocity deficit that is only dependent of the distance behind the rotor, see figure 2-1. This figure shows the wake at a horizontal plane through the hub of a GE1.5sl having a rotor diameter D modeled with the Jensen model. The wake diameter is given by

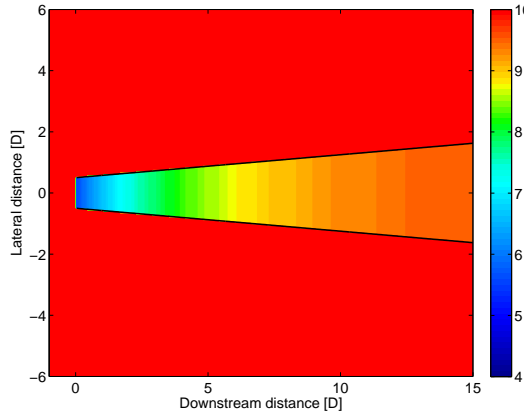


Figure 2-1: Wake behind a turbine: Jensen model. $U_\infty = 10 \text{ m/s}$, $k = 0.075$

$$D_w = D(1 + 2ks) \quad (2-1)$$

and the velocity in the (fully developed) wake by

$$u = U_\infty \left[1 - \frac{1 - \sqrt{1 - CT}}{(1 + 2ks)^2} \right] \quad (2-2)$$

Both depend on the relative distance behind the rotor, $s = x/D$ and the Wake Decay Constant (WDC) k . Because the velocity in the wake is constant for a given downstream distance, the velocity profile is called ‘hat-shaped’. The value of k is generally taken to be 0.075, which is adequate for land cases, but for offshore use a value of 0.04 is recommended.

It can easily be seen from Eq. (2-2) that just behind the rotor ($s = 0$) the velocity in the wake is

$$u|_{s=0} = U_\infty \sqrt{1 - CT} \quad (2-3)$$

Hence due to its simplifications the Jensen model requires that the thrust coefficient of the rotor is smaller than one.

The Jensen model is the wake model in WAsP and is also included in Garrad Hassan (GH) WindFarmer. Until the upgrade to version 2.5 it was also the only velocity deficit model available in WindPRO. In WindPRO 2.5 several other wake models are available including a modified version of the Jensen model. This modified version allows the Jensen model to be able to work together with turbulence models that have also been included in WindPRO 2.5. Besides that the algorithms for to handle multiple wakes have been changed. Originally the Jensen model in WindPRO was fine-tuned to mimic results obtained with WAsP. In the

modified Jensen (2005) model, the wake combination method described by Katic [8] is used. This allows wind farms to consist of turbines with different hub heights or contain different turbine types.

Because of the fact that EMD has only recently provided some (though still limited) insight and documentation about the validity of the new wake models in WindPRO, the original Jensen model still was the model used for micrositing by the Application Engineering group at GE at the start of this thesis work.

2.1.2 Larsen model

The model by G.C. Larsen (referred to as the Larsen model from now, but also known as the EWTSII model) is based on the Prandtl turbulent boundary layer equations and has closed-form solutions for the width of the wake and the mean velocity profile in the wake. In order to obtain the closed form solutions a self-similar velocity profile is assumed and Prandtl's mixing length theory is used. The flow is further assumed to be incompressible and stationary and wind shear is neglected, hence the flow is axisymmetric.

Larsen showed both a first-order and a second-order approximate solution to the boundary layer equations [9], of which the last one is capable of resolving the double dip in the velocity deficit profile of the near wake.

Below the governing equations of the first order solution will be given. For the second order solution, see appendix D Using the first order approximation, the following equations for the rotor wake radius R_w and the axial velocity deficit in the wake $(\Delta U)_1$ are obtained

$$R_w(x) = \left(\frac{35}{2\pi} \right)^{\frac{1}{5}} (3c_1^2)^{\frac{1}{5}} (C_T A (x + x_0))^{\frac{1}{3}} \quad (2-4)$$

$$\begin{aligned} (\Delta U)_1(x, r) = -\frac{U_\infty}{9} \left(C_T A (x + x_0)^{-2} \right)^{\frac{1}{3}} & \left[r^{\frac{3}{2}} (3c_1^2 C_T A (x + x_0))^{-\frac{1}{2}} + \right. \\ & \left. - \left(\frac{35}{2\pi} \right)^{\frac{3}{10}} (3c_1^2)^{-\frac{1}{5}} \right]^2 \end{aligned} \quad (2-5)$$

There are still two unknown constants, namely c_1 , which is related to the Prandtl mixing length, and the position of the rotor with respect to the applied coordinate system, x_0 . WindPRO uses the relations given in the EWTS II¹:

$$c_1 = \left[\frac{D_{\text{eff}}}{2} \right]^{\frac{5}{2}} \left(\frac{105}{2\pi} \right)^{-\frac{1}{2}} (C_T A x_0)^{-\frac{5}{6}} \quad (2-6)$$

$$x_0 = \frac{9.5D}{\left(\frac{2R_{9.5}}{D_{\text{eff}}} \right)^3 - 1} \quad (2-7)$$

¹However, the equation for c_1 in EWTS II is erroneous, the correct one is given in Larsen [10] and is used here.

The effective rotor diameter D_{eff} is given by

$$D_{\text{eff}} = D \sqrt{\frac{1 + \sqrt{1 - C_T}}{2\sqrt{1 - C_T}}} \quad (2-8)$$

and the wake radius at a distance 9.5 rotor diameters downstream of the turbine, $R_{9.5}$, is taken from [11] to be

$$R_{9.5} = 0.5 [R_{\text{nb}} + \min(H, R_{\text{nb}})] \quad (2-9)$$

with the empirically found relation

$$R_{\text{nb}} = \max(1.08D, 1.08D + 21.7D(I_a - 0.05)) \quad (2-10)$$

Equation 2-9 accounts for the blockage effect of the ground, if the wake radius were to be larger than the hub height. Besides on the coordinates x and r the Larsen models depends on the thrust coefficient C_T , the undisturbed wind speed U_∞ , rotor diameter D , hub height H and the ambient turbulence intensity I_a . An example of the axial velocity development behind a turbine calculated with the Larsen model is shown in figure 2-2. In this plot the wake boundary as given by R_w is shown as a black line.

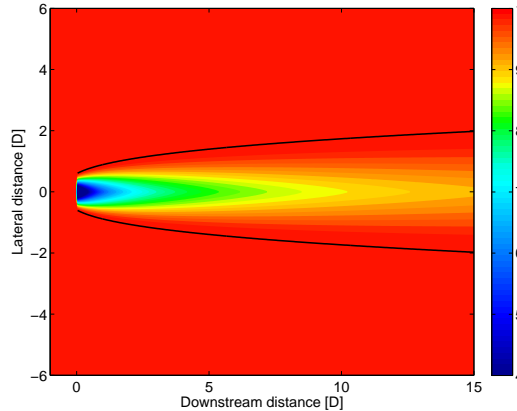


Figure 2-2: Wake behind a GE 1.5sl: Larsen model. $U_\infty = 10$ m/s, $I_a = 0.1$

2.1.3 Analytical model by Frandsen

A more recent method than the Jensen and Larsen model is the Storpark Analytical Model (SAM) that was presented at the European Wind Energy Conference and Exhibition 2006 [12]. While the SAM was designed to predict the wind speed deficit in large offshore wind farms with a rectangular grid and constant spacing between rows, work is ongoing to make the model suitable for irregular grids. This of course is a requirement for the model to be useable for general wind farm calculations.

The model distinguishes three different wake regimes: in the first regime single or multiple wake flow is present without interaction between neighboring wakes. The second regime starts when two neighboring wake flows interact. The expansion of the wake is then limited to an expansion in vertical direction only. The wake is in the third and last regime when the wake

flow is in balance with the planetary boundary layer. This occurs when the wind farm can be seen as infinitely large.

Similar to the Jensen model, the velocity deficit in the wake is assumed to be hat-shaped. Originally in the SAM the wake diameter in the first regime was given by

$$D_w(x) = D(\beta^{k/2} + \alpha s)^{1/k} \quad (2-11)$$

with the wake expansion parameter β given by

$$\beta = \frac{1 + \sqrt{1 - C_T}}{2\sqrt{1 - C_T}} = \left(\frac{D_{\text{eff}}}{D} \right)^2 \quad (2-12)$$

and the values of k and α being 2 and 0.7 respectively. Later studies showed that a different description of the wake diameter corresponded better with measurements in the far wake.

$$D_w(x) = D \max [\beta, \alpha s]^{1/2} \quad (2-13)$$

However, using this relation will result in a discontinuity in the wake diameter in the near wake.

In a single wake the velocity deficit is assumed constant and is given by:

$$u = \frac{U_\infty}{2} \left(1 \pm \sqrt{1 - 2 \frac{A}{A_w} C_T} \right) \quad (2-14)$$

where the sign in the term between parentheses depends on the value of C_T . The axial velocity calculated using this model is shown in figure 2-3.

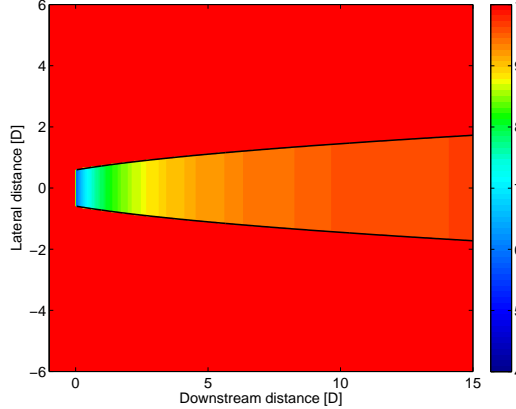


Figure 2-3: Wake behind a GE 1.5sl: Larsen model. $U_\infty = 10$ m/s, $k = 2$, $\alpha = 0.7$

In the case of composite wakes (wakes consisting of multiple wakes originating from upstream turbines) the wakes are divided in several sections (called mosaic tiles) each having a constant but different velocity deficit. In order to calculate the mean wind speed over the rotor area, a semi-linear method is used. See the paper by Rathmann et al. [13] for more details regarding the method for wake combination.

Up to this date no validation studies using this model have been published.

2.2 Field models

Field models calculate the complete flow field through a wind farm, or a part of the wind farm when the wind farm is regular, hence the name field models. In order to do so field models solve the Reynolds-averaged Navier-Stokes equations with a turbulence model for closure. This chapter will describe the best known field models which can be divided in two- and three-dimensional models.

2.2.1 Two-dimensional field models

Two-dimensional field models assume axial symmetry in the wakes. Since this leads to fewer equations to be solved simultaneously less time is needed for the calculation of the flow field. This approach was first used by J.F. Ainslie [14] and several models are based on his work.

The model by J.F. Ainslie (referred to as Ainslie model) uses axisymmetrical, time averaged Navier-Stokes equations for incompressible flow with eddy viscosity closure to calculate wake behavior. The continuity equation in cylindrical coordinates is given by

$$\frac{1}{r} \frac{\partial(rv)}{\partial r} + \frac{\partial u}{\partial x} = 0 \quad (2-15)$$

and the momentum equation in free stream direction by

$$u \frac{\partial u}{\partial x} + v \frac{\partial u}{\partial r} = -\frac{1}{r} \frac{\partial(r \bar{u}' v')}{\partial r} \quad (2-16)$$

The Reynolds stress is modeled with the eddy viscosity

$$-\bar{u}' \bar{v}' = \varepsilon(x) \frac{\partial u}{\partial r} \quad (2-17)$$

Ainslie splitted the eddy viscosity in the ambient eddy viscosity of the atmospheric flow and the eddy viscosity generated by the wind shear in the wake

$$\varepsilon(x) = \varepsilon_a + \varepsilon_w(x) \quad (2-18)$$

$$(2-19)$$

where the latter part of the right hand side is given by

$$\varepsilon_w(x) = kb(U_\infty - u_c(x)) \quad (2-20)$$

and depends on the wake width b , the velocity deficit at the center line of the wake ($U_\infty - u_c(x)$) and a constant k , empirically found to be 0.015.

One of the simplifications of the model is that pressure gradients in the wake are neglected. This assumption however is not valid just behind the rotor and the model cannot be used in that region. Hence the wake model has to be initialized after the near wake with an empirical wake profile. Ainslie assumed the length of the near wake to be $2D$ and used a Gaussian profile

$$1 - \frac{u}{U_\infty} = (U_\infty - u_c) \exp \left(-3.56 \left(\frac{r}{b} \right)^2 \right) \quad (2-21)$$

The initial velocity deficit at the centerline of the wake ($U_\infty - u_c$) was found to be

$$(U_\infty - u_c) = C_T - 0.05 - (16C_T - 0.5) \frac{I}{10} \quad (2-22)$$

based on wind tunnel studies and the wake width b (defined as the distance at which the velocity deficit is 2.83% of its centerline value) was then found from momentum conservation to be

$$b = \sqrt{\frac{3.56C_T}{4(u_\infty - u_c)(2 - (u_\infty - u_c))}} \quad (2-23)$$

An example of the axial velocity development downstream of a turbine is given in figure 2-4. Note that in the first part of the wake the velocities are constant.

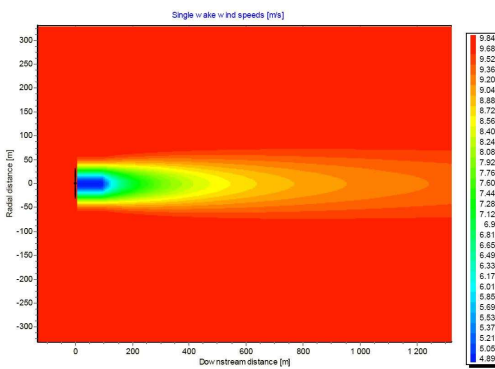


Figure 2-4: Calculated flow field behind a turbine at hub height using the Ainslie model. Source: EMD [15]

Implementations of the Ainslie model

While in WindPRO the Ainslie model is implemented as described above, there are other implementations of the model that differ in some or more aspects from the equations just given. These differences are given below.

GH WindFarmer In the commercially available software package WindFarmer by Garrad Hassan the Ainslie model is implemented as the Garrad Hassan Eddy Viscosity Wake model. In the WindFarmer Theory manual [16] the same equations could be found as given above.

FLaP The Farm Layout Program (FLaP) [17] was developed by the University of Oldenburg (UO) and is also based on the Ainslie model. During the Efficient Development of Offshore Windfarms (ENDOW) project (see chapter ??) several improvements were made to the program in order to make it usable for offshore conditions [18]. The eddy viscosity model was improved and the effect of the turbulence and atmospheric stability on the length of the near wake was taken into account. To calculate the near wake length the approach suggested by Vermeulen was used (see appendix E for details).

2.2.2 Three-dimensional field models

WAKEFARM

ECN has developed the model WAKEFARM which is based on a modification of the UPMWAKE wake model by Universidad Polytechnica de Madrid.

WAKEFARM (and hence UPMWAKE) is a 3D parabolized Navier-Stokes code for the far wake using a $k-\varepsilon$ turbulence model. To model the near wake, momentum theory is used together with some empirical corrections. Originally the far wake was initialized with a hat-shaped velocity deficit at $2.25D$ downstream of the rotor (this is the main difference between the modified and the original UPMWAKE which assumes the wake is fully expanded at the rotor disc). This hat-shape was changed to a Gaussian velocity deficit during the ENDOW project [19]).

The initial wake shape used during ENDOW is given by

$$u_{initial}(y, z) = 1.3(1 - \sqrt{1 - C_T})U_\infty(e^{-0.5(y/r\sigma_y)^2}e^{-0.5((z-H)/r\sigma_z)^2}) \quad (2-24)$$

where σ_y and σ_z are tuned to wind tunnel measurements

$$\sigma_y = \sigma_z = \frac{1}{2}\sqrt{\frac{1-a}{1-2a}} \quad (2-25)$$

and a is given by

$$a = \frac{1}{2}(1 - \sqrt{1 - C_T}) \quad (2-26)$$

An anisotropic turbulence model was initially used. Since this model was overestimating the turbulence in free-stream direction, an isotropic model for the added turbulence was later validated. While using an isotropic model yields decreased values of the turbulence in free-stream direction, turbulence in other directions are increased. No measurements were available for these, so no complete validation was possible. For multiple wake cases, the far wake was initiated just at the rotor plane, since again initializing it $2.25D$ did not show good results. The WAKEFARM program experienced some convergence problems, but these could be circumvented. The initialization of the wake is needed because of the parabolization. Were an fully elliptic model to be used, this initialization would not be necessary, since the near wake is a part of the solution. However, according to ECN the extra calculation time necessary (about 12 hours for the fully elliptic equations and in the order of minutes for the parabolized ones) does not weigh up to the slight increase in accuracy. ECN suggested further improvements could be made by initializing the velocity deficit as a double dip profile instead of a Gaussian. This shape is seen in both measurements and near wake results of more elaborate models. Also improvements may be seen when atmospheric conditions are allowed to influence initial wake shape and near wake length.

Recent improvements to WAKEFARM Recently ECN has made improvements to the WAKEFARM model, although not the ones suggested after the ENDOW project. The need for the initialization lies in the fact that the model is parabolized. While better results could be achieved by a further improvement of the initial wake shape, a removal of the need for

this tuning is preferred. This can be achieved by prescribing the pressure gradient in the near wake. In order to calculate the pressure gradient a free vortex wake model is used. Using this improved model similar results to the WAKEFARM with tuned parameters were obtained [20].

Elliptic field models

Several elliptic field models have been developed to study the flow around wind turbines and through wind farms. In these models wind turbines are modeled either using generalized actuator discs (Ammara et. al [21]) or actuator lines (Mikkelsen [22] and Troldborg et. al [23]). Though these models are able to capture a lot of detail in the (near) wake, they are computationally very intensive. Mikkelsen only studied a single wind turbine, Troldborg et. al a row of 3 turbines and Ammara a two row periodic wind farm.

The Robert Gordon University (RGU) used a fully elliptic three-dimensional Navier Stokes code with a turbulent $k-\varepsilon$ closure during the ENDOW project (see chapter ??). It required about 12 hours of calculation time in 2001 (see Schepers et. al [24]) compared to seconds or minutes for the other models, while not yielding significant better results. For general micrositing work with random wind farm layouts calculations using elliptic models are not yet feasible, therefor these models will not be subject of this thesis.

As has been mentioned, several of these models have been used in a validation study called ENDOW. The findings from this study will shortly be discussed in chapter ??.

2.3 Wake added turbulence models

As stated earlier, the kinematic wake models have to be combined with turbulence models when used for load calculations. In WindPRO the turbulence models available are Danish Recommendation (DR), Larsen, the Frandsen or DIBt model and the Quarton / TNO turbulence model.

2.3.1 Danish Recommendation

The model used in the Danish Recommendation specifies a design turbulence intensity I_d normalized with respect to the ambient mean wind speed at hub height.

$$I_d = \sqrt{I_a^2 + I_w^2} \quad (2-27)$$

in which the wake added turbulence is specified by

$$I_w = 0.15\beta_v\beta_l \quad (2-28)$$

where β_v and β_l are correction factors related to wind speed and wind farm configuration and can be obtained from figure 2-5 (reproduced from Dekker and Pierik [11]). Using these correction factors it can be derived that the value of I_w lies in between 0.066 and 0.15.

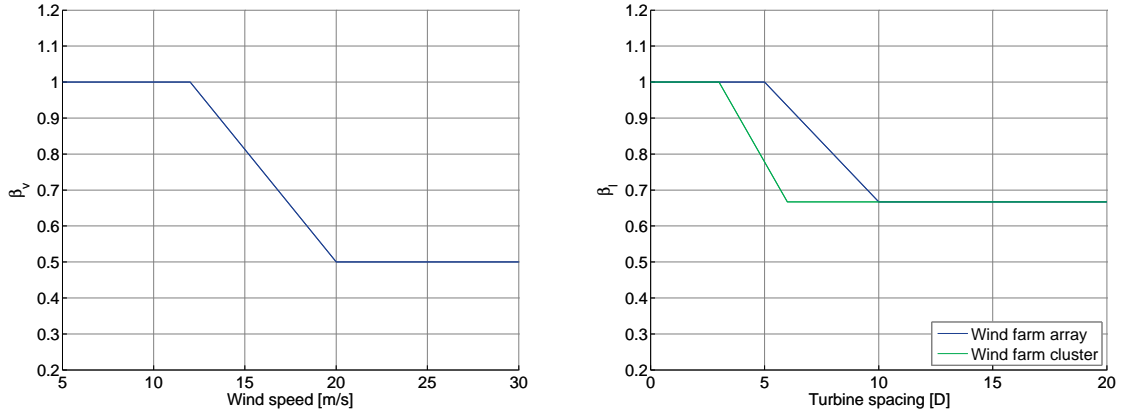


Figure 2-5: Wind speed correction factor (left) and distance correction factor (right) for the Danish Recommendations design turbulence

2.3.2 Larsen model

The turbulence model of Larsen is based on the assumptions that only surface and wake shear mechanisms contribute significantly to turbulence production and that these mechanisms are statistically independent, thus additive. The component of the total turbulence intensity in the wake in the direction of the undisturbed wind, I_{wt}^u is given by

$$I_{wt}^u = \sqrt{I_a^2 + I_w^2} \quad (2-29)$$

The wake added turbulence (for spacings larger than 2D) is given by

$$I_w = 0.29 s^{-1/3} \sqrt{1 - \sqrt{1 - C_T}} \quad (2-30)$$

2.3.3 Frandsen / DIBt model

The Frandsen model and the Deutsche Institut fr Bautechnik (DIBt) model are identical. They are given in WindPRO as two separated options, mainly because users in Germany are more familiar with the DIBt naming. The model states the following: if the smallest separation between two wind turbines in a wind farm is more than 10 rotor diameters, wake effects do not have to be accounted for. However, if the minimum separation is less than 10 rotor diameter, the wake effects in the form of the added turbulence have to be calculated as follows. The turbulence intensity in a wake, which Frandsen calls ‘effective turbulence’, is given by

$$I_{eff} = \left[(1 - p_w N) I_a^m + p_w N \sum_{i=1}^N I_T^m(s_i) \right]^{\frac{1}{m}} \quad (2-31)$$

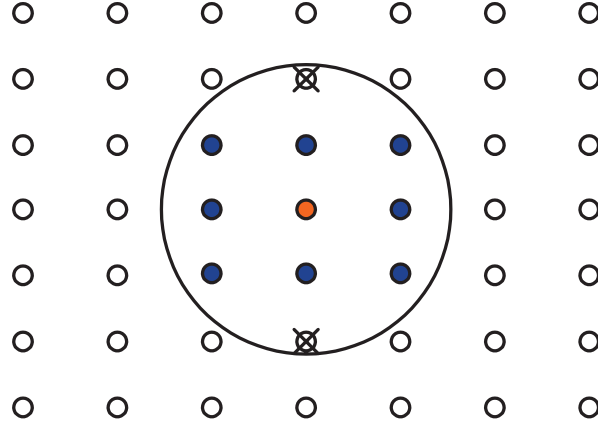


Figure 2-6: Turbines taken into account in the Frandsen model. Reproduced from Frandsen and Thøgersen [25].

where

- m is the Wöhler curve exponent depending on the material of the structural component under consideration
- N is the number of neighboring turbines
- p_w is the wake probability and is taken to be 0.04
- s_i is the distance to the neighboring turbine i
- I_a depends on the considered load case

and the maximum center wake turbulence intensity I_T is given by

$$I_T = \sqrt{\frac{1}{1.5 + 0.3s_i\sqrt{U_\infty}} + I_a^2} \quad (2-32)$$

The wake of a turbine that is ‘in front’ another turbine from the point of view of the turbine in consideration is not taken into account. So in a rectangular grid the number of neighboring turbines is 8, see also figure 2-6.

In large wind farms, where there can be more than 5 turbines between the turbine under consideration and the edge of the wind farm, or when the turbines are spaced less than 3 rotor diameters from each other in the direction perpendicular to the predominant wind direction, a different value for the ambient turbulence intensity, I'_a , has to be used:

$$I'_a = \frac{1}{2}(\sqrt{I_w^2 + I_a^2} + I_a) \quad (2-33)$$

with

$$I_w = \frac{0.36}{1 + 0.2\sqrt{\frac{s_r s_f}{C_T}}} \quad (2-34)$$

The values s_r and s_f are the relative spacings in the rows and between the rows respectively.

Though having a different name, the Frandsen and DIBt models available in WindPRO are identical. However, when using the default settings for the models there will be small differences in the results due to an override of the step size setting within wind speed distribution with the DIBt model. When this setting is set equally, the results are identical as expected.

2.3.4 Quarton / TNO models

The wake added turbulence as defined by the Quarton and TNO models is given by the following relation:

$$I_w = K_1 C_T^{\alpha_1} I_a^{\alpha_2} \left(\frac{x}{x_n} \right)^{\alpha_3} \quad (2-35)$$

Based on wind tunnel test, Quarton proposed an alternative to his original model. The values of the parameters are given for the different models in table 2-1.

Turbulence model	K_1	α_1	α_2	α_3
Quarton original	4.8	0.7	0.68	-0.57
Quarton alternative	5.7	0.7	0.68	-0.96
TNO	1.31	0.7	0.68	-0.96

Table 2-1: Parameters for the Quarton and TNO turbulence models

The TNO model requires the ambient turbulence intensity to be fraction, while the Quarton model requires a percentage. Combining this with the difference in parameters it can easily be calculated that the only difference between the Quarton alternative and the TNO model is the definition of the near wake length. In the alternative Quarton model the near wake length defined by Vermeulen is used (see appendix ??) while the TNO model uses its own definition.

$$\frac{I_{w_{Quarton}}}{I_{w_{TNO}}} = \frac{5.7}{1.31} \frac{*100^{0.68}}{1^{0.68}} \left(\frac{x_{n_{TNO}}}{x_{n_{Quarton}}} \right)^{-0.96} = \left(\frac{x_{n_{TNO}}}{x_{n_{Quarton}}} \right)^{-0.96} \quad (2-36)$$

2.3.5 Lange model

Only available in combination with the Ainslie model, the turbulence model by Lange models the turbulence intensity created by wind shear by means of the eddy viscosity like was done in FLaP:

$$I_{mean} = \varepsilon \frac{2.4}{\kappa u_\infty H} \quad (2-37)$$

2.3.6 Model by ForWind

All turbulence models available in WindPRO assume that the turbulence intensity in the wake is constant for a given distance downstream of the turbine, just like the Jensen model does with the velocity deficit. However, most turbulence is generated near the hub region and at the rotor blade tips. At a certain distance downstream a Gaussian-like profile remains due to diffusion. To capture this turbulence shape a new model was developed by ForWind which was presented at the EWEC 2006 conference.

In the ForWind model the wake added turbulence consists of a part due to shear and a smoothing part due to diffusion. The velocity in the wake is assumed axisymmetrical and this model should thus not be used together with the Jensen or Frandsen models discussed

in chapter ???. At ForWind the model was used in combination with FLaP, see Wessel et al. [26]. Using the following relation for the relative axial velocity deficit

$$\tilde{u}(r, x) = 1 - \frac{u(r, x)}{U_\infty} \quad (2-38)$$

the added turbulence is given by

$$I_{add}(r, x) = I_{shear}(\tilde{u}(r, x)) + I_{diff}(\tilde{u}(r, x)) \quad (2-39)$$

The parts due to shear and diffusion are given by

$$I_{shear}(\tilde{u}(r, x)) = AI_{mean}(x) \frac{\partial \tilde{u}(r, x)}{\partial(r/R)} \quad (2-40)$$

$$I_{diff}(\tilde{u}(r, x)) = B\tilde{u}(r, x) \quad (2-41)$$

where A and B are empirically found constants.

To calculate I_{mean} equations (2-37) and (2-18) to (2-23) are used, leading to

$$I_{mean}(x) = I_a + \frac{2.4}{\kappa U_\infty z_H} k R_w(x) [U_\infty - u_c(x)] \quad (2-42)$$

2.4 Previous validation results

As mentioned earlier, while the upgrade of WindPRO to version 2.5 introduced several wake models, a thorough validation of these models was not available. At European Wind Energy Conference (EWEC) 2006 Sørensen et al. from EMD presented a paper with a preliminary validation study of the models [27, 28]. Clear conclusions from these papers could not be drawn.

Actually, only recent results were found for the field models. The SAM still has to be validated and calibrated at the time of writing of this literature study. This chapter tries to summarize -and compare when possible- the results of other previous validation studies. Since some of the field models were validated during ENDOW, a short description of this project will be given first.

2.5 Introduction to the ENDOW project

Because of the differences in for instance turbulence and the propagation of wakes behind wind turbines between onshore and offshore application of wind energy, the European project EfficieNt Development of Offshore Windfarms (ENDOW) was started. The goal of ENDOW was to evaluate, enhance and interface wake and boundary layer models for offshore wind farm utilization. Wake models of six partners were investigated during ENDOW, namely those of Risø, ECN, Garrad Hassan (GH), Robert Gordon University (RGU), University of Uppsala (UU) and University of Oldenburg (UO). For validation the Vindeby wind farm in Denmark and the Bockstigen wind farm in Sweden were used.

Three variables were considered to generate the wake model scenarios: free wind speed at hub height, turbulence intensity at hub height and the Monin-Obukhov length, which is a measure for the stability of the atmosphere. The effect of the atmospheric stability will not be considered in this study, for more details about the Monin-Obukhov length, see for instance Lange et al. [17]

In the Vindeby wind farm measurement for single, double and quintuple wake cases were made, while in the Bockstigen wind farm only single wake cases were measured.

2.6 Results from ENDOW

The results for the single wake case in neutral atmospheric conditions are given in [29]. Some general observations can be made from the comparison with measurements. All the models based on approximations of the Navier-Stokes equations predict consistent turbulence intensity levels in the wake. The three-dimensional models of the Robert Gordon University and ECN (after the modifications) show good agreement in both velocity deficit and turbulence intensity.

For the double wake case all models overestimate the wake effects. The models from GH, UO and ECN perform best. The FLaP model from the UO showed most improvement after the adjustments, though the improvements made by ECN were also significant. The GH

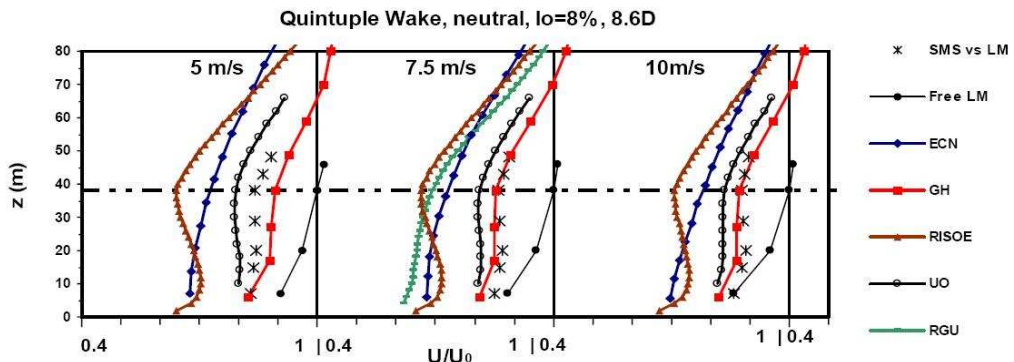


Figure 2-7: Results of the models used during ENDOW for the quintuple wake case after improvements made by the participants. Obtained from: Barthelmie (ed.) [30]

model showed very good agreement with the measurements in the quintuple wake case, see figure 2-7. Only for the lowest wind speed was the wake effect underestimated. All other models overestimated the velocity deficit. The UO showed again great improvement with their modifications. It is suggested that for multiple wake cases wake meandering can become important (see also appendix ???. This effect is not included in any of the models.

No results were available of the multiple wake cases using the model by UU or the Risø Computational Fluid Dynamics (CFD) model.

Chapter 3

Wind farm measurements and validation

This chapter describes the validation of the WindPRO velocity deficit models with measurements from operating wind farms and the influence of the available turbulence models on the results. In order to be useful for validation purposes, a site must of course have wake situations, operating data from the turbines and meteorological data of at least one met mast. Besides that the data set should be sufficiently large. For micrositing analysis at least one full year of date is preferred as wind conditions vary over the year (multiple years are even better).

Data from three locations were available at GE for this study: Prettin in Germany, Colorado Green in the United States and Wieringermeer in the Netherlands. Data from the prototype site in Wieringermeer was not used however for reasons described in appendix F. The analyses for the other two wind farms will be given below.

3.1 Prettin wind farm

The first wind farm under consideration is the Prettin wind farm. As this is a rather small site, it was a good farm to use for both learning WindPRO and doing initial work on the Matlab routines. However, as will be shown the wind farm has as drawback that only one wake case can be investigated.

3.1.1 Location and layout

Prettin is a small village that is located about 50 kilometers northeast of Leipzig, in the eastern part of Germany, see figure ???. Near this village (approximately at the coordinates $51^{\circ}40'20''\text{N}$ $12^{\circ}57'00''\text{E}$) a small wind farm is located of which an overview is given in figure 3-1 as well.

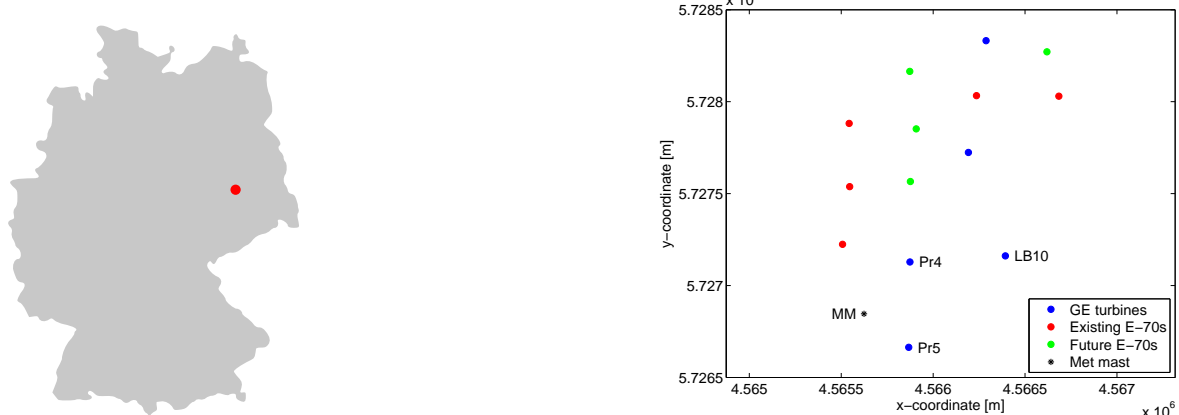


Figure 3-1: Location of the Prettin wind farm within Germany (left) and the coordinates of the Prettin wind farm in the Gauß-Krüger coordinate system (right)

From two turbines in the wind farm a data set was available, designated with ‘Pr4’ and ‘Pr5’ in the layout. Besides these turbines the wind farm consists of several other GE turbines as well as some (future) Enercon turbines. From these turbines no measurement data was available though. There is one met mast which is equipped with several anemometers, a wind vane, and sensors measuring pressure and temperature, see appendix G.

As can be seen from photographs taken at the site the terrain around it is quite flat although there are disturbances in the form of the villages of Prettin and Labrun, a small forest on a little hill and some trees aligning the roads. Turbines Pr4 and Pr5 are both GE 1.5sl turbines



Figure 3-2: Views from the top: looking from Pr4 to the Enercons (left) and to the LB10 (right).

(see appendix ?? for an overview of GE turbines) with a hub height of 96m, but they are equipped with different blades: GE 37c blades are mounted on Pr4 while Pr5 uses LM 37.3P2 blades. This difference in blades will result in a small difference in performance.

Data was available from April 2002 until May 2006 to use in this analysis. Besides the data collected from the met mast, the status of the two turbines is known, which is also used in the filtering process. The data set contains 10 minute average values of the variables.

3.1.2 Flow qualification

Figure 3-3 shows the qualification of the incoming flow at the met mast and wind turbines Pr4 and Pr5 using the method described in appendix ??.

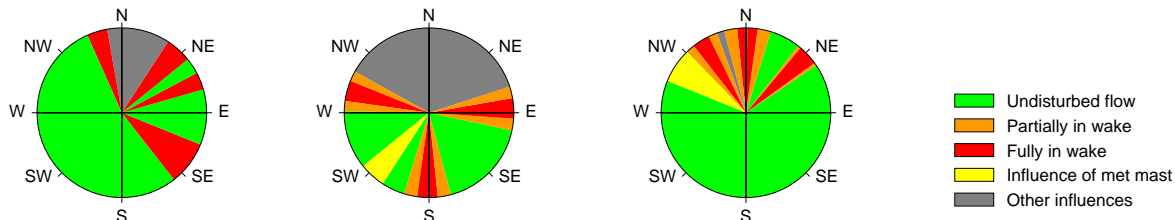


Figure 3-3: Flow qualifications at met mast (left), Pr4 (middle) and Pr5 (right)

The color green indicates that for that wind direction the met mast or turbine is not in a wake, orange and red mean a partial or full wake, yellow indicates the ‘influence’ of the met mast and grey means either multiple overlapping wakes and/or uncertainty about wake occurrence.

Ideally one would have data from two met masts available for wake analysis, one being in a wake and the other met mast in free stream conditions. While only one met mast is located at Prettin (which is sufficient for power curve measurements), the possibilities for wake analysis are somewhat limited.

For the investigations it is required that the met mast and one turbine are in undisturbed flow and the other turbine is in the wake of the first turbine. Taking into account the possible disturbances of the village and the hill as well, two sectors for investigation were chosen. One sector for the wake investigation, when the wind is blowing from the south (180°) and Pr4 is in the wake of Pr5 and as a check a free sector, when the wind is blowing from between the east and southeast and both turbines and the met mast are in undisturbed flow.

The influence of the village and the forest might be found from a different roughness length for certain wind directions. When the wind speed is known at two different heights, this roughness length can be calculated using a logarithmic wind speed profile. Doing so at Prettin resulted in unrealistic values, hence this method was not used and the wind directions were the forest and village could be of influence were neglected. The reason for the unrealistic values probably is that the highest anemometer is located at a height of 87 meters. Around this height there is a transition from the atmospheric boundary layer into the so called Ekmann layer where the logarithmic wind speed profile (or the profile using the power law) is not valid anymore.

3.1.3 Analysis of measurement data

The measurement data is cleaned to ensure that no data is used from periods that either one of the turbine was offline or not in normal operation. Also care is taken at temperatures below 3 degrees Celsius as it is possible that for instance the wind vane or cup anemometer is not functioning correctly due to icing. This cleaned data is used as well as input for the simulations in WindPRO.

Turbulence intensity

A plot of the turbulence intensity at the met mast as a function of wind direction can show distinct peaks. These peaks indicate the wind directions at which the met mast is in the wake of a turbine and hence this plot can also serve as a check on the calibration of the wind vane.

When the wake sectors are clearly indicated in this plot by peaks, the wake added turbulence can be determined. Plotting the turbulence intensity at the met mast versus the wind direction gives the plot as shown in figure 3-4.

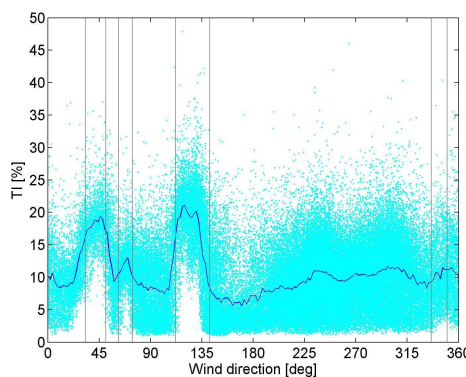


Figure 3-4: Turbulence intensity at the met mast for all wind speeds greater than 3 m/s

The various wake situations are clearly visible. Besides the measurement points, the mean line is shown. The vertical lines mark the wind directions where the met mast was in a wake according to the flow qualification tool (see the left pie chart of figure 3-3). The first and third peak occur when the met mast is in the wake of turbines Pr4 and Pr5 (at a distance of 3.9D and 4.9D respectively). The second smaller peak is the wake from LB10. This peak is lower due to its greater distance to the met mast, namely 10.8D, but also since it was not possible to filter on the operation of LB10. It could thus be the case that this turbine was not operating for some measurement points.

Power residual

The power residual of a turbine is defined as the difference between the actual power that the turbine produces and the power it should produce according to a reference power curve at the wind speed as measured at the nearby met mast.

$$P_{residual} = P - P_{pc}(V_{met}) \quad (3-1)$$

Similar to a plot of the turbulence intensity, a plot of the power residual versus the wind direction can quickly show different wake situations and can also serve as a check on wind vane calibration.

When a wind turbine is in another turbines wake, it is operating at reduced wind speeds and hence produces less power than it would according to the power curve at the undisturbed

wind speed. If at the same time the met mast is in free stream conditions, the power residual will be negative. If on the other hand the met mast is in a wake and the turbine not, the turbine is producing more power than it would when the wind was blowing according to the wind speed measurement at the met mast, hence the power residual will be positive.

In figure 3-5 the power residuals of all measurement points for both Pr4 and Pr5 are plotted. From these two plots it can be concluded that Pr4 is in a wake when the wind is coming from roughly 85 degrees and 180 degrees and that the met mast is in the wake when the wind comes from roughly 125 degrees, which correspond with the angles found using the simple flow qualification tool.

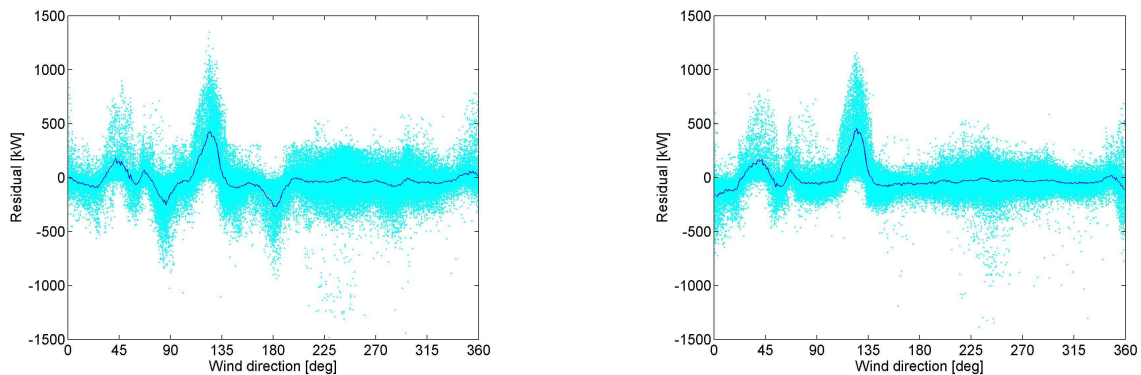


Figure 3-5: Power residual of Pr4 (left) and Pr5 (right)
Power Residuals of Pr4 (left) and Pr5 (right)

Normalized power

The normalized power of a turbine is the instantaneous power that turbine produces divided by the instantaneous power of a reference turbine. A nearby met mast is used to connect this value to the wind direction and wind speed. This tool is considered valid when the turbine and reference turbine are positioned not too far from each other and from the met mast.

The advantage of this tool is that variations in atmospheric conditions have no influence, since at both the turbine under investigation and the reference turbine these conditions can be assumed equal. The same holds for the free stream turbulence intensity.

As stated earlier two sectors have been designated for investigation, a reference sector where both turbines and the met mast are in undisturbed flow and a sector where Pr4 is in the wake of Pr5. The normalized power of Pr4 with respect to Pr5 is shown in figure 3-6.

As the wind direction is concerned the data is put in bins of 2 degrees. This ensures a good 'resolution' of the wake, while leaving enough data points per bin. The wind speed range used for these plots is between cut-in and cut-out wind speed.

Of course it would be interesting to look at these plots for different wind speed bins. The reason for taking the whole wind speed range is that this can be compared to the simulations in WindPRO. WindPRO was designed for calculation of AEP and had problems handling 'singular' wind speed distributions. When the normalized power is plotted for different wind

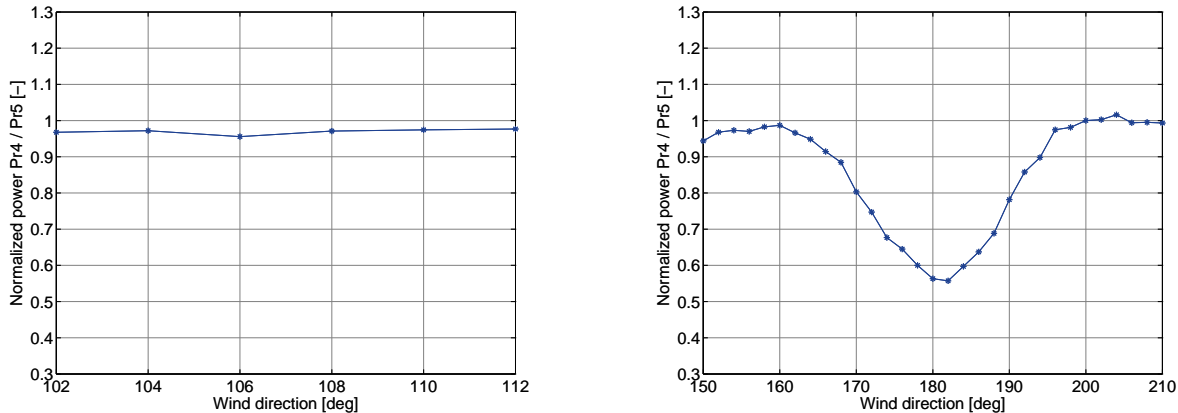


Figure 3-6: Normalized power of Pr4 in free stream (left) and in the wake of Pr5 (right)

speed bins, it can be seen that the power loss increases first with increasing wind speed until between 8 and 10 m/s and then decreases again. This is as expected and relates to the thrust coefficient.

3.1.4 Simulation with WindPRO

WindPRO was used to calculate the wake losses using the different wake models and turbulence models available. It is also capable of calculating the turbulence intensities at the turbine locations when the turbulence models are used. But since there is no measurement data available of the turbulence intensity at the turbines, these results were not evaluated.

The available wake models are the original Jensen model (no combination with turbulence model possible), the EMD modified version of the Jensen model that can be combined with turbulence models, an implementation of the Ainslie model and the model proposed by EWTS II, based on Larsen. As for the (wake added) turbulence models, the following are available: Danish Recommendations (1992), EWTS II (1999), Effective turbulence by Frandsen (1999), Empirical turbulence model by Quarton/Ainslie (1989) or TNO (1999) and finally the DIBt added turbulence model (2004). When the Ainslie model is chosen as wake model, there is an extra turbulence model available, from Lange (2002).

Using the same cleaned measurement data that was used to generate the plots in the previous section as input and selecting the Jensen model the normalized power of Pr4 for several values of the WDC is shown in figure ???. One can see that with a WDC of 0.075 the wake loss is underestimated. Instead of manually setting a value for the WDC one can let WindPRO calculate it from the meteo data as laid out in appendix H. As this value then changes from sector to sector, WindPRO names this setting Sector Wise Parameters (SWP).

Since the prediction of the velocity (deficit) with the Jensen model does not depend on the turbulence intensity, combining the Jensen (EMD) model with any wake added turbulence model does not yield different results as far as power is concerned. The results obtained using the original Jensen model and the Jensen (EMD) model were exactly the same, so in figure 3-7 only results for the original Jensen model are shown. The key parameter for the Jensen model is the WDC and as can be seen from the figure, the influence of this parameter

on the results is quite large. For onshore use the value of the WDC is suggested to be 0.075 which is at the moment the standard setting within GE. Note that the measurements and the results from the simulations are not aligned with each other. A misalignment of the wind vane could be a cause of this and since this misalignment also occurs using the other models this is very likely to be the case.

When the Ainslie model is used, the normalized power of Pr4 does depend on the chosen turbulence model, however the influence is not very big, see figure 3-7.

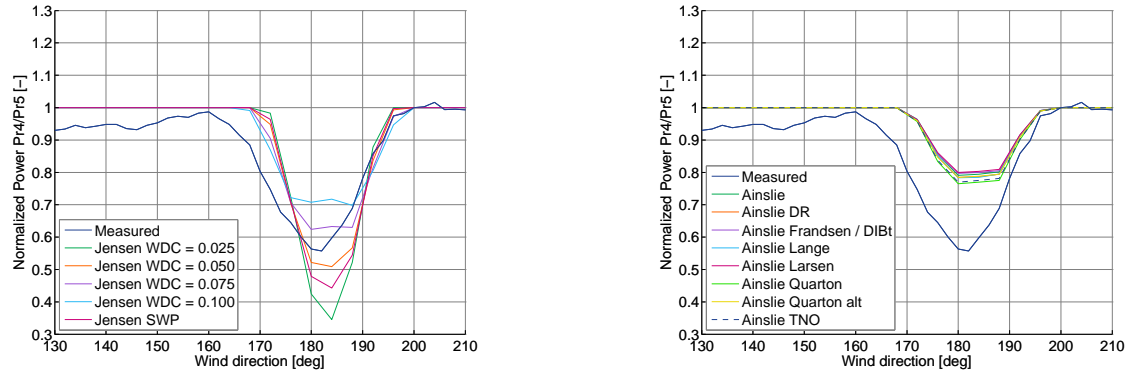


Figure 3-7: Normalized power of Pr4 simulated with the Jensen model (left) and the Ainslie model (right)

The results obtained with the Larsen model are shown in figure 3-8. As can be seen the wake is predicted very badly: it is much too wide and the power loss (velocity deficit) is much too low. During communication with EMD at a later stage of the thesis work I became aware of an error in the documentation describing the model and considering the good performance of the Larsen model when I programmed it, it may be that the implementation of the model by EMD is erroneous as well. What also is striking is that the application of a turbulence model does not influence the results. The simulations with the Ainslie and Larsen models have been

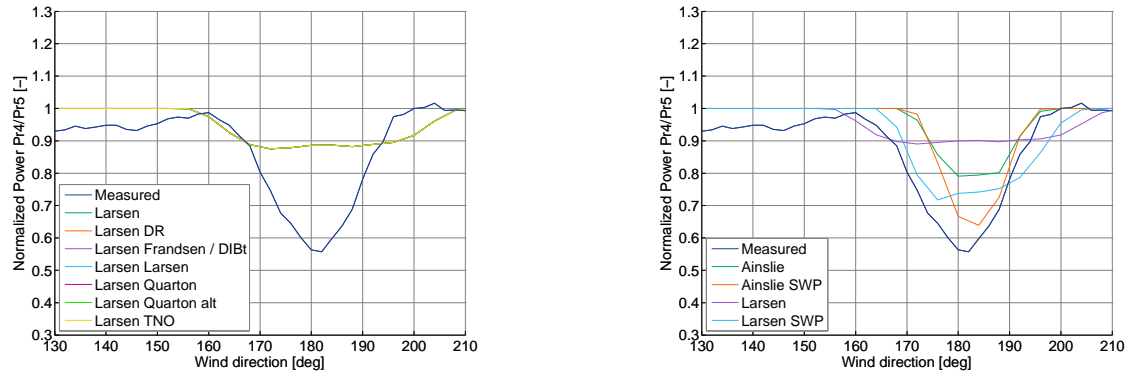


Figure 3-8: Normalized power of Pr4 simulated with the Larsen model (left) and the influence of the ambient turbulence on the Ainslie and Larsen model (right)

performed using the standard setting for the ambient turbulence intensity in WindPRO, which is $I_a = 0.147$. This corresponds to a terrain classification of ‘open farmland’, see appendix H.

However, from figure 3-4 it can be seen that the ambient turbulence intensity is lower than this, around 10%. On the right side of figure 3-8 the normalized power of Pr4 is plotted for both the Ainslie and Larsen model with no added turbulence model. It can be seen that the influence of the ambient turbulence intensity on the prediction of the normalized power using the Ainslie or Larsen model is of the same order of magnitude as the influence of the WDC on the prediction using the Jensen model. Although using the measured turbulence intensity as input for the Ainslie and Larsen model leads to better results, the Larsen model is still off and the Ainslie model still underpredicts the power loss.

3.2 Colorado Green wind farm

With the Prettin wind farm there it was only possible to investigate a single wake case. To investigate the performance of the models for multiple wake situations the Colorado Green wind farm was used.

3.2.1 Location and layout

The Colorado Green wind farm is located near the town of Lamar in Prowers County in the southeastern part of Colorado. With 108 GE 1.5s wind turbines it is one of the largest wind farms in the United States. The wind farm was built in 2003 and is owned by PPM Energy Inc. and Shell WindEnergy Inc. in a 50/50 joint venture. The layout of the wind farm is given in figure 3-9. The center of the wind farm is approximately at the coordinates $37^{\circ}42'00''$ N $102^{\circ}38'00''$ W. The wind farm is located in flat terrain, as can be seen from figure 3-10. Only

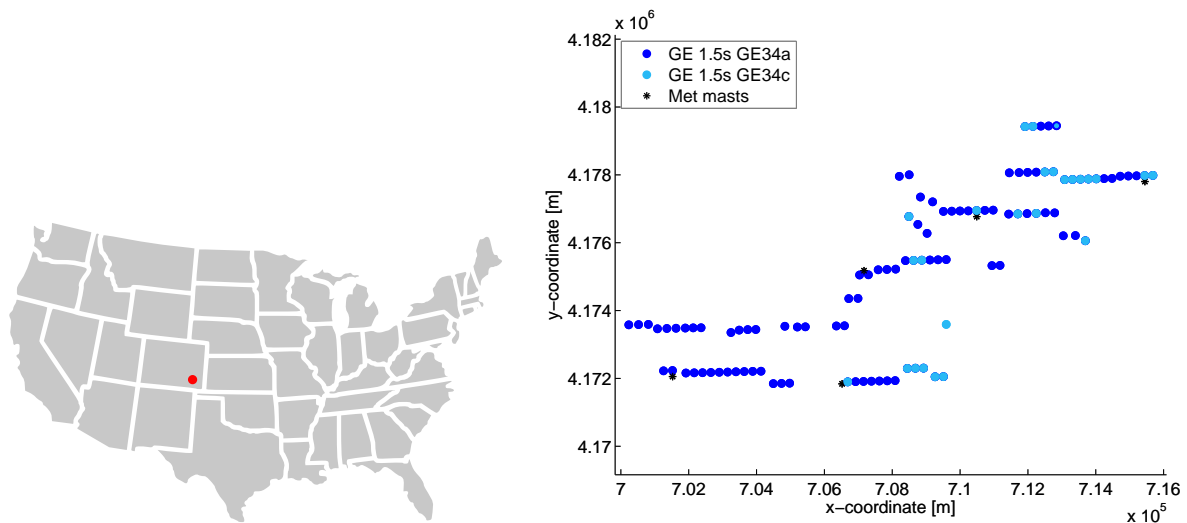


Figure 3-9: Colorado Green wind farm location and layout

low vegetation covers the desert-like surface.

There are 5 met mast located at the wind farm. It was investigated if data from all met masts could be used simultaneously to reproduce a single set of undisturbed wind data. Although this was possible, combining the data of several met masts in WindPRO would limit the



Figure 3-10: Terrain at the Colorado Green wind farm

number of available sectors to 36. Instead I focussed on parts of the wind farm consisting of a single met mast and multiple turbines. Similar as has been done at Prettin only a specific sector of wind directions would be considered. For the wake analysis two parts of the wind farm were selected: an array from the northeast corner of the wind and an array from southwest corner, both located close to a met mast. The two parts are shown in figure 3-11. The first part contains turbines 14 to 25 (shown right) and the second part turbines 85 to 96 (the left plot). In the right subplot several of the nearest turbines are plotted as well. The spacing within the row consisting of turbines 14 to 25 is about 3.5 rotor diameters. Turbines 13 and 31 are located 5.8 and 14.5 rotor diameters away from turbine 14 respectively, the others more than 22 rotor diameters. Since only specific sectors are considered for the analysis, these turbines will be neglected in the simulations.

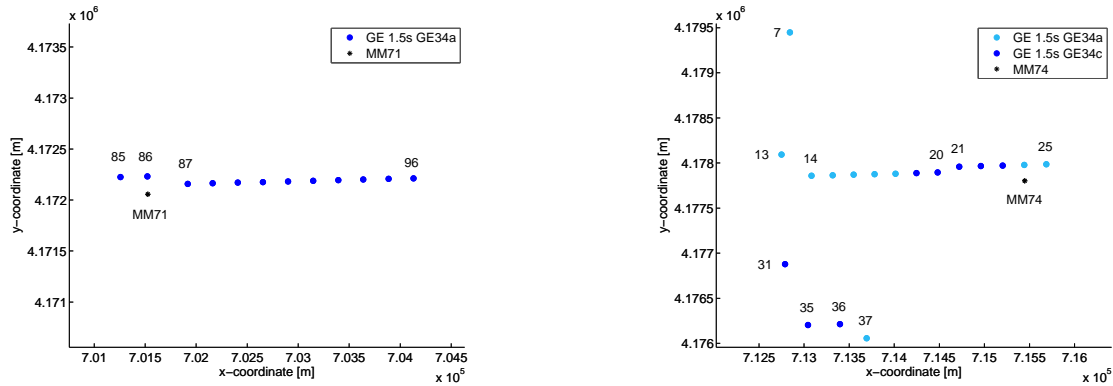


Figure 3-11: Parts of the Colorado Green wind farm used for analysis

3.2.2 Measurement data

Measurement data was available from April 2004 until July 2006. A two year subset was extracted that providing the best data fill. Subsequently the data was cleaned to make sure all turbines in the part under investigation were operating and functioning normally and that readings from the sensors were not abnormal.

Met mast	V_{mean} [m/s]	TI_{15} [%]	TI_{mean} [%]
70	8.3	11.7	18.1
71	8.1	11.7	19.2
72	8.0	11.8	20.0
73	7.8	12.4	20.0
74	8.0	11.5	20.0

Table 3-1: Wind statistics at the met masts

Turbulence intensity

Plotting the turbulence intensity measured at met mast 74 versus the wind speed and versus the wind direction (wind speeds between 5 and 25 m/s) results in figure 3-12. The turbulence intensity is relatively constant for all wind directions and no real wake situations can be derived from these plots.

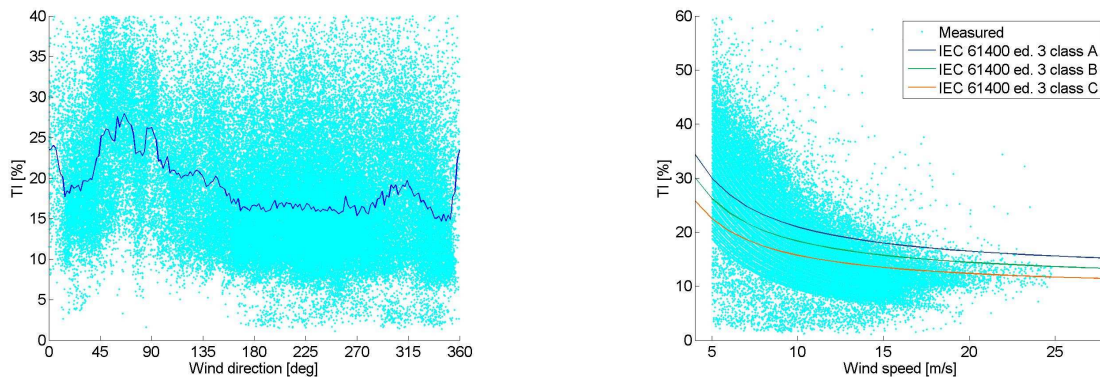


Figure 3-12: Turbulence intensity at met mast 74 versus wind direction (left) and wind speed (right)

For wind speeds lower than 10 m/s the turbulence intensity is quite high, as can be seen on the right side of the figure. The mean turbulence intensity and the turbulence intensity at a wind speed of 15 [m/s] at all met masts is given in table 3-1.

Power residual

To find the wind directions for wake investigation again the power residuals were investigated; it was known that the wind direction data that was available originated from a non-calibrated wind vane. A quick look at the right part of figure 3-11 shows that turbine 24 will be in the wake of turbine 25 when the wind is coming from the east and that both turbines will be in the wake when the wind is blowing from the west. Plotting now the residual power for both turbine 24 and 25 results in figure 3-13.

The plots of the power residual of turbine 24 and turbine 25 show a lot of resemblance, but there is one difference (indicated in the plots by the red arrow). At about 230 degrees the power residual of turbine 24 shows a clear dip, whilst that of turbine 25 doesn't. This indicates that turbine 24 is in the wake of turbine 25 (expected at about 90 degrees) and that

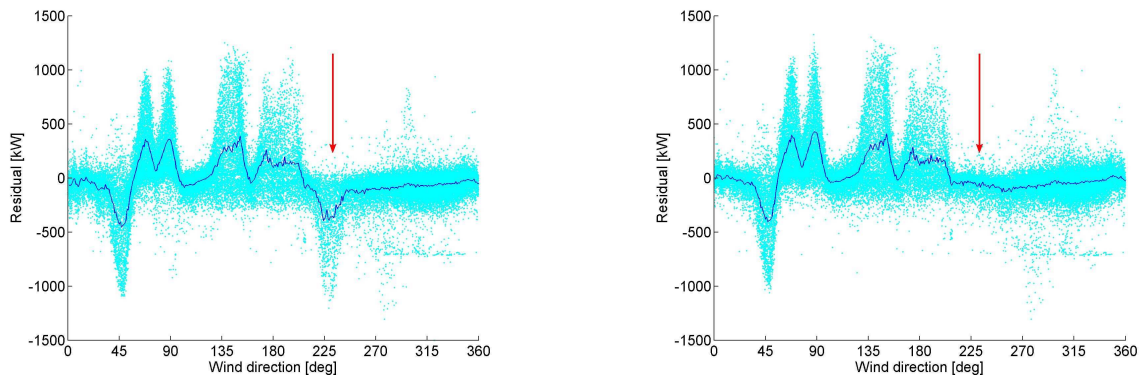


Figure 3-13: Power residual of turbine 24 (left) and 25 (right)

the wind vane is way off. At the opposite direction, at about 50 degrees in the plot, both turbines show a wake situation, which is expected when the wind is coming from the west. This indicates that the wind direction in the SCADA data is 140 degrees off. The peaks in the plot indicate when the met mast is in the wake and also match the expected values when this offset is taken into account.

Normalized power

Using this correction the normalized power of turbine 14 to 25 with respect to turbine 25 versus the wind direction is plotted left in figure 3-14 (doing the same for the second part of the wind farm results in the plot on the right).

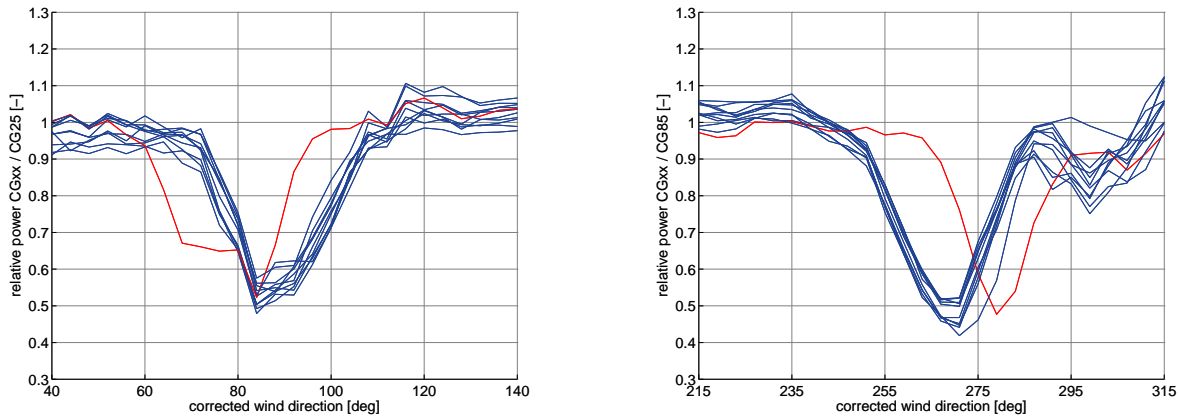


Figure 3-14: Normalized power of turbines 14 to 24 in wake (left) and turbines 85 to 95 (right)

All turbines perform similar, there is no trend in the order of the lines: the biggest losses are not from the turbines experiencing the highest number of multiple wakes. The red line shows the normalized power of turbine 20. Turbines 14 to 25 are actually standing in two rows, one being turbine 14 to 20, the other 21 to 25. Both these rows have the same direction with respect to the North: 89°. The direction from turbine 20 to 21 differs with 15 degrees from this main direction, the same shift seen in the plot between the normalized power of

turbine 20 and that of the other turbines. The wake that turbine 20 is experiencing is just as wide as that of the other turbines, only shifted. So it seems that the wake from the first upstream turbine dictates the power loss. The same holds for turbines 85 to 95, the jump being between turbines 86 and 87. What is striking is the dip on in relative power at around

From the left of figure 3-14 it can be observed that for corrected wind directions greater than 110 degrees (on the ‘right’ side of the wake) turbines 14 to 24 perform better with respect to turbine 25 than for corrected wind directions lower than 70°(‘left’ of the wake). The reason for this is unknown. One could make a similar observation for turbines 86 to 96 with respect to turbine 85, see the right of figure 3-14. But here the turbines 86 to 96 perform better than turbine 85 for wind directions than 240°. Unfortunately the dip in normalized power at around 300°makes prohibits one to compare the normalized power on the ‘left side’ of the wake with the that on the ‘right side’ of the wake for these turbines. May be this effect can be contributed to the rotational direction of the rotor.

3.2.3 Simulation with WindPRO

Since this site is located in the USA, digital elevation data with sufficient accuracy is freely available from the website of NASA. Using various software tools, both an elevation model and a roughness map can be created which can be used in WAsP and WindPRO. Using this model and the data from multiple met masts a single wind regime for the whole wind farm can be calculated. However, this results in a reduction of the maximum number of sectors to 36, too few in my opinion for detailed wake analysis. So it was chosen not to use this possibility and instead use data of just one met mast for this analysis. The wind resource map calculated using WAsP was reasonably constant over the site, which is very flat, so in this case I believe it is justified.

Because of the fact that the measurements show very similar results for the two parts of the Colorado Green wind farm, only one of these two has been simulated. The normalized power outside the wake sector of the turbines 14 to 24 is more clean than that of turbines 86 to 96, hence the part including turbine 14 to 24 is modeled.

This section will show the power of the three turbines 24, 19 and 14 which are the first wake effected turbine, a turbine halfway row 14 to 25 and the last wake effected turbine when the wind is blowing from the east (90 degrees). The power is normalized with respect to turbine 25, which encounters undisturbed flow in this situation. A comparison between the measured data and the simulation is made.

Jensen models

The impact of the Wake Decay Constant (WDC) is clearly visible from the plots. Note that for a single wake case (turbine 24) there is no difference between the original Jensen model and the one modified by EMD, referred to in the figure as Jensen (EMD), see figure 3-15. This was observed as well when simulating the Prettin wind farm. However, there is a difference for multiple wake situations. While with the original Jensen model the addition of wakes results in increasing power losses, the power loss remains relatively constant with the Jensen (EMD) model, which corresponds with the measurements.

Using the Jensen (EMD) model with wake decay constant and turbulence intensity calculated from the meteo data leads to the best results overall (in the plots referred to as SWP, for sector wise parameters). Using this setting the WDC varies from sector to sector between 0.074 and 0.117. For details about the procedure to obtain the sector wise parameters, see appendix H.

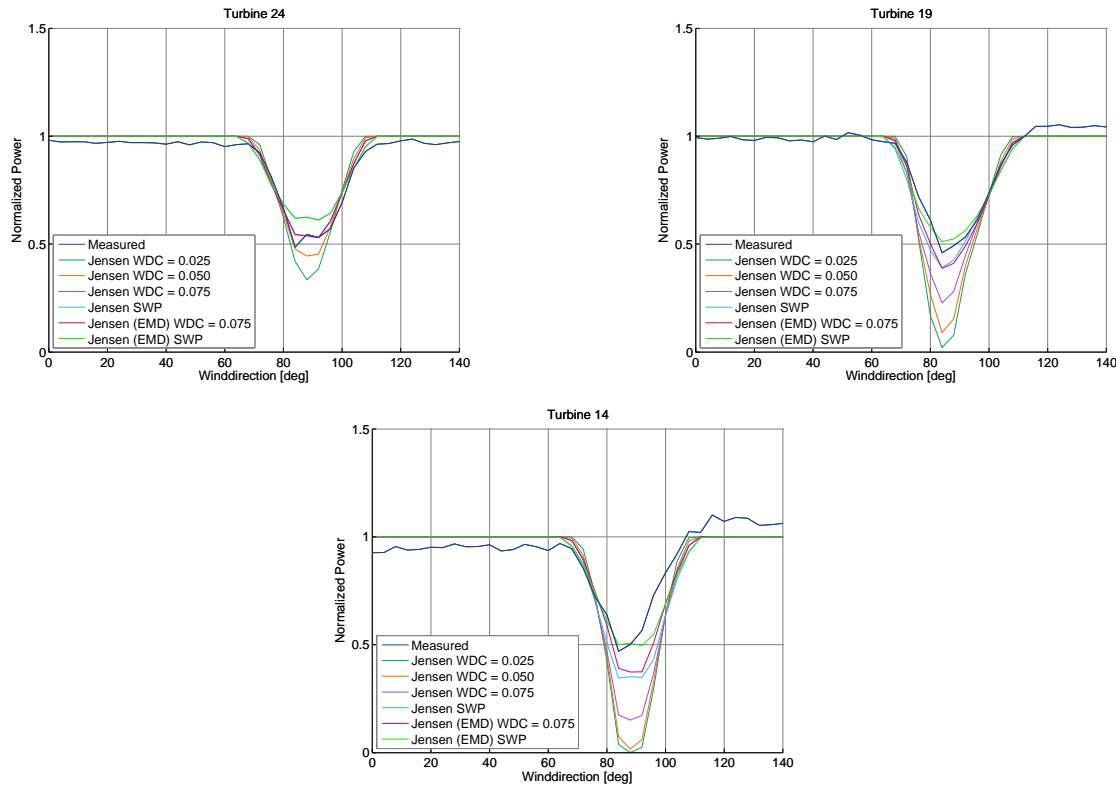


Figure 3-15: Normalized power of CG24, CG19 and CG14 using the Jensen model

Like with the Prettin wind farm no influence of the turbulence models on the power calculation with the Jensen models was found. This makes sense, as the Jensen model is not dependent of turbulence. Hence, changing the turbulence intensity only does not yield different results as far as energy production is concerned.

Ainslie model

The results of the calculations with the Ainslie model are shown in figure ???. As turbulence intensity is an input parameter for the calculation of the velocity deficit, an influence of both the value of the ambient turbulence intensity and the turbulence model is expected.

For the following plots using the Ainslie model the setting of the turbulence intensity was taken from the measurement data (SWP). As the different turbulence models result in a different wake added turbulence, the effect of the turbulence models becomes more clear after multiple turbine passings. The turbulence model of Lange, which only is available in combination with the Ainslie model, shows a slightly different behavior from the other models. For the

first wake effected turbine, turbine 24, no difference between the turbulence models can be distinguished, which was also the case with the Prettin wind farm.

Each calculation took between 2 and a half and 3 hours, as opposed to less than one minute with the Jensen (EMD) model (and in the order of seconds for the original Jensen model).

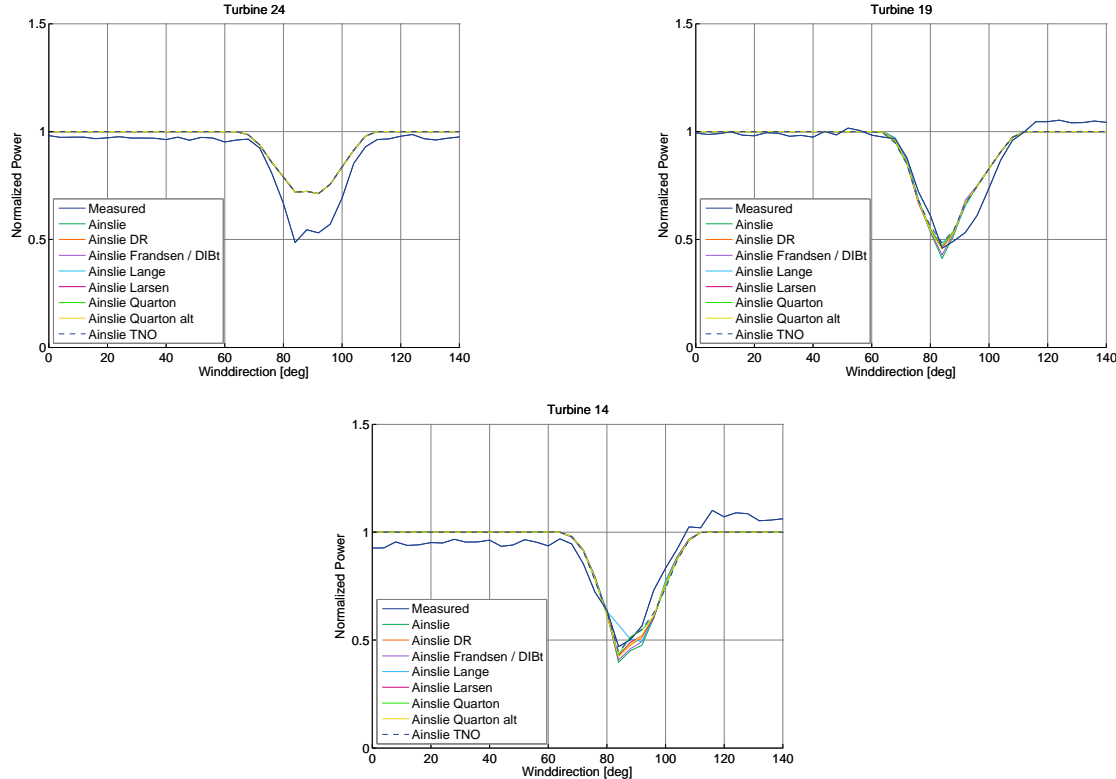
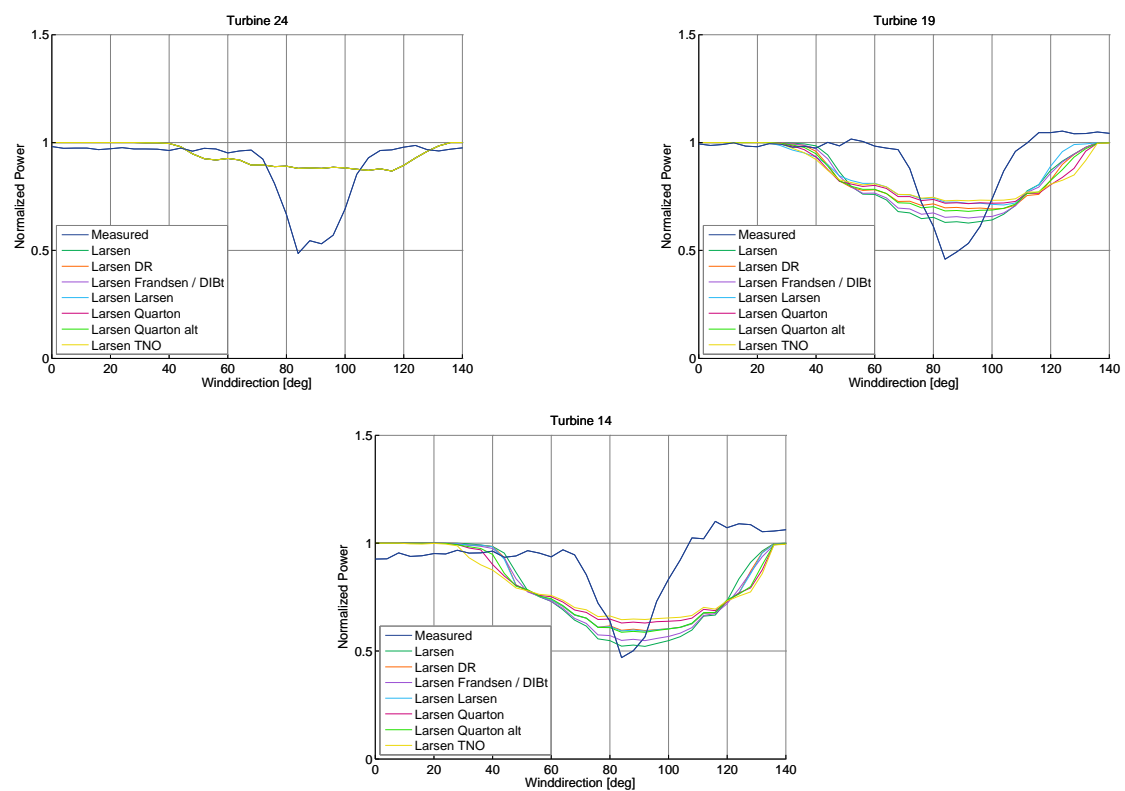


Figure 3-16: Normalized power of CG24, CG19 and CG14 using the Ainslie model

Larsen model

Using the Larsen model similar results to that obtained with Prettin are found. For the single wake (turbine 24) the wake is far too wide. The different turbulence models produce the same result as power is concerned, see figure 3.2.3. For multiple wakes the power loss increases, while the different turbulence models show different results. Still the wake is much too wide. The second order version of this model did not produce different results compared to the first order one and is not shown here.



captionNormalized power of CG24, CG19 and CG14 using the Larsen model

Analysis of the results

For a further analysis of the results I have looked at several wake characteristics in the previous plots:

- The width of the wake
- The maximum power loss in the wake
- The energy loss in the wake

For an explanation of these characteristics, see figure 3-17.

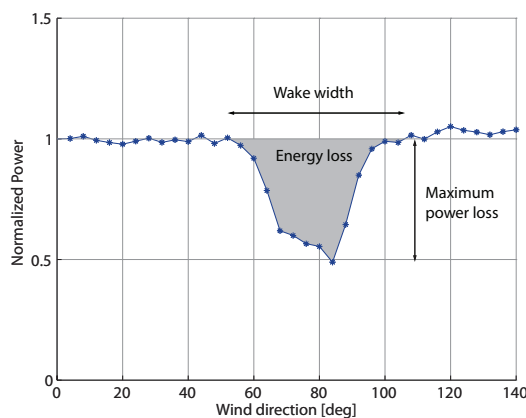


Figure 3-17: Explanation of the wake characteristics

The energy loss mentioned here is not real energy loss, but a synthetic non-dimensional value. It is calculated as 100 times the area between the normalized power and the line having a normalized power value of 1. This means that the wind rose is not taken into account. The resulting value would be a real energy loss, if the wind rose was uniform. According to the used procedure the normalized energy value a turbine would produce without wake effects equals $100 * 360 * 1 = 36,000$.

In the simulations the normalized power is perfectly equal to 1 outside the wake and the width of the wake and the energy loss are easily determined. However, when looking at the measurement data, there is a certain variation in the normalized power. The main reason for this is that the rotor inflow is not exactly the same at every turbine. This makes it hard to obtain these characteristics from the measurement data. For example, looking at turbine 14 (figures 3-15, 3-16 and 3.2.3) on the ‘left side’ of the wake the normalized power never reaches the value of 1. On the other hand, on the ‘right side’ of the wake the value of the normalized power seems a little higher than 1 suggesting an intersection with the normalized power equal to 1 doesn’t capture the boundary of the wake on that side. Especially the width of the wake is very sensitive to at which level of the normalized power the intersecting line is drawn. Combined with the fact that the width of the wake is not as important as the energy loss, I chose not to compare the simulated wake widths with the measured ones.

For the energy loss, the intersecting line was taken to be the normalized power equal to 1 where possible. When this was not possible a lower value was taken and the result was multiplied by a correction factor. This multiplication factor was obtained using the other turbines where the line could be taken at normalized power equal to 1. Because of this extrapolating procedure the turbines at which this procedure has been used are identified in the plots.

The maximum power loss in the wake for the Jensen models are shown on the left of figure 3-18. This plot shows again that the power loss keeps increasing with the increasing number of multiple wakes using the original Jensen model, but flattens when the Jensen (EMD) model is used. This is due to the difference the method of combining wakes. Also the ‘jump’ from turbine 21 to turbine 20 is clearly visible in the simulations, though in the measurements this is not so clear. With most parameter settings the maximum power loss in the wake is overestimated quite a lot. Using the standard setting at GE, the original Jensen model with a WDC of 0.075, the maximum power loss at turbine 14 would be almost 85%, while measurements indicate a value of just over 50 %. The only parameter setting not leading to an overestimation of the power loss is the Jensen (EMD) model, when the WDC is calculated from the measured turbulence intensity.

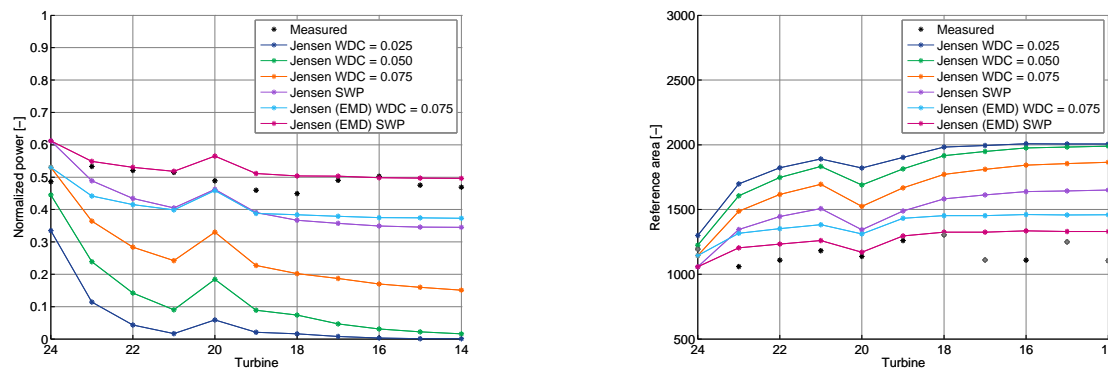


Figure 3-18: Maximum power loss (left) and energy loss (right) in the wake using the Jensen models

On the right of figure 3-18 the synthetic energy loss is plotted. Note that several measurement points are grey. These points belong to the turbines where a correction had to be made. Again the Jensen (EMD) model with SWP is the best combination. Neglecting turbines 14 to 17 (at three of which the measured energy loss had been extrapolated) the energy loss is predicted with this model remained within 10% of the measured value, while the other models would be up to 50% off.

The Ainslie model shows quite good correspondence with the measurements, see figure 3-19. Only at turbines 24 and 23 the maximum power loss is underestimated. Using the Ainslie model in combination with the turbulence model by Lange leads to the best results. Note that for the plot of the energy loss a different scale is used on the y-axis because the results are much more close to each other. Except for turbines 14, 16 and 17 the energy loss is slightly underpredicted for all combinations of Ainslie and a turbulence model.

Figure 3-20 clearly shows the poor performance of the Larsen model compared to the Jensen and Ainslie model with large deviations from the measurements, both in maximum power loss

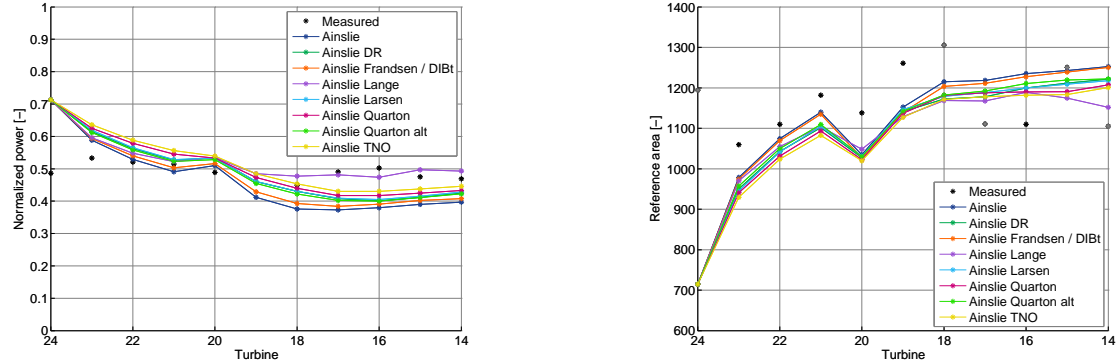


Figure 3-19: Maximum power loss (left) and energy loss (right) in the wake using the Ainslie model

as in energy loss. It is also clear from these plots that multiple wakes have a strong effect and that the Larsen model is more sensitive to the turbulence model than the Ainslie model.

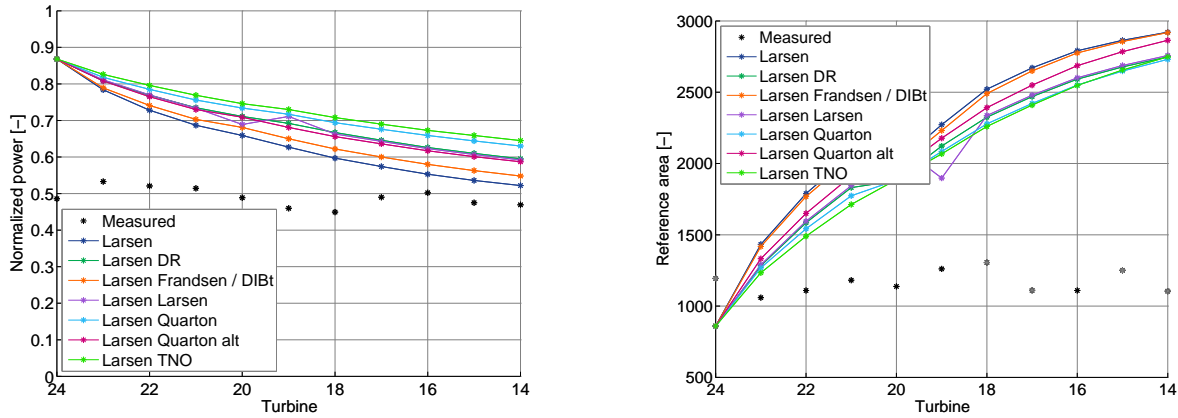


Figure 3-20: Maximum power loss (left) and energy loss (right) in the wake Larsen model

Chapter 4

Wind tunnel measurements and validation

Though in the previous chapter the influence of the turbulence models on the prediction of the power could be shown, the performance of the turbulence models itself could not be validated, because of the availability of one met mast only at the wind farms. Besides that, the prediction of the velocity deficit in the wake could be evaluated at a single distance behind the turbine only in an indirect manner by comparing the normalized power. Using the nacelle anemometer for the evalution of the turbulence is very unlikely to produce reliable results. One way to get the measurements at various locations in the wake is by using wind tunnel measurements, though this leads to other problems such as the influence of the wind tunnel and scaling effects, see table 4-1. The scaled wind farm mentioned in the table has yet to be built by ECN (according to the present planning it will be operational after summer 2007), therefor it cannot be taken into account. To gain insight in the capabilities of wake models in predicting both velocity deficit and turbulence throughout the wake (meaning at varying distances behind a turbine), I had to resort to wind tunnel measurements. During the years 2003 and 2004 ECN has performed several wind tunnel test campaigns of which data have been made available for this study.

	Wind tunnel	Full scale	Scaled farm
Scaling effects	--	++	+
Wall influence	+/-	++	++
Representative external	+/-	++	+/-
Stochastic nature of external	++	--	-
Meteo measurements	++	--	+
Turbine measurements	+	--	++
Turbine operation	++	+/-	++
Farm layout	++	--	+

Table 4-1: Advantages and disadvantages of wind tunnel measurements, full scale measurements and measurements using a scaled wind farm, obtained from [31]

4.1 TNO wind tunnel

The experiments were performed in the atmospheric boundary layer wind tunnel of TNO in Apeldoorn. The wind tunnel is an open Eiffel type wind tunnel, see figure 4-1. The test

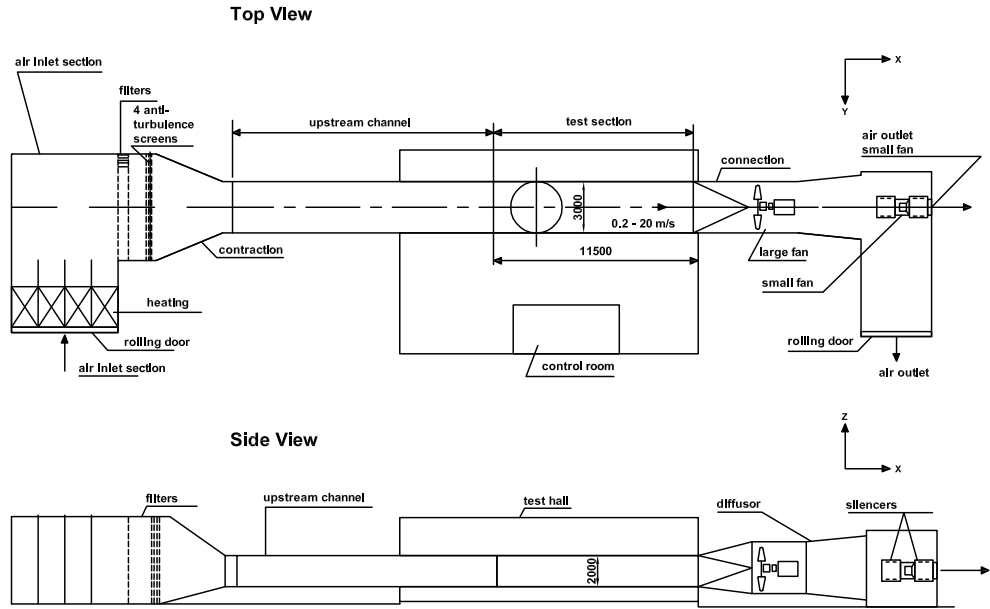


Figure 4-1: Schematics of the atmospheric boundary layer wind tunnel of TNO

section has a cross section of 2 by 3 m and a length of 11.5 m. However, this length can be extended to 20 m when necessary. By applying different roughness elements in the channel upstream of the test section, 6 different atmospheric boundary layer types can be simulated, including an offshore boundary layer. This latter type was used mostly and figure 4-2 shows vertical profiles of the wind speed for various location in an empty tunnel using a tunnel wind speed of 8.27 m/s (which is close to the tunnel wind speed used during later measurements). Note that the profiles for $x > 0$ are offset by 1 m/s with respect to the preceding profile. For a fit to the logarithmic profile representative for neutral boundary layer flows

$$u(z) = \frac{u_*}{\kappa} \ln \left(\frac{z}{z_0} \right) \quad (4-1)$$

values of the friction velocity u_* and roughness length z_0 of 0.24 ± 0.006 m/s and $(1.9 \pm 0.7) \cdot 10^{-4}$ mm were found, see Blaas et al. [32]. Ambient turbulence intensity for the offshore profile was 8%.

4.2 Wind turbine models

The turbine models used during the wind tunnel test are variable speed turbines supposed to represent current commercial wind turbines having a rotor diameter of 100 m. As the scale

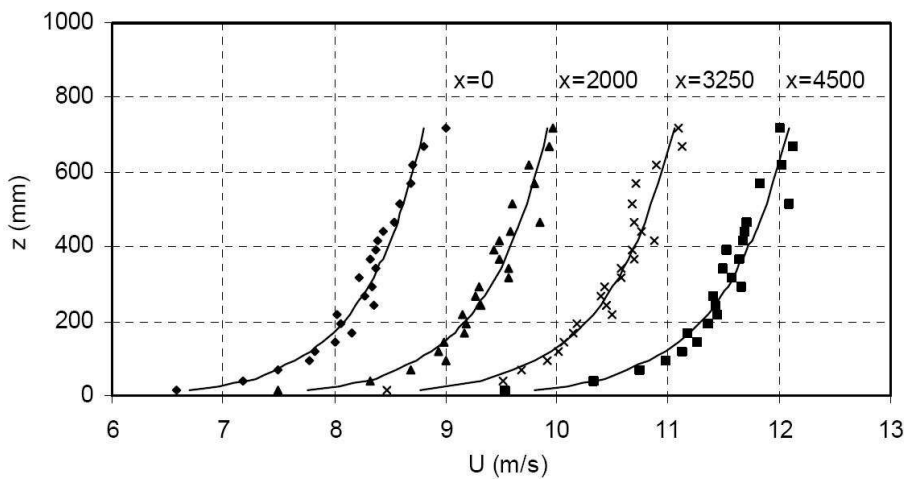


Figure 4-2: Wind profile in the TNO tunnel for

of the boundary layer that builds up in the channel upstream of the test section is 1:400, the rotor diameter of the wind turbine models is 25 cm, which is equal to the hub height. The main concern when performing the wind tunnel tests is that the flow in the wind turbine wakes should behave similar to the flow in the wake of a full scale wind turbine. In order to do so, the wind turbine models are not simply geometrically scaled models of existing wind turbines: the model turbines have 2-bladed rotors with a relatively large chord, in order to ensure that the chord based Reynolds number is higher than 25,000. The rotor blades use the NACA 0009 airfoil which has a relatively low Reynolds dependency (near the root NACA 0012 is used). This ensures that the thrust and wake properties are as close as possible to that of full scale wind turbines. The wind turbine model used in the wind tunnel tests is shown in figure 4-3.

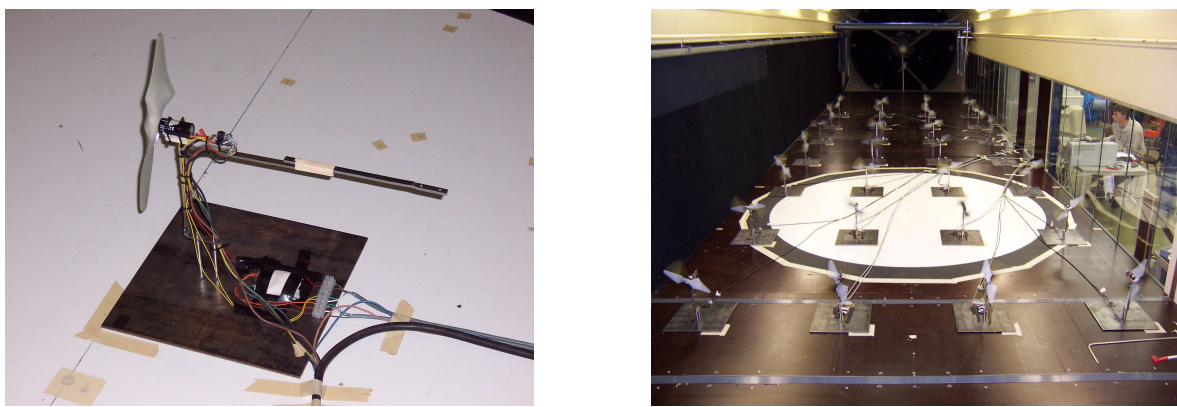


Figure 4-3: Wind turbine model zoomed (left) and in a wind farm set up (right). Courtesy of ECN.

Five different rotors can be mounted on the turbines, each rotor having a fixed but different pitch angle. The thrust curves for the different pitch angles are given in figure 4-4, together with a comparison of the the thrust curve of the model at zero degree pitch (the rotor that was used most) with the curves of the turbines of the GE 1.5 series.

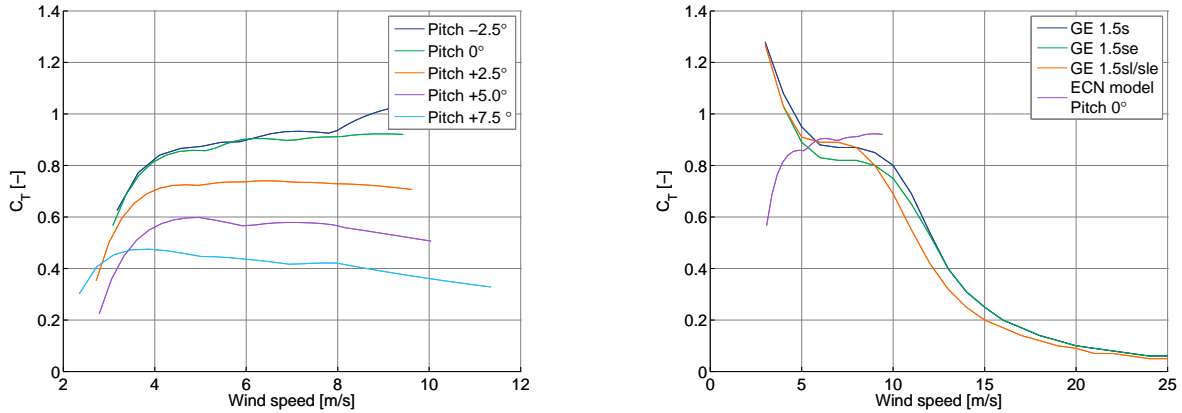


Figure 4-4: Thrust curves of ECN's wind turbine models and the GE 1.5 series of turbines

In the wind speed range of 6 to 9 m/s the thrust curve of the ECN model is very similar to that of the GE 1.5 turbines, the wind turbines that the wind farms considered in chapters ?? and ?? consist of. This wind speed range is exactly the wind speed range used during the wind tunnel tests.

4.3 Measurement campaigns

Three measurement campaigns were performed, the first one in March 2003, the second one in November 2003 and the last one in October 2004. The experiments used during this thesis work were done during the second and third series. Some results of the measurement campaigns have already been published, see [33] and [34].

The goal of the measurements was to investigate wind turbine interaction in large offshore wind farms and to validate ECN's wake reducing concepts 'Heat and Flux' and 'Controlling Wind'. These wake reducing concepts will not be discussed in this thesis, more information about 'Heat and Flux' can be found in [35].

4.4 Measuring system

The wind speed throughout the wind tunnel was measured by a hot-wire traversing probe which measured at a frequency of 200 Hz. At each measurement point 2 measurements of 10.24 seconds each were taken, from which the average wind speed and turbulence was determined. The readings from this probe were corrected with data obtained from a Schiltknecht propeller anemometer placed at the beginning of the test section. See figure 4-5 for an impression of the measurement devices. The turbines were instrumented as well, and of each turbine the generator voltage was measured. From this voltage several physical quantities could be derived, one of those being the wind speed at the rotor, using predefined calibration curves.

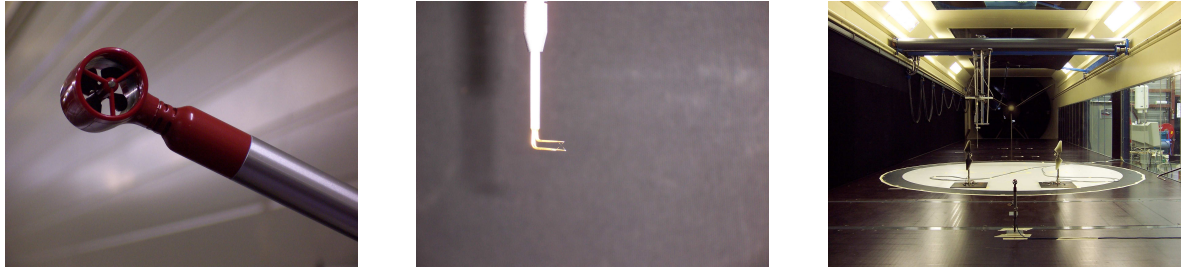


Figure 4-5: Schiltknecht propeller anemometer (left), hot-wire probe (middle) and both together with two model turbines (right). Courtesy of ECN.

4.5 Wake measurements behind a single turbine

Both horizontal and vertical velocity and turbulence intensity profiles have been measured at several stations behind a single turbine. The plots of the horizontal profiles for a pitch setting of 0° and 5° are shown in figure 4-6 and 4-7. Note that at some distances the measurements were only taken for negative values of y up to $y = 0$. The offsets used in these plots are given in table 4-2.

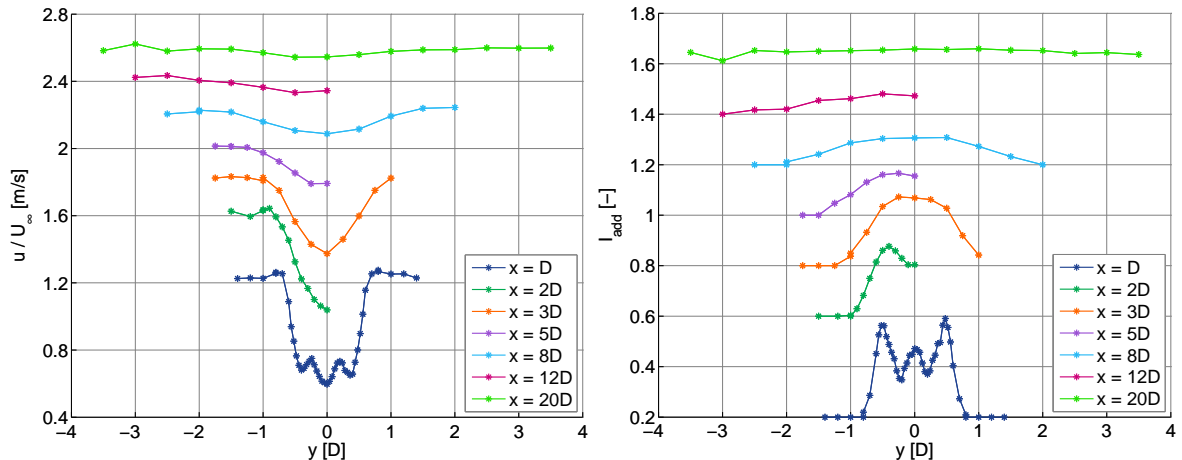


Figure 4-6: Normalized velocity(left) and generated turbulence (right) in the wake behind a single turbine with a pitch setting of 0° , $C_T = 0.91$

Downstream position	Offset
$x = D$	0.2
$x = 2D$	0.6
$x = 3D$	0.8
$x = 5D$	1.0
$x = 8D$	1.2
$x = 12D$	1.4
$x = 20D$	1.6

Table 4-2: Used offset in (single) wake plots

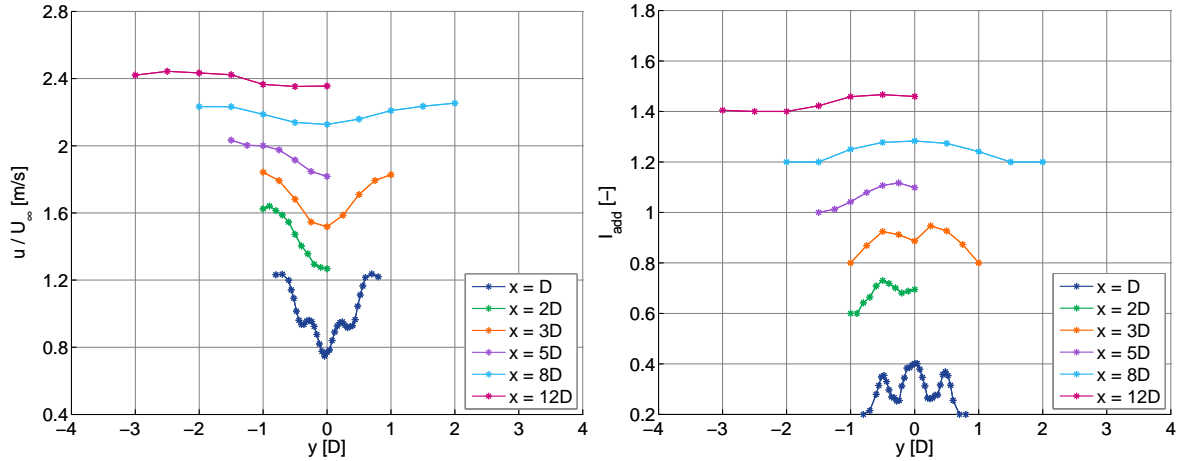


Figure 4-7: Normalized velocity(left) and generated turbulence (right) in the wake behind a single turbine with a pitch setting of 5° , $C_T = 0.56$

Measurements using a rotor with a 2.5° pitch setting were also performed, however the resolution of these measurements was much lower, so this data will not be used. Both figures 4-6 and 4-7 show that at short distances downstream the velocity deficit and turbulence show local maxima at the blade tips and the hub region, the latter being especially visible at the a pitch setting which results in a lower thrust coefficient. The velocity deficit has already taken a Gaussian-like shape after $2D$, it takes a little longer for the turbulence intensity. Because of the scale of the figures on might think that the added turbulence intensity for distances of $8D$ and beyond is equal for the two C_T -settings, however in the center of the wake (e.g. $y = 0$) the added turbulence for a C_T of 0.56 is with a value of 0.083 more than 0.02 lower than for a C_T of 0.91.

4.6 Validation of the kinematic wake models

The measurements performed in the wind tunnel provide the opportunity to validate the kinematic wake models discussed in ??, namely the models by Jensen, Larsen and Frandsen. The comparison of the wake velocity relative to the undisturbed wind speed calculated using the kinematic wake models with the measurements is shown for the two rotor pitch settings at a downstream distance of $3D$ in figure 4-8. For the figures at all downstream distances, see appendix I.

From this appendix it can be observed that the Larsen model actually performs quite well¹: ignoring the double-dip shape and the influence of the hub at $1D$, the depth of the wake is estimated reasonably well (it is underestimated at $2D$ and $3D$ and overestimated slightly from $5D$ or $8D$, depending on the pitch setting. The width of the wake however is estimated very well. For wind farm modeling the accuracy of the velocity and turbulence at $1D$ downstream of a turbine is of less importance, as the blades of neighboring turbines could hit each at a

¹These observations do not match the ones found after the simulations with WindPRO. The fact that I had a discussion with the programmer of EMD about the equations of the Larsen model as stated in their manual, makes me question EMD's implementation of the Larsen model.

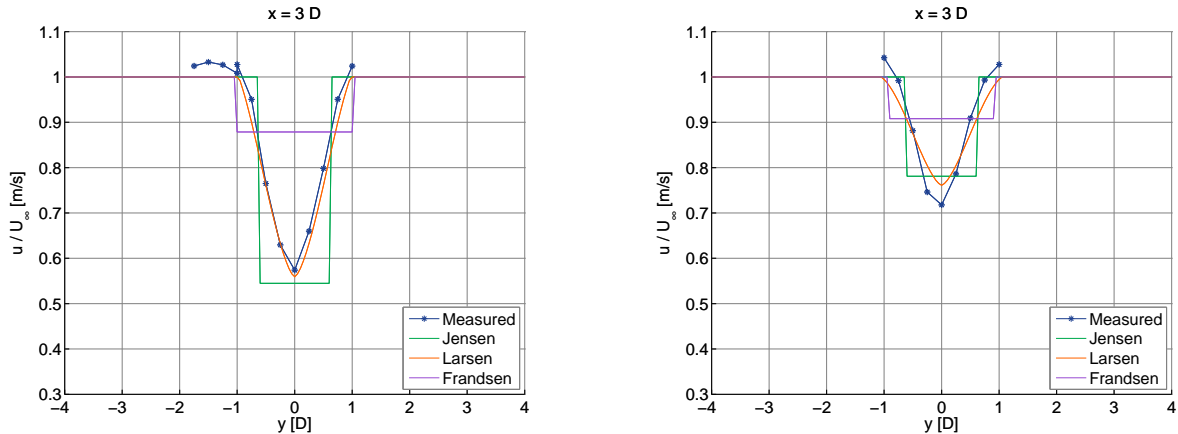


Figure 4-8: Wake velocities at $3D$ behind the rotor, with $C_T = 0.91$ (left) and $C_T = 0.56$ (right)

spacing of $1D$. Usually the smallest spacing for a wind farm is closer to $2D$ than to $1D$, although a wind farm has been built by GE with a spacing of $1.3D$ perpendicular to the dominating wind direction.

4.7 Validation of the turbulence models

Using the turbulence models available in WindPRO and the same flow characteristics as were present with the wind tunnel tests yielded the values shown in table 4-3.

Turbulence model	Downstream position						
	1D	2D	3D	5D	8D	12D	20D
DR	0.15	0.15	0.15	0.15	0.114	0.09	0.09
Frandsen	0.2016	0.188	0.1714	0.1468	0.1267	0.1154	0.1121
Larsen	0.2426	0.1926	0.1682	0.1419	0.1213	0.106	0.0894
Quarton	0.3325	0.224	0.1777	0.1328	0.1016	0.0807	0.0603
Quarton alt.	0.5901	0.3033	0.2055	0.1259	0.0802	0.0543	0.0333
TNO	0.592	0.3043	0.2062	0.1263	0.0804	0.0545	0.0334

Table 4-3: Generated turbulence using several turbulence models

A plot of these values is shown in figure 4-9.

As can be seen, the Frandsen / DIBt model, Larsen model and Danish Recommendation model yield high values for the generated turbulence for downstream distances larger than $5D$. As they are design codes this is expected. The line corresponding to the alternative Quarton model cannot be seen, as the values are almost identical to the values of the TNO model; both yield very high values for the generated turbulence for distances smaller than $3D$. All these models for the added turbulence have in common that they result in a constant turbulence intensity throughout the wake at a certain distance downstream of the turbine, similar to the Jensen model does for the velocity deficit. However, in reality most turbulence is generated near the hub region and at the blade tips. At a certain distance downstream

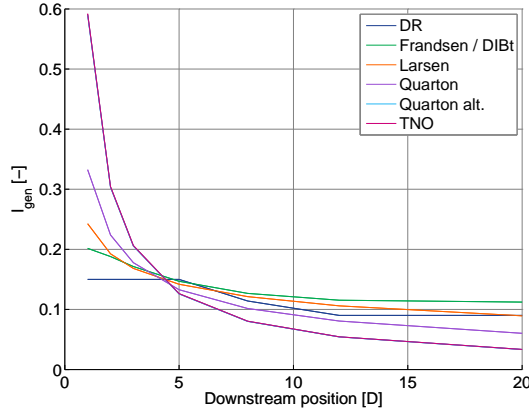


Figure 4-9: Development of the generated turbulence downstream a single turbine for different turbulence models

a Gaussian-like profile remains due to diffusion. The ForWind model discussed in chapter 2 tries to capture this shape.

Because of the fact that the wake velocity predicted with the Larsen model corresponds with the measurements quite well, the ForWind model was connected to it. Since the Larsen model has analytical solutions for the wake radius and velocity in the wake, a wind farm tool using these two models could calculate velocity and turbulence intensity at desired turbine positions quickly and provide input on velocity, turbulence intensity, but also wind shear over a rotor unlike the other kinematic models.

The constants A and B were empirically found by Wessel [26] from experiments at other wind farms to be 1.42 and 0.54 respectively. These values have been used in this work as well.

4.7.1 Turbulence intensity using the Larsen/ForWind model

In figure 4-10 the results obtained using the ForWind model as outlined above are shown, together with the measurements and the results of the Frandsen model at a downstream distance of $3D$. Only the Frandsen model is shown as well, as this is the basis of the existing model in TBONTB at the moment. The settings used for the Frandsen turbulence model are a Wöhler curve exponent of 3 and a wake probability of 0.06. The Frandsen velocity deficit model uses the standard settings $\alpha = 0.7$ and $k = 2$. As an input for the ForWind model the velocity profiles obtained with the second order Larsen model [36] and [10] were used. These equations are given in D as well. In appendix the plots for all measurement locations are shown, for both the rotor with a C_T of 0.91 and the rotor with a C_T of 0.56.

As can be seen from this figure the added turbulence intensity at $3D$ can be predicted very well with the combination of the Larsen velocity deficit model and the ForWind turbulence model for a C_T -value of 0.56. For a C_T -value of 0.91 the maximum increase in turbulence is underestimated, but qualitatively the shape of the increase is modeled well. The results for all downstream distances are shown in appendix I. From these figures it can be seen for a high C_T -value of 0.91 the model performs well until a distance of $3D$. Except for the large peaks at $1D$, the predicted turbulence stays within 0.05 of the measurements, while Frandsen can be more than 0.1 off. At distances larger than $5D$ the velocity deficit is overpredicted, like the

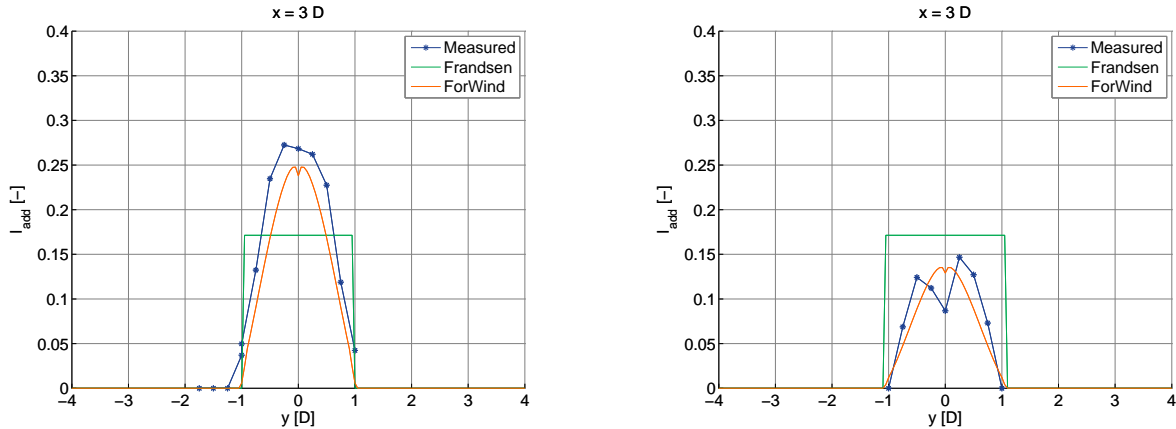


Figure 4-10: Turbulence intensities at $3D$ behind the rotor, with $C_T = 0.91$ (left) and $C_T = 0.56$ (right)

Jensen model, and the turbulence intensity as well. The Frandsen model does not perform better. The Larsen models performs very well up to $5D$ for a lower C_T of 0.56, almost exactly following the measurements. At larger distances it overpredicts the velocity deficit a little. The shape of the turbulence intensity is captured by the ForWind model, but unfortunately it is not conservative.

A better match for the different C_T values may be achieved by changing the parameters of the constants A and B in the ForWind model. However, these parameters were set using full scale measurements at the Nibe wind farm and used in verifications at the Vindeby and Middelgrunden wind farms, so changing them to fit this wind tunnel data does not seem like a logical step. A verification of these values with GE turbines should be performed instead.

4.8 Wake superposition

For the model to be suitable for wind farm application it should not only predict the effect of a single wind turbine correctly, but also the interaction of multiple wakes as well. An algorithm is hence needed to take these multiple wake situations into account. Several methods for this wake adding already exist, the ones most commonly used will be described below. First however, rotor averaging will be discussed.

4.8.1 Rotor averaging

Most wake models assume that a uniform flow enters the swept area of a rotor, but this is generally not the case, neither in reality nor with a simple wake model. Although the Jensen and the Frandsen model generate a uniform wake flow for a given downstream position, even when using these models a uniform inflow over the rotor area will only be the case if the turbines downstream have a rotor diameter smaller than the width of the expanded wake and are precisely in the wake of the upstream turbine (yaw misalignment is not considered). In any other situation the rotor of the downstream turbines will be only partially in the wake, thus experiencing both undisturbed and wake affected flow. Hence in order to be able to

apply the wake models an averaging of the wind speed over the rotor is performed to obtain a equivalent uniform inflow. Using momentum conservation the equivalent uniform inflow u_{rotor} is generally calculated as

$$(U_\infty - u_{rotor})^2 = \frac{1}{A} \int_{rotor} (U_\infty - u_w)^2 dA \quad (4-2)$$

The value of u_w can be influenced by wakes of different turbines and can vary from point to point on the rotor disk. Therefor the contributions of all upstream turbines need to be added in a certain manner.

4.8.2 Wake adding

For the addition of multiple wakes several methods can be used [37]: geometric sum, linear superposition, energy balance and sum of squares. The equations belonging to these models are given below.

Geometric sum	$\frac{u_i}{U_\infty} = \prod_j \frac{u_{ij}}{u_j}$
Linear superposition	$\left(1 - \frac{u_i}{U_\infty}\right) = \sum_j \left(1 - \frac{u_{ij}}{u_j}\right)$
Energy balance	$U_\infty^2 - u_i^2 = \sum_j (u_j^2 - u_{ij}^2)$
Sum of squares	$\left(1 - \frac{u_i}{U_\infty}\right)^2 = \sum_j \left(1 - \frac{u_{ij}}{u_j}\right)^2$

In these equations u_i is the wind speed at turbine i , u_{ij} is the wind speed at turbine i due to (the wake of) turbine j and the summations and the product are taken over the j turbines upstream of turbine i .

All four of these methods can be chosen in WindFarm [38]. In the documentation of WindFarm a comparison of these models is made with wind tunnel data from GH. In this comparison, the sum of squares method was found to be the best performing method for almost all situations, followed by the energy balance. Furthermore, the maker of WindFarm suggests not to use the methods geometric sum and linear superposition, since they tend to overestimate the velocity deficit. The sum of squares method is the only wake combination method available in WindPRO. In their software tool FluxFarm ECN uses the geometric sum surprisingly [39].

Combining a slightly different formulation of the sum of squares with the method to calculate the rotor averaged wind speed (equation 4-2), yields:

$$(U_\infty - u_{rotor})^2 = \frac{1}{A} \int_{rotor} \sum_{i,allwakes} (u_{rotor(i)} - u_{w(i)})^2 dA \quad (4-3)$$

which can be found in Lange [17], where modifications to FLaP are described.

Adding wakes of two turbines

As a part of the wind tunnel campaign measurements were performed to assess the effect of the combination of two wakes, although not as extensive as has been done with the single wake measurements. During these measurements two wind turbines (turbines A and B) were put in the wind tunnel, turbine A spaced $4D$ downstream of turbine B and either $1D$ or $2D$ in lateral direction from turbine B, see figure 4-11. Note that the two possible positions of turbine A are shown simultaneously.

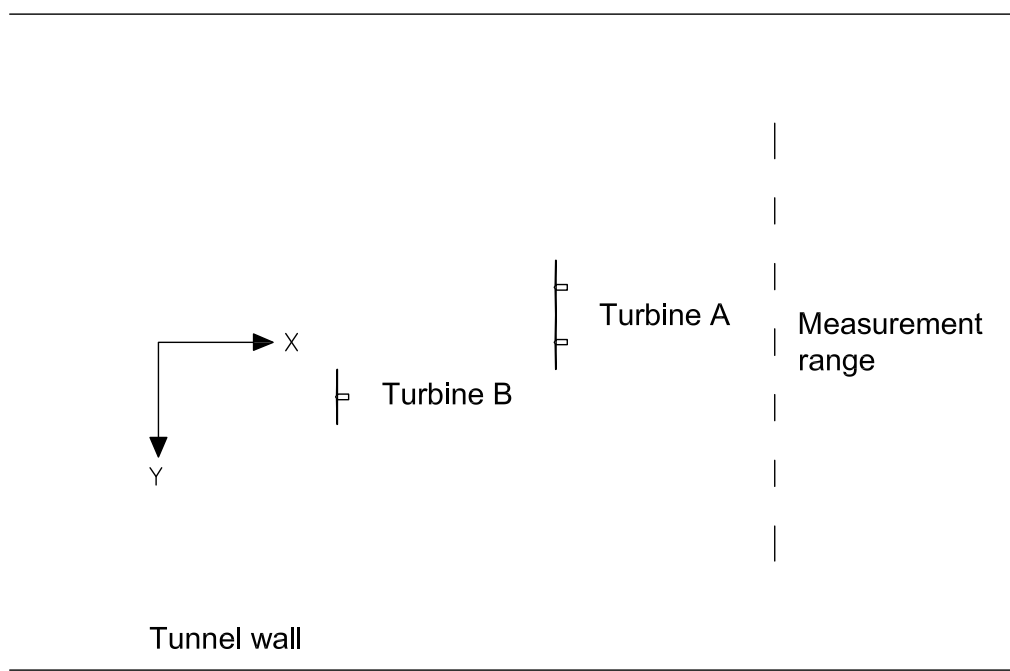


Figure 4-11: Overview of the wind tunnel set up for the wake adding measurements. Both possible positions of turbine A are shown.

The effects of turbines A and B together were measured another $4D$ downstream turbine A (thus $8D$ downstream turbine B) at hub height. Also the effects of the turbines separately was measured. See figure 4-12 for the case when the lateral spacing was $2D$.

For the wake of turbine B to just ‘touch’ the rotor disc of turbine A, the wake radius has to expand to $1.5D$ over a downstream distance of $4D$. Looking at the influence at $4D$ downstream of a single turbine (this is comparable with the blue line in the graph, when only turbine A is present) one can see that the wake radius after $4D$ indeed is about $1.5D$. So the wake of turbine B does not cover the rotor area of turbine A. Repeating this at the measurement distance, one finds that the two wakes merely overlap. The resulting velocity deficit and generated turbulence intensity seem to be equal to the maximum effect of turbine A and B.

For a lateral spacing of only $1D$ the results are shown in figure 4-13. At this lateral spacing the rotor of turbine A is indeed partially in the wake of turbine B² and especially for the

²Since the turbines have the same hub height the amount of overlap between the wake of turbine B and turbine A has its maximum at hub height, where the measurements were taken as well.

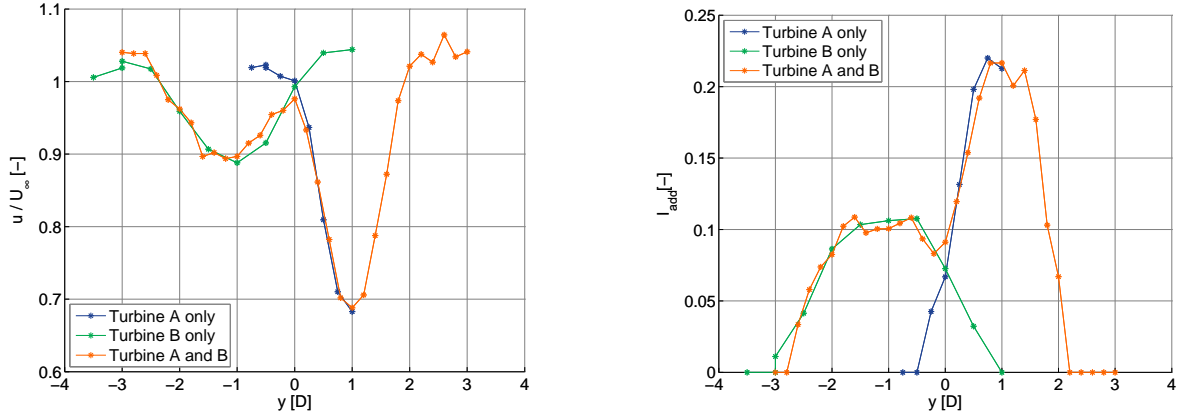


Figure 4-12: Velocity deficit (left) and generated turbulence intensity (right) when turbines A and B are separated 2D

velocity deficit a difference with figure 4-12 can be seen.

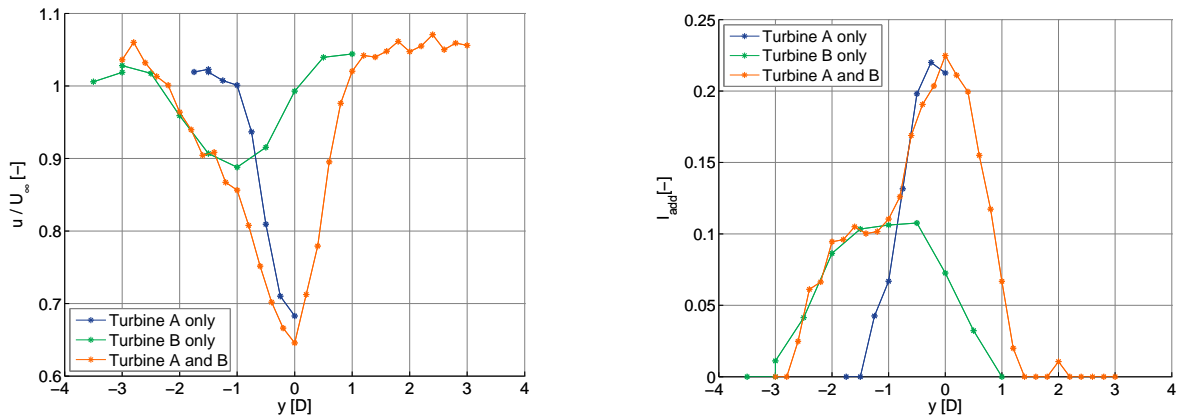


Figure 4-13: Velocity deficit (left) and generated ... turbulence intensity (right) when turbines A and B are separated 1D

Because turbine A is influenced by the wake of turbine B, it will not experience free stream conditions. Hence the velocity and turbulence intensity at positions downstream -even if these points are only influenced by turbine A- will be different depending if turbine B is present or not. This effect has to be incorporated in the superposition model.

4.8.3 Rotor averaged wind speed

To be able to validate the wake superposition models the rotor averaged wind speed over turbine A has to be calculated. Figure 4-14 shows on the left the method how this is done. It is a schematic plot of the y - z plane of the wind tunnel at the location of the turbine under consideration. The right circle represents the rotor of this wind turbine, the concentric circles on the left the expanded wake of an upstream turbine (for the Larsen model the velocities in the wake are axisymmetrical). The color red represents the free stream wind speed, while blue represents the lowest value of the wind speed. The rotor averaged wind speed can now be calculated by using the procedure outlined in appendix J.

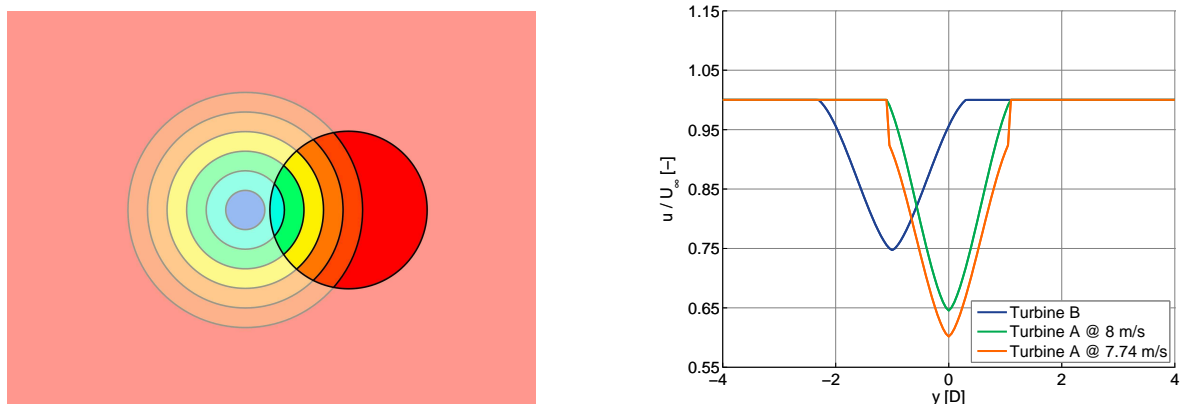


Figure 4-14: Calculating the rotor averaged wind speed (left) and the effect on the velocity deficit

Using this procedure the rotor averaged wind speed on turbine A is equal to the free stream value, 8 m/s when the lateral spacing is $2D$ (see figure 4-12) and 7.74 m/s when the spacing is only $1D$ (see figure 4-13). Using this value to calculate the velocity deficit behind turbine A with the Larsen model (there are no measurements for this slightly reduced wind speed), results in the plot shown on the right side of figure 4-14. The velocity deficit is a little bigger, which is as expected when using a lower wind speed as input. However, since the wake radius is not increased, discontinuities can be seen near the edge of the wake which may cause difficulties later on. Note also that the velocity deficit at $8D$ downstream of turbine B is overestimated, which was already observed, see ?? A similar procedure has to be used for the turbulence intensity, as a different value of the turbulence intensity influences the wake as well. This will be discussed at a later stage.

4.8.4 Results using superposition models

The prediction of the velocity using the geometric sum (in figure: Geo) and the sum of squares methods (in figure: Sos) for the situation of figure 4-13 is shown in figure 4-15. Both methods were applied with or without the calculation of the rotor averaged wind speed at turbine A. As can be seen from the figure, both methods do not perform very well, which is partly due to the fact that the velocity deficit of turbine B is overestimated. That said, the sum of squared method seems to follow the measurements better. As far as the rotor averaging is concerned, it seems that it no averaging performs better than using the rotor averaging. However in this test the increase in turbulence intensity that turbine A experiences is not taken into account yet. This may change the results to such extend that a different conclusion has to be made.

4.9 Wind turbine array

To further assess the model, a validation with a situation where more wake interaction takes place than when only two turbines are present is preferable. This is possible with data from another test run where the development of the velocity and turbulence profile was measured through a wind farm consisting of 2 columns having 14 turbines each. The turbine rows were

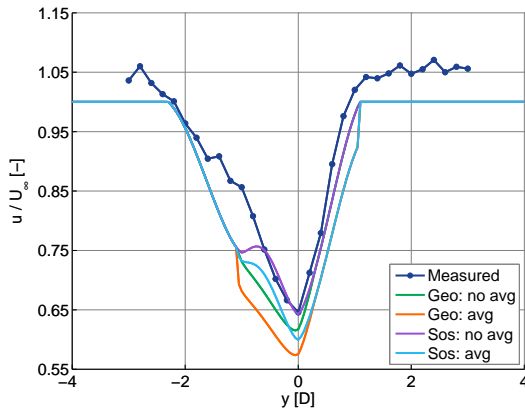


Figure 4-15: Comparison of wake superposition methods

spaced $4D$ from the wind tunnel walls and hence were spaced $4D$ from each other. Within the columns the turbines were spaced $4D$ from each other as well, see figure 4-16.

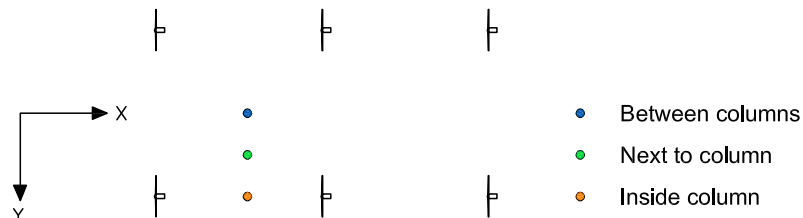


Figure 4-16: Layout of the first three rows of the wind turbine array in the wind tunnel and the measurement locations

Using the hotwire probe the velocity and turbulence intensity was measured for a height range at several locations: before and after the first row of turbines, after three rows and after seven rows of turbines. This was done Between the columns (BC) of turbines, next to a column -which means at a distance of $1D$ from one column and $3D$ from the other- and inside a column. Vertical profile plots of the normalized velocity and turbulence intensity are shown in figures 4-17 and 4-18. Note that $z = 0$ corresponds with the hub height, so the tips of the rotors extend to a height of $0.5D$. The velocity is normalized with respect to the velocity measured before the first turbine, the added turbulence intensity is the increase in turbulence intensity with respect to the situation before the first row. The wind tunnel speed was 8 m/s , while the ambient turbulence intensity was 0.06 .

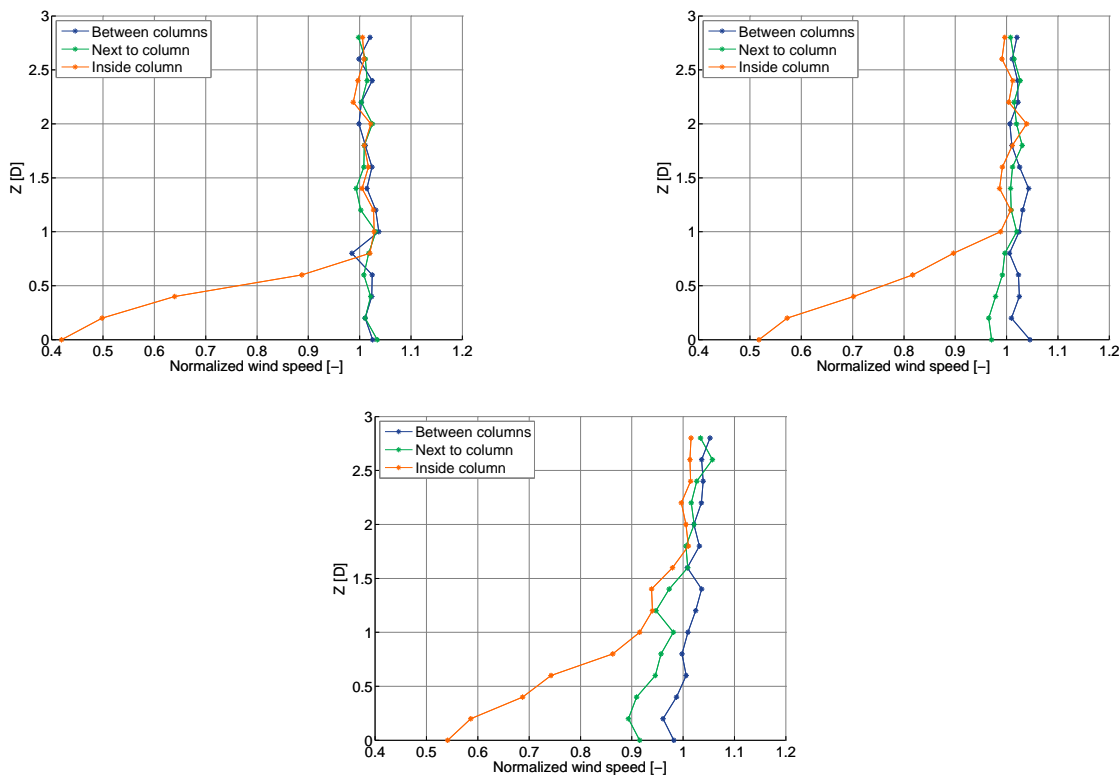


Figure 4-17: Normalized velocity in the model wind farm after one row (top left), three rows (top right) and after five rows (bottom).

4.9.1 Results of the Larsen/ForWind model

The results for the velocity deficit and the turbulence intensity using the new model combination for the different locations through the wind farm are given in this subsection. Applying the rotor averaged wind speed at every turbine yielded better results than using only the ambient wind speed. However, the question was whether the rotor averaging needed to be implemented for the turbulence intensity as well. In appendix K.1 the results for the new model are shown using the ambient turbulence intensity as input for each turbine and using the rotor averaged turbulence intensity, calculated similarly to the rotor averaged wind speed.

For both the velocity deficit and the turbulence intensity the measurements lie in between the results obtained with the ambient turbulence intensity as input and the results obtained with the rotor averaged turbulence intensity. The influence of the increased turbulence intensity in the wake on turbines downstream -although present - is overestimated with the currently used method. The values of the turbulence intensity at the rotors thus have to be closer to the ambient value. The rotor averaged values of the wind speed at the turbines was measured and is used for the tuning, see figure 4-19. This figure shows the values of the rotor averaged wind speeds at the turbines in the 14×2 wind farm, converted from the measured generator voltage using the calibration curves, together with the values calculated with the combination of the Larsen en ForWind models using a modified rotor averaged turbulence intensity defined

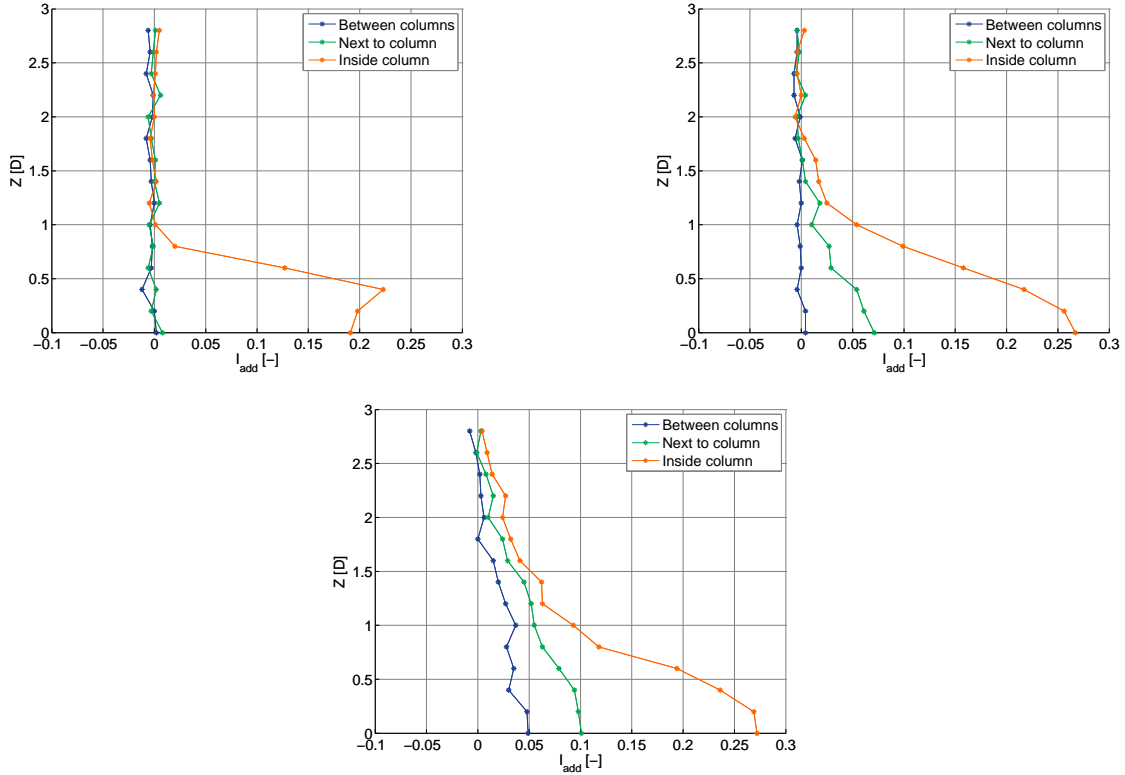


Figure 4-18: Added turbulence velocity in the model wind farm after one row (top left), three rows (top right) and after five rows (bottom).

as

$$I_{rotor_{new}} = \sqrt{\frac{2I_{amb}^2 + I_{rotor}^2}{3}} \quad (4-4)$$

Note that for both turbines in row 13 and 14 and one turbine in each of the rows 5, 6, 8 and 9 the generator voltage was not recorded. Except for the first two rows of turbines and ignoring one of the measurement points from row 7, the rotor averaged wind speed is predicted rather well.

Using this reduction new relation of the rotor averaged turbulence intensity, the prediction of the velocity deficit and turbulence at the measurement stations are as shown in figures 4-20 to 4-22.

The predictions inside the column after seven rows -and to a lesser extend after three rows as well- still do not match the measurements very well. Figure ?? shows the effect of the different inputs of the turbulence intensity on the prediction capabilities of the model: only the ambient turbulence intensity I_{amb} , the rotor averaged value of the turbulence intensity I_{rotor} and the reduced rotor averaged turbulence intensity $I_{rotor_{new}}$. It is clear the use of $I_{rotor_{new}}$ yields results that still are rather close to using the original rotor averaged turbulence intensity. Hence there is some room for improvement in defining $I_{rotor_{new}}$.

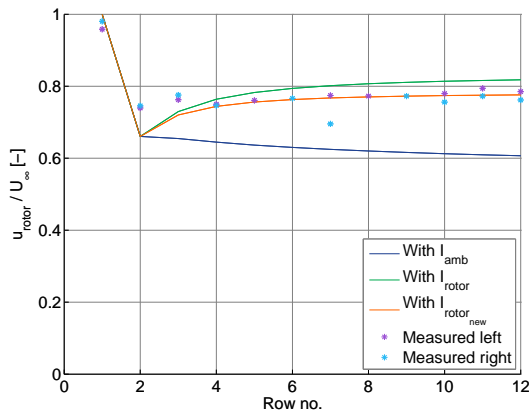


Figure 4-19: Measured and simulated rotor averaged wind speed at the turbines

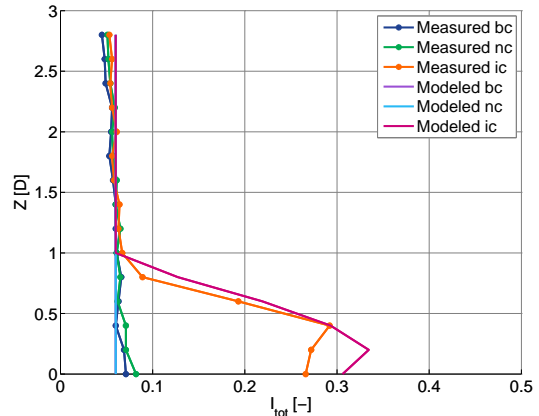
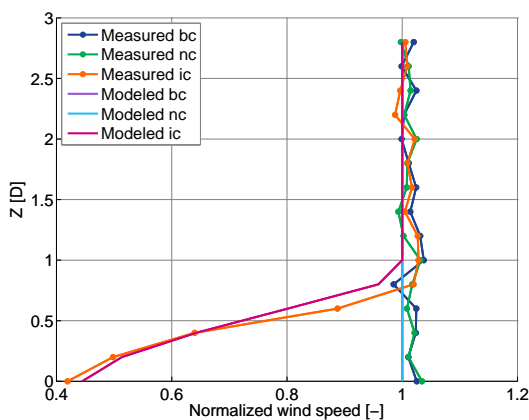


Figure 4-20: Velocity deficit (left) and total turbulence intensity (right) after the first row of turbines

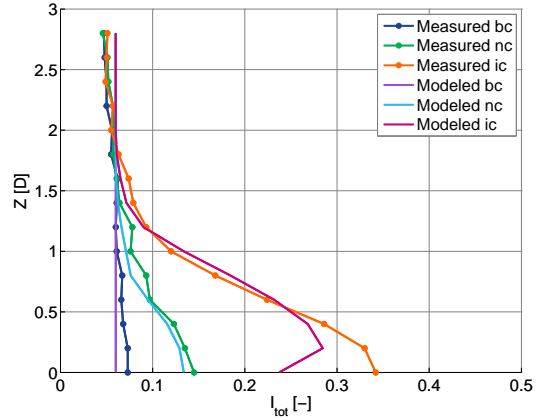
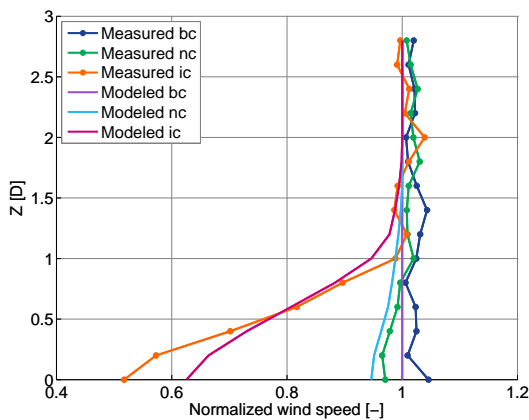


Figure 4-21: Velocity deficit (left) and total turbulence intensity (right) after the third row of turbines

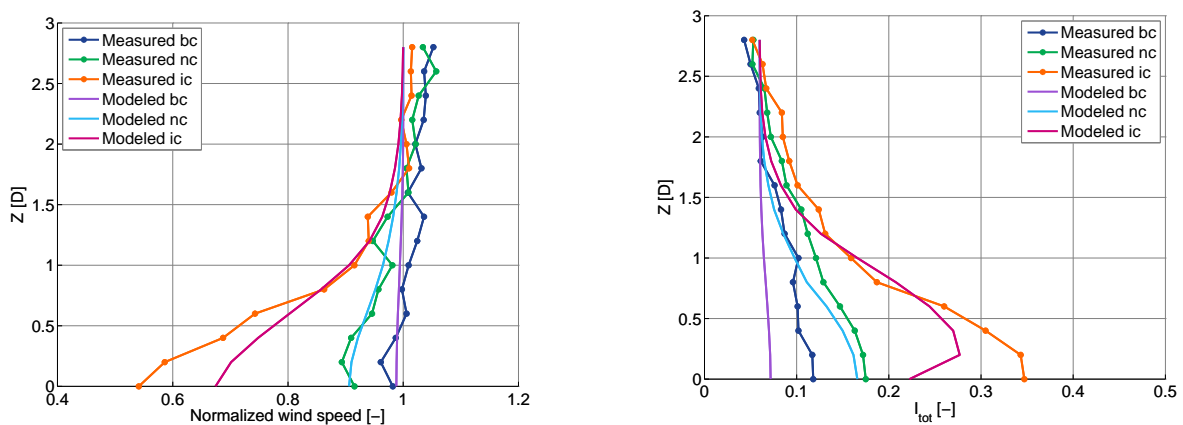


Figure 4-22: Velocity deficit (left) and total turbulence intensity (right) after the seventh row of turbines

Chapter 5

Conclusions and recommendations

5.1 WindPRO modeling

5.1.1 Conclusions

The performance of the available wind turbine wake models in WindPRO has been evaluated using wind farm data available at GE. The objective was not to accurately predict the total wind farm efficiency, but to get an insight in the way these models model the wake effects. As such, much smaller sectors than normally used in micrositing were used. The study found large differences in the prediction capabilities of the models.

The implementation of the Larsen model in WindPRO was found to perform badly, as the wakes are estimated much too wide and much too shallow. This is probably due to errors in the implementation by EMD. The Larsen model is quite sensitive to the turbulence model chosen. The Ainslie model performs consistently and shows only little variation when different turbulence models are used. The wake losses are underpredicted slightly. Note that the Ainslie model needs considerably more calculation time than the other models. The newly introduced Jensen (EMD) model performs much better in multiple wake situations than the original, and when the right settings are chosen for the wake decay constant, the model can be about as accurate as the Ainslie model. The wake decay constant can best be calculated from the turbulence intensity using the Sector Wise Parameter option.

5.1.2 Recommendations

I recommend the Micrositing team based on the findings to discontinue using the original Jensen model and instead use the Jensen (EMD) model for wind farm calculations, at least when the layout is likely to change. The Ainslie model can be used as a check when the layout is fixed. As the Ainslie model slightly underpredicts the wake losses, it is best to use the most conservative combination of the Ainslie model and turbulence model, which is using no added turbulence model.

Wake effects are known to be dependent on thermal stratification, etc, etc. These effects have not been taken into account in this work.

5.2 Wind tunnel measurements

By using the wind tunnel measurements from ECN the development in space of the velocity and turbulence behind a single turbine and though a wind farm could be evaluated. A combination of the Larsen velocity deficit model and the turbulence model introduced by ForWind was able to very quickly estimate velocity and turbulence intensity in space and is able to model wind shear in the wakes. Only close to the hub of the turbines the model is not able to match the measurements closely, but the calculation of the rotor averaged wind speed compares very well with measurements.

5.3 Future work

The model should be validated outside the wind tunnel as well. In order to do so, turbulence measurements should be available inside the wind farm. Providing an existing wind farm with extra met masts would create this possibility. Also the proposed scaled wind farm from ECN should be considered as a good opportunity to further test this model.

Bibliography

- [1] John D. Anderson. *Fundamentals of Aerodynamics*. McGraw-Hill, 4th edition, February 2006.
- [2] J.F. Manwell, J.G. McGowan, and A.L. Rogers. *Wind Energy Explained*. John Wiley & Sons, Ltd, April 2002.
- [3] Tony Burton, David Sharpe, Nick Jenkins, and Ervin Bossanyi. *Wind Energy Handbook*. John Wiley & Sons, Ltd, September 2001.
- [4] G.J.W. van Bussel. *The aerodynamics of horizontal axis wind turbine rotors explored with asymptotic expansion methods*. PhD thesis, Delft University of Technology, June 1995.
- [5] L.J. Vermeer, J.N. Sørensen, and A. Crespo. Wind turbine wake aerodynamics. *Progress in Aerospace Sciences*, (39):467–510, 2003.
- [6] A. Crespo, J. Hernández, and S. Frandsen. Survey of modelling methods for wind turbine wakes and wind farms. *Wind Energy*, 2(1):1 – 24, 1999.
- [7] T. Hegberg, G.P. Corten, and P.J. Eecen. Turbine interaction in large offshore wind farms. Technical Report ECN-C-04-033, Energy research Centre of the Netherlands, August 2004.
- [8] I. Katić, J. Højstrup, and N.O. Jensen. A simple model for cluster efficiency. European Wind Energy Association Conference and Exhibition, 7-9 October 1986, Rome, Italy, 1986.
- [9] N.O. Jensen. A note on wind generator interaction. Risø-M-2411, Risø National Laboratory, November 1983.
- [10] Gunner C. Larsen, Helge Aagaard Madsen, and Niels N. Sørensen. Mean wake deficit in the near field. In *European Wind Energy Conference and exhibition 2003, Madrid, Spain*, 2003.

- [11] J.W.M. Dekker and J.T.G. Pierik, editors. *European Wind turbine standards II*.
- [12] Sten Frandsen, Rebecca Barthelmie, Sara Pryor, Ole Rathmann, Søren Larsen, Jørgen Højstrup, and Morten Thøgersen. Analytical modelling of wind speed deficit in large offshore wind farms. *Wind Energy*, 9.
- [13] Ole Rathmann, Rebecca Barthelmie, and Sten Frandsen. Turbine wake model for wind resource software. In *European Wind Energy Conference 2006, Scientific Proceeding*, 2006.
- [14] J.F. Ainslie. Calculating the flowfield in the wake of wind turbines. *Journal of Wind Engineering and Industrial Aerodynamics*.
- [15] Morten Lybeck Thøgersen. WindPRO / PARK. Technical report, EMD Internation A/S, 2005.
- [16] Garrad Hassan and Partners Ltd. GH WindFarmer Theroy Manual, 2004.
- [17] Bernhard Lange, Hans-Peter Waldl, Rebecca Barthelmie, Algert Gil Guerrero, and Detlev Heinemann. Modelling of offshore wind turbine wakes with the wind farm program FLaP. Technical report.
- [18] Bernhard Lange, Hans-Peter Waldl, Rebecca Barthelmie, Algert Gil Guerrero, and Detlev Heinemann. Improvements of the wind farm model FlaP for offshore applications. Technical report.
- [19] J.G. Schepers. ENDOW: Validation and improvement of ECN's wake model. Technical Report ECN-C-03-034, Energy research Centre of the Netherlands, March 2003.
- [20] S.P. van der Pijl and J.G. Schepers. Improvements of the WAKEFARM wake model. Presented at the Workshop on wake modelling and benchmarking of models of Annex XXIII (Offshore Wind Energy Technology Deployment) of IEA Wind, Denmark, September 2006.
- [21] Idriss Ammara, Christophe Leclerc, and Christian Masson. A viscous three-dimensional differential/actuator-disk method for the aerodynamic analysis of wind farms. *Journal of Solar Energy Engineering*, 124:345–356, November 2002.
- [22] Robert Mikkelsen. *Actuator Disc Methods Applied to Wind Turbines*. PhD thesis.
- [23] Niels Troldborg, Jens N. Sørensen, and Robert Mikkelsen. Numerical simulations of wakes of wind turbines in wind farms. Technical report, 2006.
- [24] Gerard Schepers, Rebecca Barthelmie, Kostas Rados, Bernhard Lange, and Wolfgang Schlez. Large off-shore windfarms: Linking wake models with atmospheric boundary layer models. *Wind Engineering*, 25(5):307–316, 2001.
- [25] Sten Frandsen and Morten L. Thøgersen. Model for turbulence in wind farms. Technical report.
- [26] Arne Wessel, Joachim Peinke, and Bernhard Lange. Verification of a new model to calculate turbulence intensity inside a wind farm. 2006.

- [27] Thomas Sørensen, Per Nielsen, and Morten Lybeck Thøgersen. Recalibrating wind turbine wake model parameters – Validating the wake model performance for large offshore wind farms. 2006.
- [28] Thomas Sørensen, Morten Lybeck Thøgersen, Per Nielsen, Anselm Grötzner, and Stefan Chun. Evaluating models for wind turbine wake added turbulence - Sensitivity study of the models and case study.
- [29] K. Rados, G. Larsen, R. Barthelmie, W. Schlez, B. Lange, G. Schepers, T. Hegberg, and M. Magnisson. Comparison of wake models with data for offshore windfarms. *Wind Engineering*, 25(5):271–280, 2001.
- [30] R.J. Barthelmie (ed.). Proceedings of the ENDOW workshop ‘Offshore wakes: measurements and modelling’. Risø-R-1326(EN), Risø National Laboratory, March 2002.
- [31] Ben Hendriks. Tunnel experiments, full scale experiments, scale farm. Presented at the Dutch Wind Workshops, October 2006, Petten, the Netherlands, October 2006.
- [32] M. Blaas, G.P. Corten, and P. Schaak. TNO boundary layer tunnel. Technical report, Energy research Centre of the Netherlands.
- [33] G.P. Corten, P. Schaak, and T. Hegberg. Velocity profiles measured above a scaled wind farm. Technical report, Energy research Centre of the Netherlands.
- [34] G.P. Corten, P. Schaak, and T. Hegberg. Turbine interaction in large offshore wind farms. Technical Report ECN-C-04-048, Energy research Centre of the Netherlands, August 2004.
- [35] G.P. Corten and P. Schaak. Heat and flux. Technical report, Energy research Centre of the Netherlands.
- [36] Gunner C. Larsen. A simple wake calculation procedure. Risø-M-2760, Risø National Laboratory, December 1988.
- [37] Hartwig Dobesch and Georg Kury. Basic meteorological concepts and recommendations for the exploitation of wind energy in the atmospheric boundary layer. Technical report.
- [38] Erik Djerf and Henrik Mattsson. Evaluation of the software program WindFarm and comparisons with measured data from alsvik. Master’s thesis, Royal Institute of Technology, Stockholm, Sweden.
- [39] E.T.G. Bot, G.P. Corten, and P. Schaak. FluxFarm. Technical report, Energy research Centre of the Netherlands.
- [40] Ib Troen and Lundtang Petersen. *European Wind Atlas*. Risø National Laboratory, 1989.
- [41] Website of WindSIM AS. <http://www.windsim.com>.
- [42] Website of EMD. <http://www.emd.dk/>.
- [43] Website of Garrad Hassan and partners ltd. <http://www.garradhassan.com/>.
- [44] Website of Resoft’s WindFarm. <http://www.resoft.co.uk>.
- [45] Website of LM Glasfiber. <http://www.lmglasfiber.com>.

Appendices

Appendix A

About General Electric

The history of GE goes back to 1890 when the inventor Thomas Edison (who stood at the cradle of the modern light bulb) founded the Edison Electric Light Company, which in 1892 merged with its main competitor the Thomson-Houston Company to form the General Electric Company. Since then GE has grown to be one of the world's largest companies. In 2006 the total revenues of GE amounted US\$ 163 billion, earnings exceeded US\$ 20 billion and the work force of GE was over 300,000 employees.

The company is structured in six businesses: Commercial Finance, Healthcare, Industrial, Infrastructure, GE Money (formerly Consumer Finance) and NBC Universal. GE Wind Energy is part of GE Energy, which in its turn is part of GE Infrastructure. GE Energy deals with power generation and energy delivery technologies, providing comprehensive solutions for coal, oil, natural gas, nuclear energy and renewable resources such as wind solar and biogas. Besides that GE Energy provides aviation and energy leasing and financing services. Both in revenue and work force GE Energy accounts for about one tenth of GE.

A.1 GE Wind Energy

GE Wind Energy was started in 2002 when GE acquired the assets of Enron Wind Corp. Enron had entered the wind energy business in 1996 after the acquisition of Zond Systems (founded in 1980) and in 1997 Tacke Windtechnik GmbH (started in 1990) was added. In 2005 GE Wind Energy delivered more than 1300 turbines with revenues exceeding US\$ 2 billion, up 200% with respect to 2004 and up 400% from 2002, the first year GE entered the wind business. In 2006 GE supplied 764 of its 1.5-megawatt wind turbines to projects in the United States alone, resulting in an installed capacity of more than one GigaWatt, which was 45 % of the installed new wind capacity in the United States. Of all wind turbine manufacturers in the world, GE Wind Energy was ranked second largest and the only one of the big four (which together hold more than 70 % of the market) that gained market share¹. In 2006 GE ranked third largest (the numbers 2, 3 and 4 having an almost equal market share).

¹Source: World Market Update 2005, BTM Consult ApS

GE has design, manufacturing and assembly facilities in Germany, Spain, China, Canada and the United States.

Wind turbines are part of GE's Ecomagination product portfolio, a commitment to expand its portfolio of cleaner energy products while reducing its own greenhouse gas emissions. That GE is committed to and sees a bright future for wind energy is also shown by the fact that it has taking ownership of several wind farms in Germany and the United States through GE Energy Financial Services.

A.2 GE turbines

GE Wind Energy's product portfolio consists of turbines with a rated capacity ranging from 1.5 MW to 3.6 MW. The latter is designed especially for offshore use and has been used in the Arklow wind farm located roughly 10 km off the coast of Ireland. This wind farm became operational in 2004 and comprises of 7 turbines, giving the wind farm a total capacity of little more than 25 MW.

The latest sibling joining the GE wind turbine family is the GE 2.5xl. A prototype of this turbine is being operated on the test field of ECN near Wieringermeer in the Netherlands. Commercial shipment is expected to begin in 2008 to key markets in Europe.



Figure A-1: Members of the GE family of wind turbines: a GE1.5 (left), a GE2.5 (middle) and one of the GE3.6 at Arklow (right)

The GE 1.5 turbine is the oldest turbine in the family, but it is still the work horse of GE Wind Energy. More than 5000 have already been installed. However, since the first GE 1.5 was installed in 1996 development have been ongoing and the GE 1.5 turbines that are manufactured nowadays are quite different than the first ones. There are several different versions of the GE 1.5 turbine, see table A-1 for the differences and the characteristics of all GE turbines.

Technical data	1.5s	1.5se	1.5sl	1.5sle	1.5xle	2.5xl	3.6sl
Rated capacity [kW]	1500	1500	1500	1500	1500	2500	3600
Cut-in wind speed [m/s]	4	4	3.5	3.5	3.5	3.5	3.5
Cut-out wind speed [m/s]	25	25	20	25	20	27	27
Rated wind speed [m/s]	13	13	14	14	12.5	12.5	14
Rotor diameter [m]	70.5	70.5	77	77	82.5	100	111
Wind Class IEC	IIa	Ib	-	IIa	IIIb	IIIa, IIb	Ic
Wind Class DIBt	II/III	-	II	-	II	-	-

Table A-1: Characteristics of the GE wind turbines

Appendix B

Wake tools used at GE

This appendix gives a short overview of the tools associated with wake effects that are currently used at GE.

WAsP

Wind Atlas Analysis and Application Program (WAsP) was introduced in 1987 by the Wind Energy and Atmospheric Physics Department at Risø National Laboratory, Denmark. It can be used for wind data analysis, wind atlas generation, wind climate estimation and siting of wind turbines. The program extrapolates wind climate statistics both vertically and horizontally based on measurements. It therefore contains several models to describe the wind flow over different terrains and close to sheltering obstacles. A simple wake model, based on the model by Jensen is implemented as well in order to be able to calculate wake losses. The background of models implemented in WAsP are described in the European Wind Atlas (EWA) [40].

WindPRO

WindPRO is an integrated software package developed by the Danish company EMD for the design and planning of wind energy projects. Since it is a modular based software, it can be accustomed to the needs of the user. Besides the basis module there are modules for noise, shadow flicker and economic calculations and modules that can produce renderings and photo montages. It is also capable of processing data from other software packages like WAsP and WindSIM, a simulator developed by WindSim AS [41] for optimizing the energy production from wind turbines based on CFD, making it suitable for more complex terrain. The most important module from the perspective of wake modeling is the PARK module. This module handles wind farm energy calculations and array losses. For a complete overview of the software, see the website of EMD [42].

Commercial packages similar to WindPRO are WindFarmer by Garrad Hassan [43] and WindFarm by ReSoft [44].

TBONTB

When a wind farm layout has been defined from an energy perspective, it has to be verified that the loads on the turbines will remain within the design envelope. The main focus of the Loads group when considering wake effects is the turbulence intensity in the wake which has a direct influence on the fatigue life. In order to assess this effect, the Loads group uses an in-house developed tool to identify the turbine with the highest Damage Equivalent Load (DEL). This tool, named ‘To Be Or Not To Be’ (TBONTB), calculates the wake influences in the form of wake turbulence intensities and combines this with the wind distribution at the location. It is based on the model by Sten Frandsen that was presented at the conference Offshore Wind Energy in the Mediterranean and other European Seas (OWEMES) in the year 2000 [25] and hence is similar to the Frandsen / DIBt added turbulence model that is described in chapter ???. This model only calculates the increase in turbulence intensity and does not consider velocity deficits.

FLEX5

FLEX5 is not as much a tool to assess the wake effects, but since it uses output from TBONTB as input, a quick explanation of the program is justified. The FLEX5 code was developed by Stig Øye at the Department of Fluid Mechanics of the Technical University of Denmark. The program can be used for all load simulations on horizontal axis wind turbines. It can simulate different operating and fault conditions such as normal production, parking, idling, start-up, stop, emergency stop, oblique inflow, network faults, icing of the blades, failing brakes etc. for both deterministic and turbulent wind. During the last couple of years FLEX5 has become an industry standard and is used by several wind turbine manufacturers as well as the largest wind turbine blade manufacturer, LM Glasfiber [45].

GE Wind Energy has made various modifications to the program and both a pre-processor and a post-processors were added in order to make it easier to use the program and to interpret the results. GE uses FLEX5 to perform detailed load calculations on the turbine with the highest DEL as identified using TBONTB.

Similar codes to FLEX5 are for instance Bladed by GH and Horizontal axis wind turbine Code (HawC) by Risø.

Appendix C

Determination of wake sectors

In order to determine at which wind directions the turbines or met mast are in wake condition, a simple linear expanding wake was assumed. This forms the basis for the Jensen model as well. See the figures below for a graphical representation.

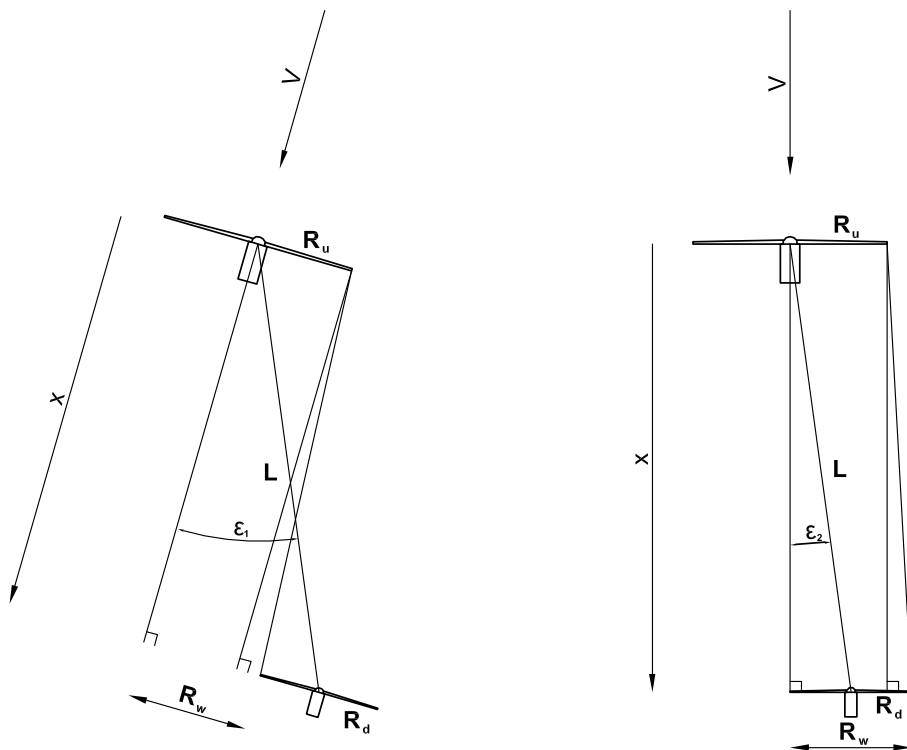


Figure C-1: Determination of wake sectors

So the angles for full and partial wake are determined as follows

$$R_u + R_d + kl \cos \epsilon_1 - L \sin \epsilon_1 = 0 \quad (\text{C-1})$$

$$R_u - R_d + kl \cos \epsilon_2 - L \sin \epsilon_2 = 0 \quad (\text{C-2})$$

The angles ϵ_1 and ϵ_2 are the angles that the wind can have with respect to the connecting line between the rotor centers of two turbines such that the downstream turbine is just experiencing the wake of the upstream turbine respectively is experiencing fully the wake of the upstream turbine.

When the angles ϵ_1 and ϵ_2 are not equal to 90° , the previous equations can be written as:

$$\epsilon_1 = \arctan \left[k + \frac{R_u + R_d}{L \cos \epsilon_1} \right] \quad (\text{C-3})$$

$$\epsilon_2 = \arctan \left[k + \frac{R_u - R_d}{L \cos \epsilon_2} \right] \quad (\text{C-4})$$

These angles can be calculated using non-linear optimization in the neighborhood of the solution of the linearized problem.

$$\epsilon_1 = \arctan \left[\frac{R_u + R_d}{L} + k \right] \quad (\text{C-5})$$

$$\epsilon_2 = \arctan \left[\frac{R_u - R_d}{L} + k \right] \quad (\text{C-6})$$

When R_d is larger than R_u it is possible for ϵ_2 to be negative. In that case the downstream turbine can never be fully in the wake of the upstream turbine. This distinction between being fully in a wake and being only partially in a wake is made, because this can be of influence for the loading of the turbine. Since for the power output of a turbine the (cube of the) wind speeds are integrated over the rotor area, it is expected that an abrupt transition from partial to full wake operation cannot be observed in the power output; instead a gradual transition will be present.

The relations for the two angles ϵ_1 and ϵ_2 hold as well for the met mast. When -instead of a downstream turbine- a met mast is considered, having a very small ‘radius’, the angle ϵ_2 will approach ϵ_1 . This means that the met mast cannot be partially in wake; it will either be in free stream conditions or in wake conditions.

Appendix D

Larsen model: second order contribution

Following the second order approach as given in [36] and [10] (however without the weighting factor that was introduced in the latter paper) yields the following equation for the velocity deficit of the Larsen model:

$$\Delta U(x, r) = (\Delta U)_1(x, r) + (\Delta U)_2(x, r) \quad (\text{D-1})$$

The first order contribution $(\Delta U)_1$ was already given in equation 2-5, the second order contribution $(\Delta U)_2$ is given by:

$$(\Delta U)_2(x, r) = U_\infty (C_T A(x + x_0)^{-2})^{2/3} \sum_{i=0}^4 d_i z(x, r)^i \quad (\text{D-2})$$

where $z(r, x)$ is given by:

$$z(x, r) = r^{3/2} (C_T A(x + x_0))^{-1/2} \left(\frac{35}{2\pi} \right)^{-3/10} (3c_1^2)^{-3/10} \quad (\text{D-3})$$

and the constants d_0 to d_4 by:

$$d_0 = \frac{4}{81} \xi_0^6 \left(-1 - 3 \left(4 - 12 \left(6 + 27 \left(-4 + \frac{48}{40} \right) \frac{1}{19} \right) \frac{1}{4} \right) \frac{1}{5} \right) \frac{1}{8} \quad (\text{D-4})$$

$$d_1 = \frac{4}{81} \xi_0^6 \left(4 - 12 \left(6 + 27 \left(-4 + \frac{48}{40} \right) \frac{1}{19} \right) \frac{1}{4} \right) \frac{1}{5} \quad (\text{D-5})$$

$$d_2 = \frac{4}{81} \xi_0^6 \left(6 + 27 \left(-4 + \frac{48}{40} \right) \frac{1}{19} \right) \frac{1}{4} \quad (\text{D-6})$$

$$d_3 = \frac{4}{81} \xi_0^6 \left(-4 + \frac{48}{40} \right) \frac{1}{19} \quad (\text{D-7})$$

$$d_4 = \frac{4}{81} \xi_0^6 \frac{1}{40} \quad (\text{D-8})$$

The parameter ξ_0 is determined by:

$$\xi_0 = \left(\frac{35}{2\pi} \right)^{1/5} (3c_1^2)^{-2/15} \quad (\text{D-9})$$

Appendix E

Near wake length of Vermeulen

The near wake length according to Vermeulen is used in both FLaP and the Quarton wake added turbulence model in WindPRO and is described in Thøgersen [15]. Vermeulen divides the near wake in two parts, where the length of the first part is given by

$$x_h = r_0 \left[\left(\frac{dr}{dx} \right)_a^2 + \left(\frac{dr}{dx} \right)_\lambda^2 + \left(\frac{dr}{dx} \right)_m^2 \right]^{-\frac{1}{2}} \quad (\text{E-1})$$

with the effective radius of the expanded rotor disc r_0 given by

$$r_0 = \frac{D}{2} \sqrt{\frac{m+1}{2}} \quad (\text{E-2})$$

and m is defined as

$$m = \frac{1}{\sqrt{1 - C_T}} \quad (\text{E-3})$$

As can be seen the length of the near wake is defined by contributions for the ambient turbulence, rotor generated turbulence and shear generated turbulence respectively, given as follows

$$\left(\frac{dr}{dx} \right)_a^2 = \begin{cases} 2.5I + 0.05 & \text{for } I \geq 0.02, \\ 5I & \text{for } I < 0.02. \end{cases} \quad (\text{E-4})$$

$$\left(\frac{dr}{dx} \right)_\lambda^2 = 0.012B\lambda \quad (\text{E-5})$$

$$\left(\frac{dr}{dx} \right)_m^2 = \frac{(1-m)\sqrt{1.49+m}}{9.76(1+m)} \quad (\text{E-6})$$

These contributions are for the ambient turbulence, the rotor generated turbulence and the shear generated turbulence respectively.

After the calculation of this first part of the near wake, the total length of the near wake follows from

$$x_n = x_h \frac{\sqrt{0.212 + 0.145m}}{1 - \sqrt{0.212 + 0.145m}} \frac{1 - \sqrt{0.134 + 0.124m}}{\sqrt{0.134 + 0.124m}} \quad (\text{E-7})$$

Appendix F

EWTW Wieringermeer

A third site of which extensive measurement data is available is the ECN Wind turbine Test station Wieringermeer (EWTW). Figure F-1 shows the layout of the site. Beside a few separate wind turbines, there are three lines of turbines, a line of 5 Nordex N80's, a line consisting of 4 prototypes and a line of NM52's. Furthermore there is a total of 3 met masts of which two are located close to the prototype locations.

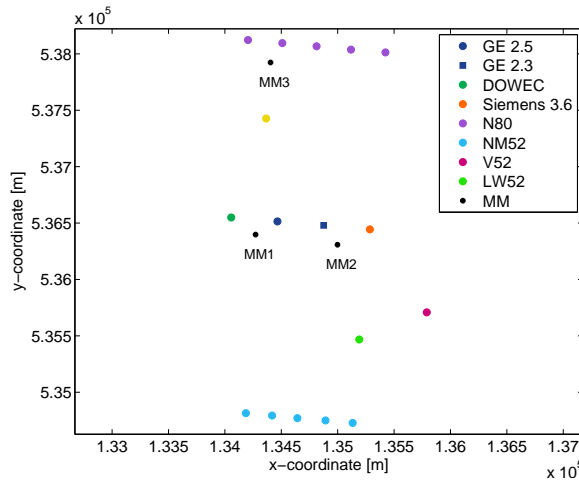


Figure F-1: Layout of the EWTW test field near Wieringermeer. Coordinates are according to the Dutch 'Rijksdriehoeks' system.

Since the prototypes are exactly in line, when one of the GE turbines is in the wake of the other GE turbine, it is also influenced by a competitor prototype. The Siemens prototype was installed just a few months after the GE 2.3, while the DOWEC was first of the four prototypes to be installed. No data (including operational status) is available from either of these two turbines.

Furthermore, although there are two met masts located close to each other and they serve perfectly for power curve measurements, for wake analysis they are not positioned very well.

In no case will one of the met masts MM1 and MM2 be in a wake of a GE turbine while the other is experiencing undisturbed flow. MM3 can not be used to fill this gap either.

Because of these reasons, it was decided not to use the data from the GE turbines at Wieringermeer.

Appendix G

Prettin met mast

The met mast located at Prettin is shown in figure G-1. Table G-1 shows the sensors with which the met mast is equipped. Since the Thies anemometer at the height of 97 m was changed during the measurement period from a Thies Classic to a Thies 1st Class and the sonic anemometer did not have reliable measurements during the whole period, the Risø anemometer was used for the wind speed measurement at hub height. Comparing values of the wind speed according to the Risø cup anemometer and the Thies anemometers showed minimal differences (especially with the 1st Class) that may be important for power curve measurements, but they are not for these wake analyses.

Sensor	Height [m]	Type
Pressure	2	
Temperature	10 93	
Wind direction	93 93	Wind vane Sonic
Wind speed	58 97 97 97	Thies Risø Sonic Thies 1 st Class / Classic

Table G-1: Sensor heights and types on the Prettin met mast

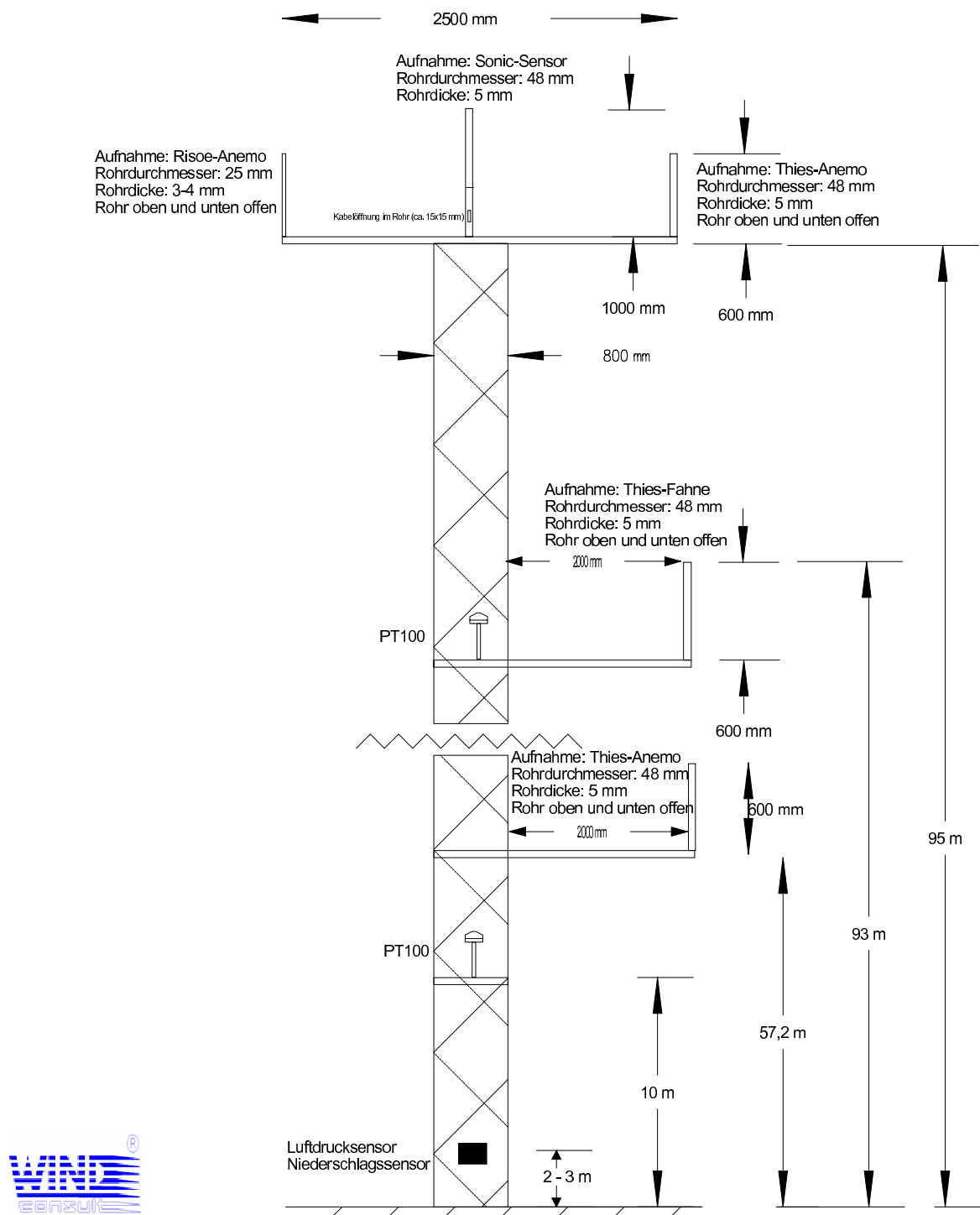


Figure G-1: Schematics of met mast at Prettin wind farm

Appendix H

Sector wise parameters

WindPRO has the option to calculate some of the parameters necessary for the energy calculations from the measured meteo data. Besides the turbulence intensity, the WDC is obtained from the meteo data.

In order to calculate the WDC two steps are needed. From the turbulence intensity the roughness length is calculated. This is done using the following relation:

$$I = A_x \kappa \left[\frac{1}{\ln(z/z_0)} \right] \quad (\text{H-1})$$

This relation is valid for homogeneous terrain. The value of A_x varies between 1.8 and 2.5, the value of the Von Karman constant κ is equal to 0.4. For the calculation of the roughness length the product $A_x \kappa$ is conservatively set equal to 1. The WDC is then obtained by interpolation using the values from table H-1.

Terrain classification	Roughness Class	Roughness Length	Wake Decay Constant	Ambient Turbulence at 50 m ^a	Ambient Turbulence at 50 m ^b
Offshore, water areas	0.0	0.0002	0.040	0.06	0.08
Mixed water and land	0.5	0.0024	0.052	0.07	0.10
Very open farmland	1.0	0.0300	0.063	0.10	0.13
Open farmland	1.5	0.0550	0.075	0.11	0.15
Mixed farmland	2.0	0.1000	0.083	0.12	0.16
Trees and farmland	2.5	0.2000	0.092	0.13	0.18
Forests and villages	3.0	0.4000	0.100	0.15	0.21
Large towns and cities	3.5	0.8000	0.108	0.17	0.24
Large build up cities	4.0	1.6000	0.117	0.21	0.29

^aUsing $A_x = 1.8$

^bUsing $A_x = 2.5$

Table H-1: Relation between wake model parameters

Appendix I

Single wake calculations: Combining Larsen and ForWind models

Pitch 0°

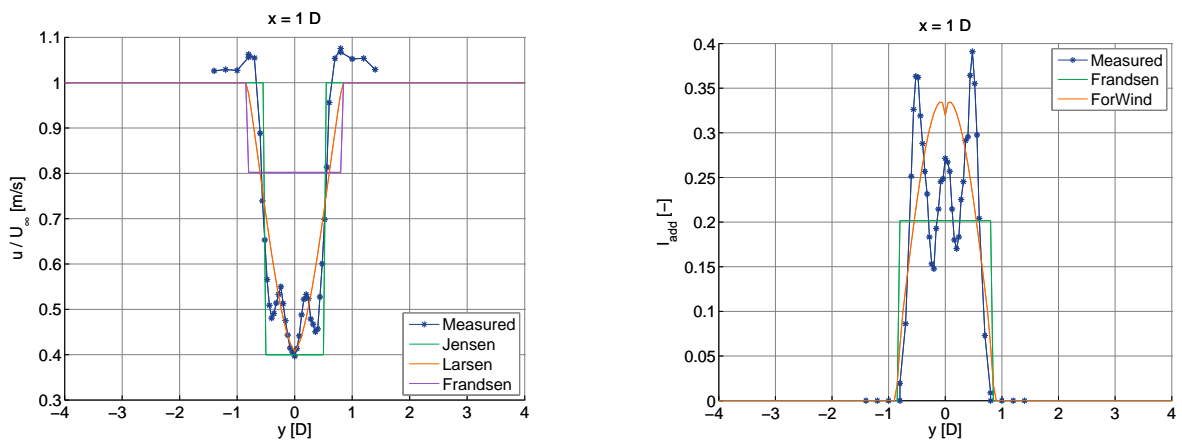


Figure I-1: Comparison of the measured and simulated velocity (left) and generated turbulence (right) behind a ECN model turbine with $C_T = 0.91$, $x = D$

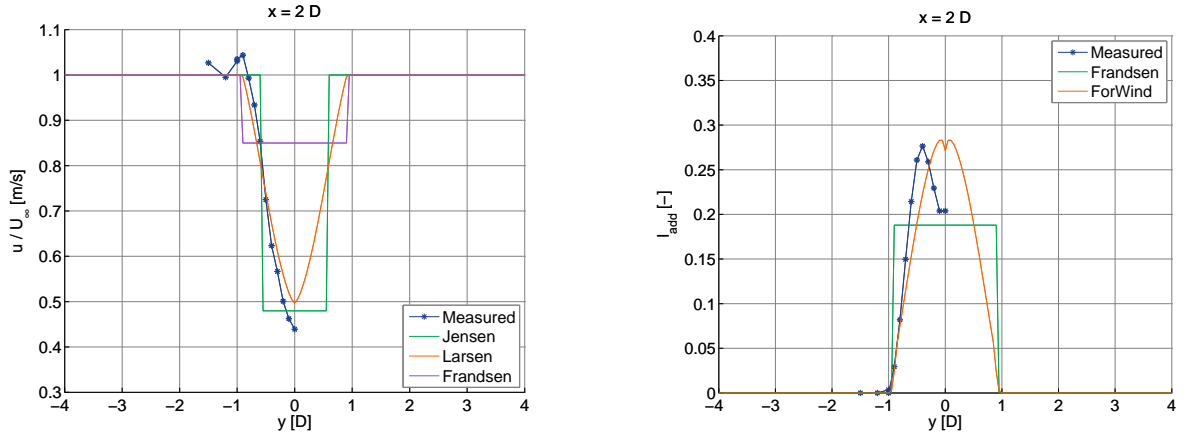


Figure I-2: Comparison of the measured and simulated velocity (left) and generated turbulence (right) behind a ECN model turbine with $C_T = 0.91$, $x = 2D$

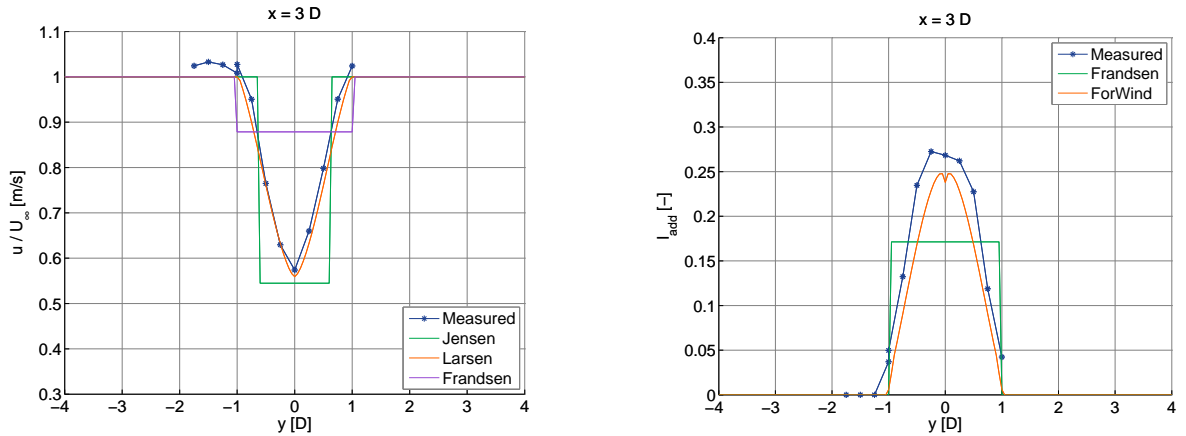


Figure I-3: Comparison of the measured and simulated velocity (left) and generated turbulence (right) behind a ECN model turbine with $C_T = 0.91$, $x = 3D$

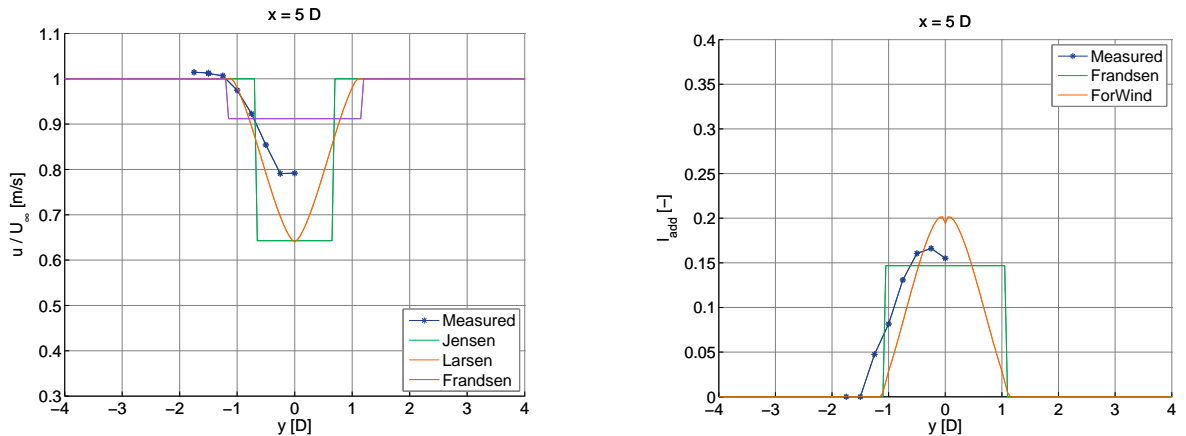


Figure I-4: Comparison of the measured and simulated velocity (left) and generated turbulence (right) behind a ECN model turbine with $C_T = 0.91$, $x = 5D$

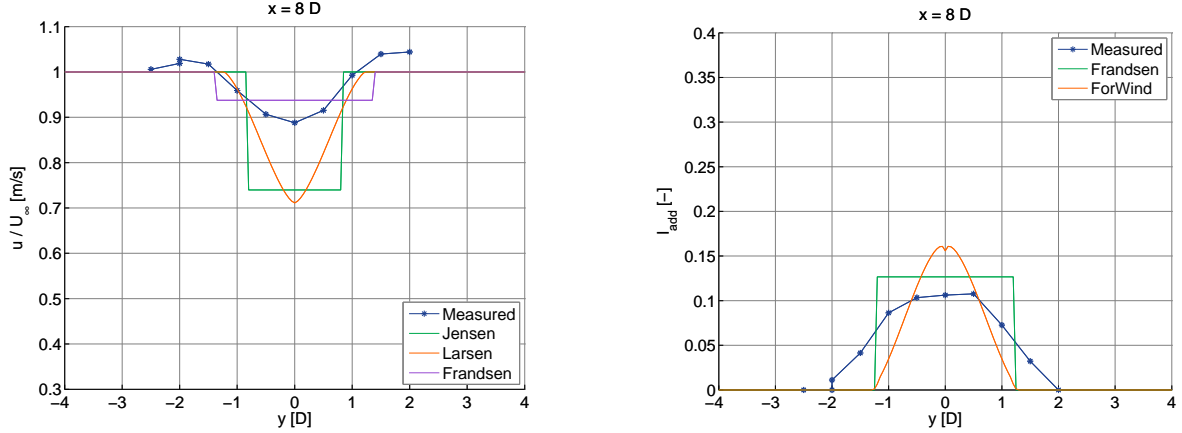


Figure I-5: Comparison of the measured and simulated velocity (left) and generated turbulence (right) behind a ECN model turbine with $C_T = 0.91$, $x = 8D$

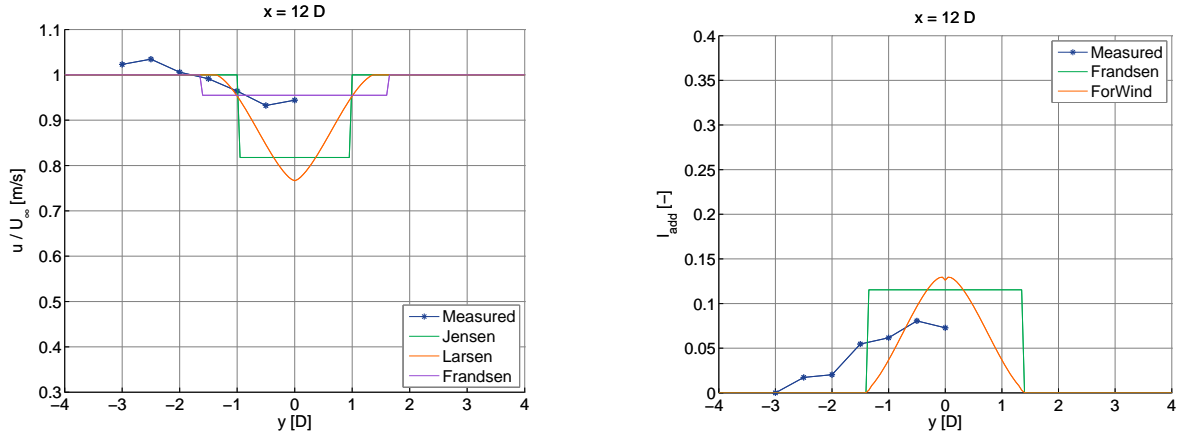


Figure I-6: Comparison of the measured and simulated velocity (left) and generated turbulence (right) behind a ECN model turbine with $C_T = 0.91$, $x = 12D$

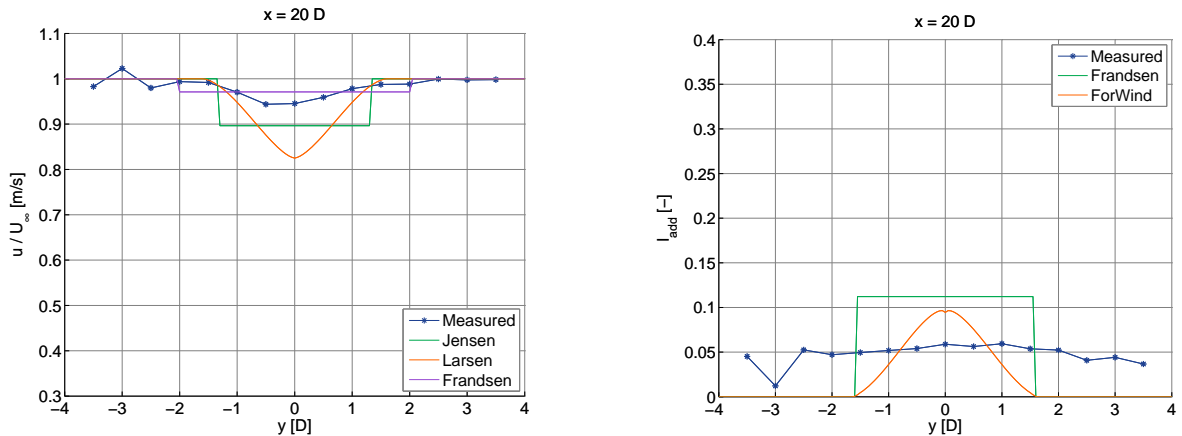


Figure I-7: Comparison of the measured and simulated velocity (left) and generated turbulence (right) behind a ECN model turbine with $C_T = 0.56$, $x = 20D$

Pitch 5°

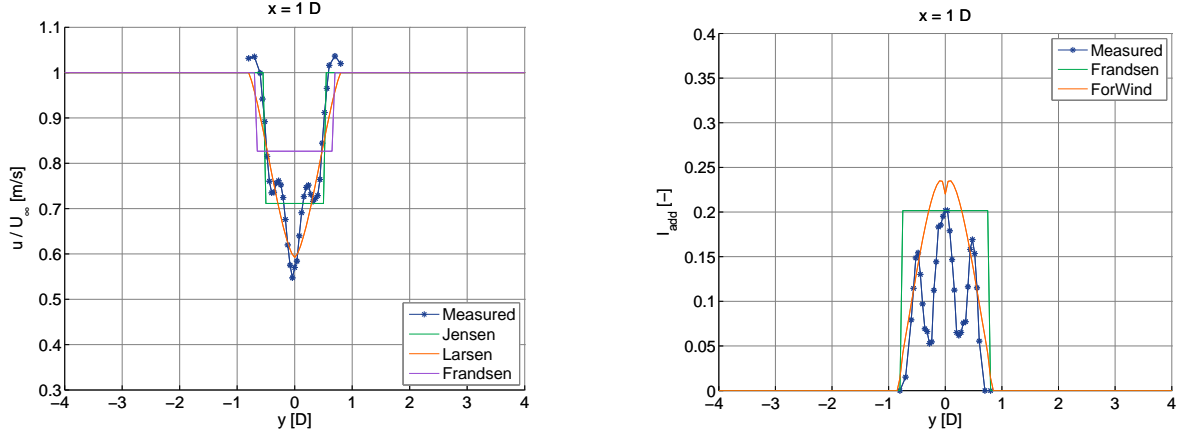


Figure I-8: Comparison of the measured and simulated velocity (left) and generated turbulence (right) behind a ECN model turbine with $C_T = 0.56$, $x = D$

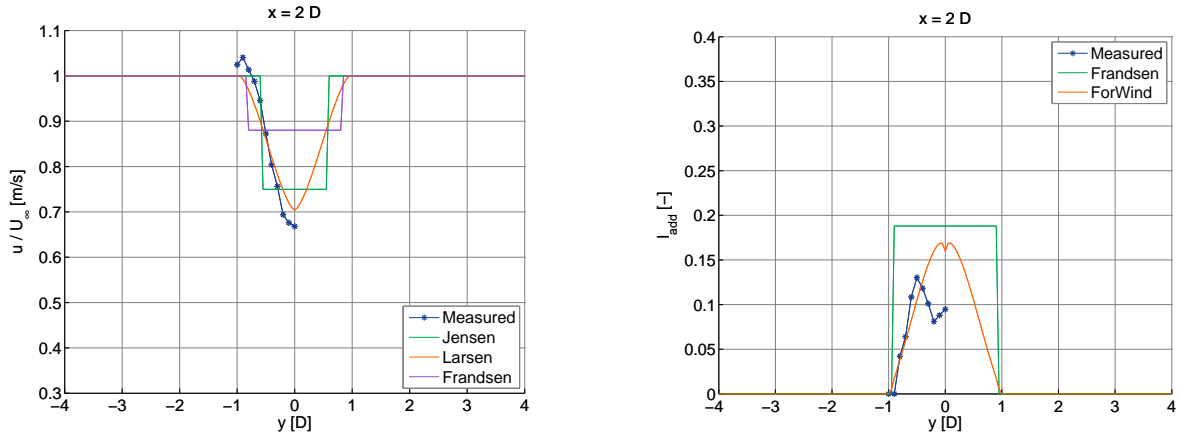


Figure I-9: Comparison of the measured and simulated velocity (left) and generated turbulence (right) behind a ECN model turbine with $C_T = 0.56$, $x = 2D$

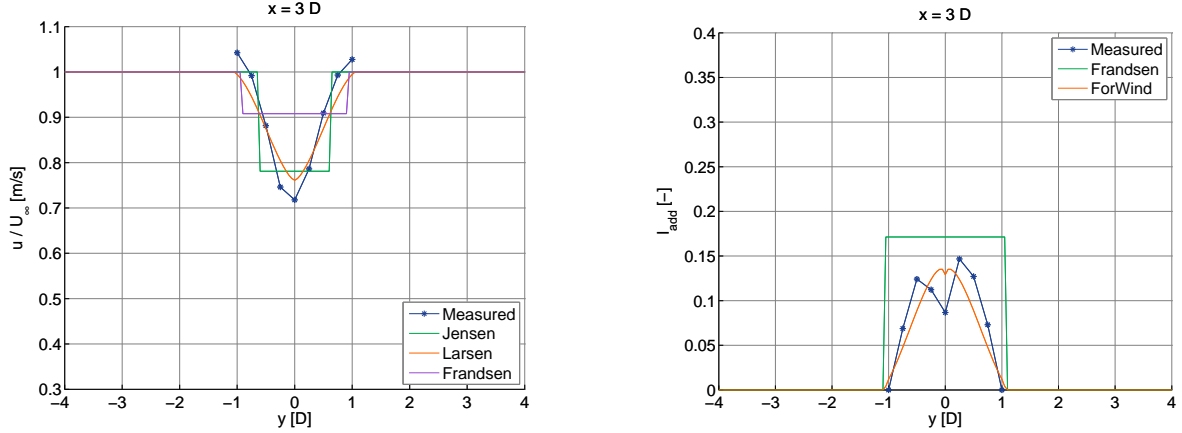


Figure I-10: Comparison of the measured and simulated velocity (left) and generated turbulence (right) behind a ECN model turbine with $C_T = 0.56$, $x = 3D$

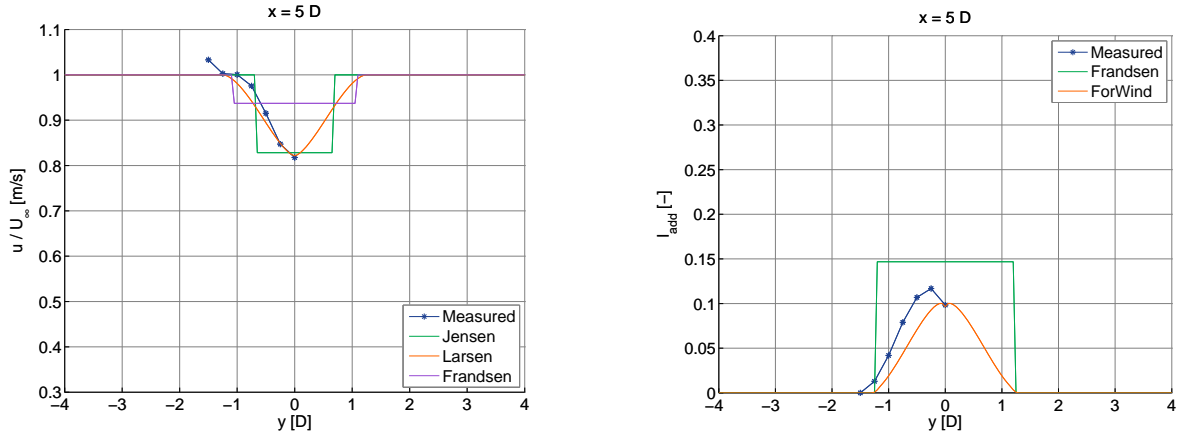


Figure I-11: Comparison of the measured and simulated velocity (left) and generated turbulence (right) behind a ECN model turbine with $C_T = 0.56$, $x = 5D$

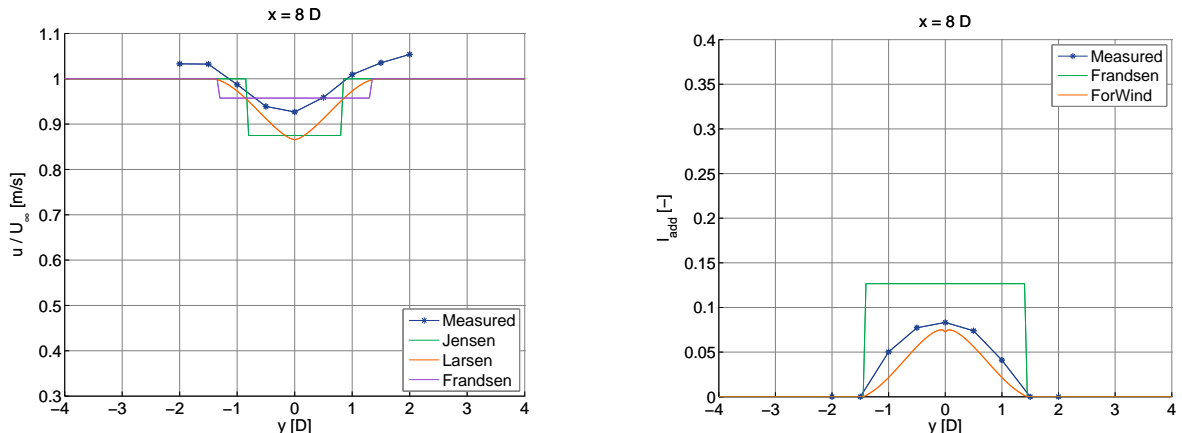


Figure I-12: Comparison of the measured and simulated velocity (left) and generated turbulence (right) behind a ECN model turbine with $C_T = 0.56$, $x = 8D$

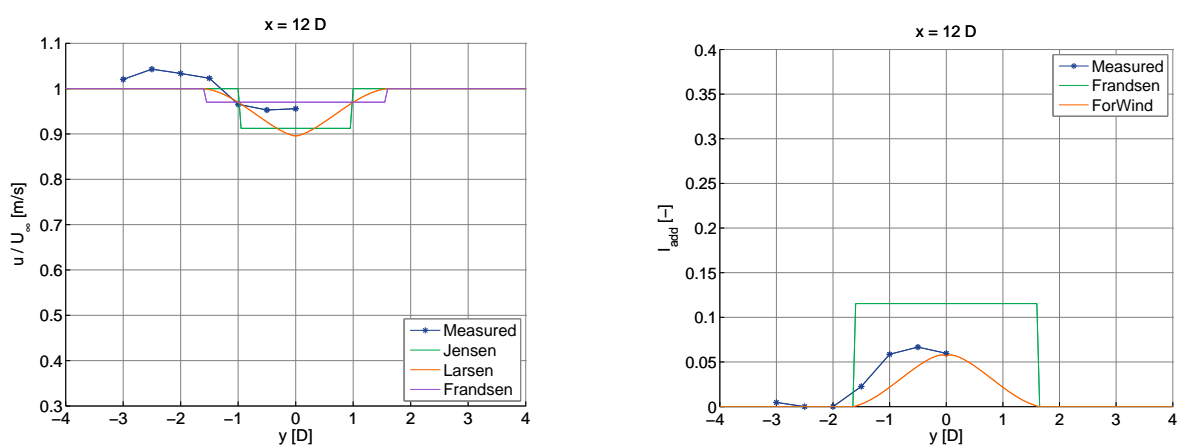


Figure I-13: Comparison of the measured and simulated velocity (left) and generated turbulence (right) behind a ECN model turbine with $C_T = 0.56$, $x = 12D$

Appendix J

Calculating rotor averaged wind speed

In order to calculate the rotor average values of the wind speed, the area of the intersection of the wake of an upstream turbine and the rotor area of downstream turbine has to be calculated as well as the momentum deficit resulting from this wake.

Suppose there are two circles with different radii, R_{exp} and R_2 , where the circle with radius R_{exp} represents the expanded wake of an upstream turbine and the circle with radius R_2 represents the turbine that is influenced by that wake.

Because the momentum deficit needs to be calculated and the velocities in the wake are axisymmetric, it would be easy to divide the intersecting area into segments of annuli as can be seen in on the right side of figure J-1.

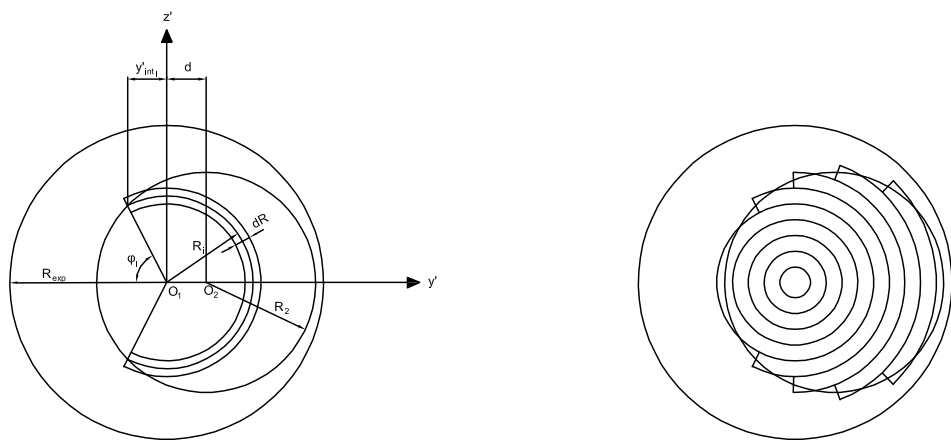


Figure J-1: Method to calculate rotor averaged wind speed

The area of segment i can be written as:

$$A_i = \frac{2(\pi - \varphi_i)}{2\pi} 2\pi R_i dR = 2(\pi - \varphi_i) R_i dR \quad (\text{J-1})$$

where φ_i is the angle between the line O_2O_1 and the line through O_1 and the point at which the center of annulus segment i intersects circle 2, y'_{int_i} .

$$\varphi_i = \begin{cases} \arccos\left(\frac{y'_{int_i}}{R_i}\right) & \text{if } R_2^2 - d^2 - R_i^2 \geq 0, \\ \pi - \arccos\left(\frac{y'_{int_i}}{R_i}\right) & \text{if } R_2^2 - d^2 - R_i^2 < 0. \end{cases} \quad (\text{J-2})$$

If such intersection does not exist and the whole annulus lies within circle 2, this angle should be equal to zero, which can be achieved by setting y'_{int_i} equal to R_i in that case:

$$y'_{int_i} = \begin{cases} \frac{|(R_2^2 - d^2 - R_i^2)|}{2d} & \text{if } R_i > R_2 - d, \\ R_i & \text{if } R_i \leq R_2 - d. \end{cases} \quad (\text{J-3})$$

The total area of the intersection can then be approximated by summing the areas of all annulus sections when dR is small enough:

$$A_{intersection} = \lim_{dR \rightarrow 0} \sum A_i \quad (\text{J-4})$$

This numerical integration introduces a small error, depending on the size of dR and hence the number of annuli.

The momentum deficit Δp can now also be easily calculated as the velocity is axisymmetric around O_1 . When the value of dR is taken small enough the velocity deficit can be assumed constant over each segment, yielding:

$$\Delta p = \sum A_i (\Delta U_i)^2; \quad (\text{J-5})$$

J.1 Analytical solution to the area

There is a simple analytical equation to calculate this area as well. While it hasn't been used to calculate the momentum deficit it was used to check the procedure described above for the calculation of the intersecting area.

[INSERT PICTURE]

For two circles with different radius the following equation holds:

$$dy = y_2 - y_1 \quad (\text{J-6})$$

$$dz = z_2 - z_1 \quad (\text{J-7})$$

The distance between the centers of the wake and the rotor d is then given by:

$$d^2 = dy^2 + dz^2 \quad (\text{J-8})$$

When dz is not zero, the xyz system can be rotated around the x-axis to a new $xy'z'$ system such that $dz' = 0$.

Take the center of the expanded wake as local zero.

In the new coordinates (y' and z') we have:

$$y'^2 + z'^2 = R_{exp}^2 \quad (\text{J-9})$$

$$(y' - d)^2 + z'^2 = R_2^2 \quad (\text{J-10})$$

The coordinates of the intersections can then be obtained

$$y'_{int} = \frac{d^2 - R_2^2 + R_{exp}^2}{2d} \quad (\text{J-11})$$

$$z'_{int} = \sqrt{R_{exp}^2 - y'_{int}^2} = \frac{1}{2d} \sqrt{4d^2 R_{exp}^2 - (d^2 - R_2^2 + R_{exp}^2)^2} \quad (\text{J-12})$$

$$= \frac{1}{2d} \sqrt{(d + R_2 + R_{exp})(-d + R_2 + R_{exp})(d - R_2 + R_{exp})(d + R_2 - R_{exp})} \quad (\text{J-13})$$

The area of the intersection can then be calculated by subtracting the area of the kite O_1AO_2Z from the sum of the area of the segment with angle 2α from circle 1 and the area of the segment with angle 2β from circle 2.

The area of the kite is:

$$\begin{aligned} A_{O_1AO_2Z} &= 2 \left(\frac{1}{2} y'_{int} z'_{int} \right) + 2 \left(\frac{1}{2} (d - y'_{int}) z'_{int} \right) = dz'_{int} \\ &= \frac{1}{2} \sqrt{(d + R_2 + R_{exp})(-d + R_2 + R_{exp})(d - R_2 + R_{exp})(d + R_2 - R_{exp})} \end{aligned} \quad (\text{J-14})$$

The sum of the areas of the two circular segments is:

$$\begin{aligned} A &= \frac{2 \cos^{-1} \left(\frac{y'_{int}}{R_{exp}} \right)}{2\pi} \pi R_{exp}^2 + \frac{2 \cos^{-1} \left(\frac{d - y'_{int}}{R_2} \right)}{2\pi} \pi R_2^2 \\ &= R_{exp}^2 \cos^{-1} \left(\frac{d^2 - R_2^2 + R_{exp}^2}{2dR_{exp}} \right) + R_2^2 \cos^{-1} \left(\frac{d^2 + R_2^2 - R_{exp}^2}{2dR_2} \right) \end{aligned} \quad (\text{J-15})$$

Note that this analytical solution only holds when the lines O_1A and O_2Z do not cross circle 2 and the lines O_2A and O_2Z do not cross circle 2, so only when the intersection does not hold the center of either circles and the overlap is not too large.

Appendix K

Influence of turbulence intensity input on the new model

This appendix shows the influence of the input that is used for the turbulence intensity at each turbine on both the velocity and turbulence predictions using the new model combination. In the plots the abbreviations bc, nc and ic stand for between the columns, next to a column and inside a column respectively. These terms were used as well in the main part of the report.

K.1 Influence on the velocity deficit prediction

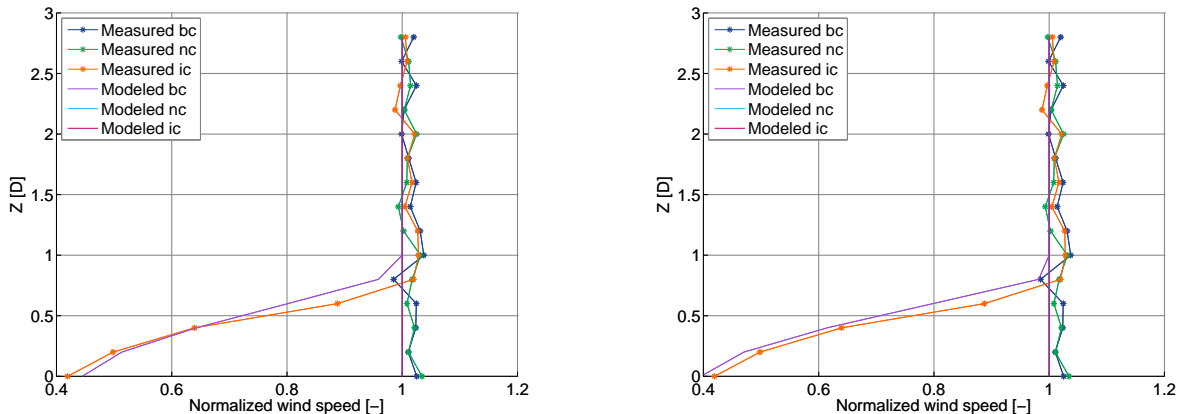


Figure K-1: Normalized velocity after the first row of turbines using ambient turbulence (left) and rotor averaged turbulence (right).

Using the rotor averaged turbulence intensity yield better results for the positions next to and between the columns. For the positions inside the column using the rotor averaged turbulence intensity yields lower values for the velocity deficit than the measurements, while using ambient turbulence intensity yields higher values. This is logical, as a higher turbulence intensity results in a less pronounced wake.

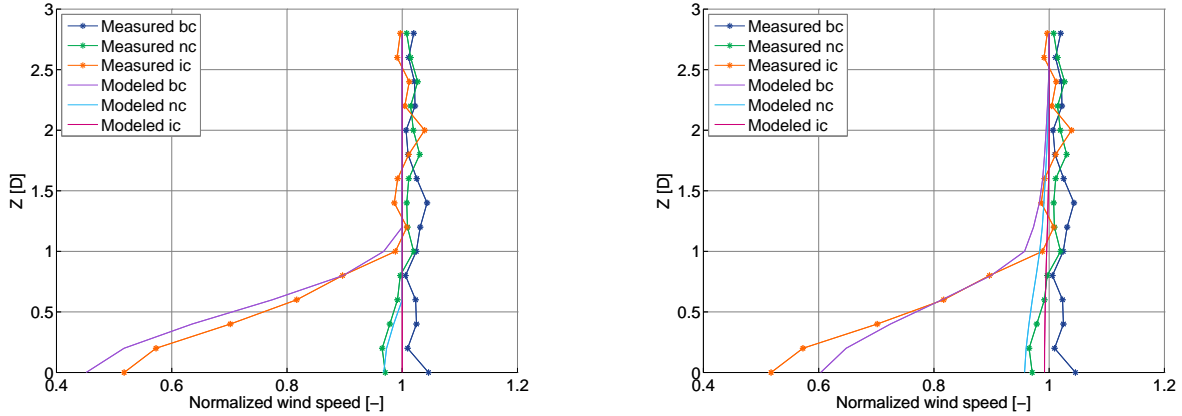


Figure K-2: Normalized velocity after the third row of turbines using ambient turbulence (left) and rotor averaged turbulence (right).

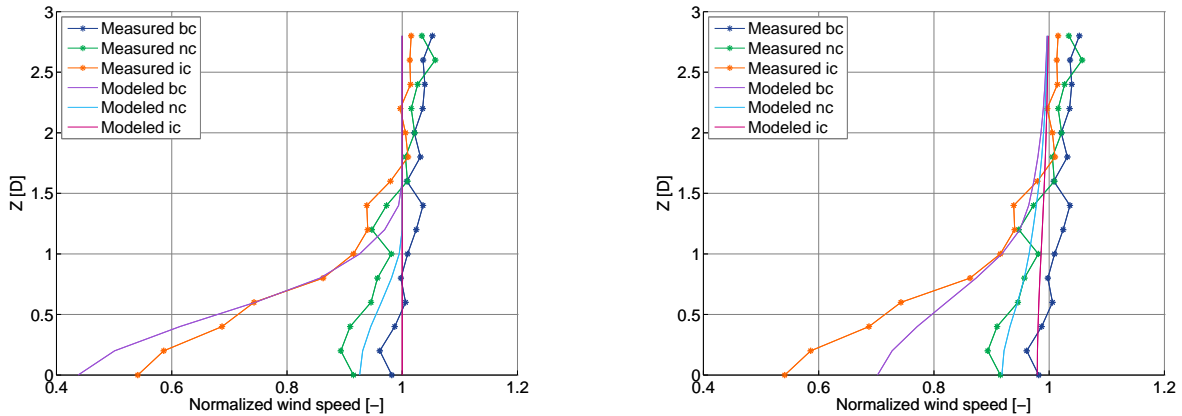


Figure K-3: Normalized velocity after the seventh row of turbines using ambient turbulence (left) and rotor averaged turbulence (right).

K.2 Influence on the turbulence intensity prediction

The same observations hold for the turbulence intensity. Using rotor averaged turbulence gives better results except for the positions inside the column; there using ambient turbulence intensity leads to too high values while using the rotor averaged ambient turbulence intensity leads too low values.

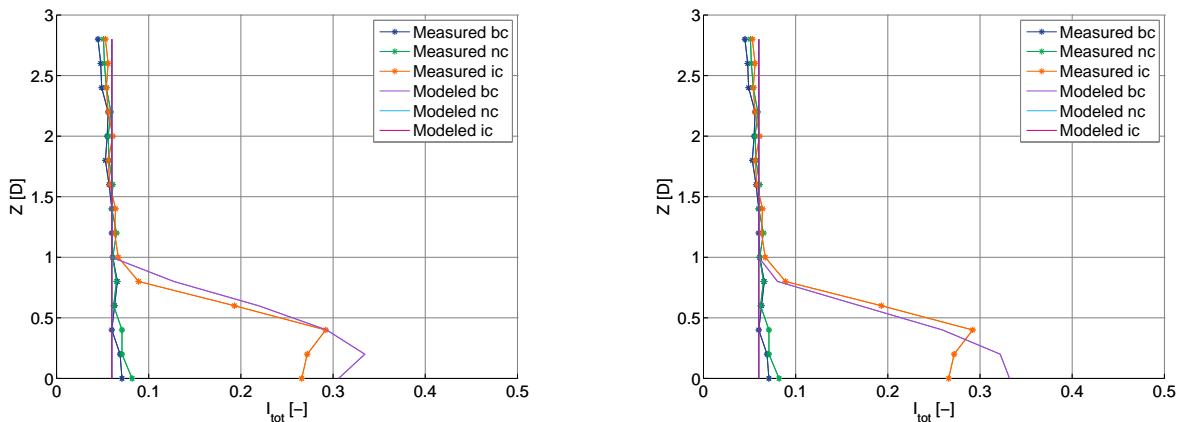


Figure K-4: Total turbulence intensity after the first row of turbines using ambient turbulence (left) and rotor averaged turbulence (right).

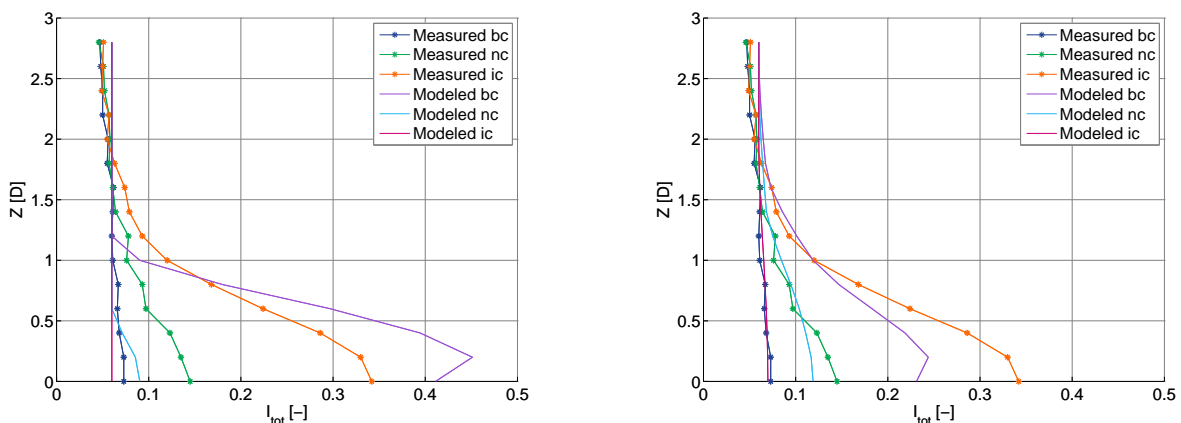


Figure K-5: Total turbulence intensity after the third row of turbines using ambient turbulence (left) and rotor averaged turbulence (right).

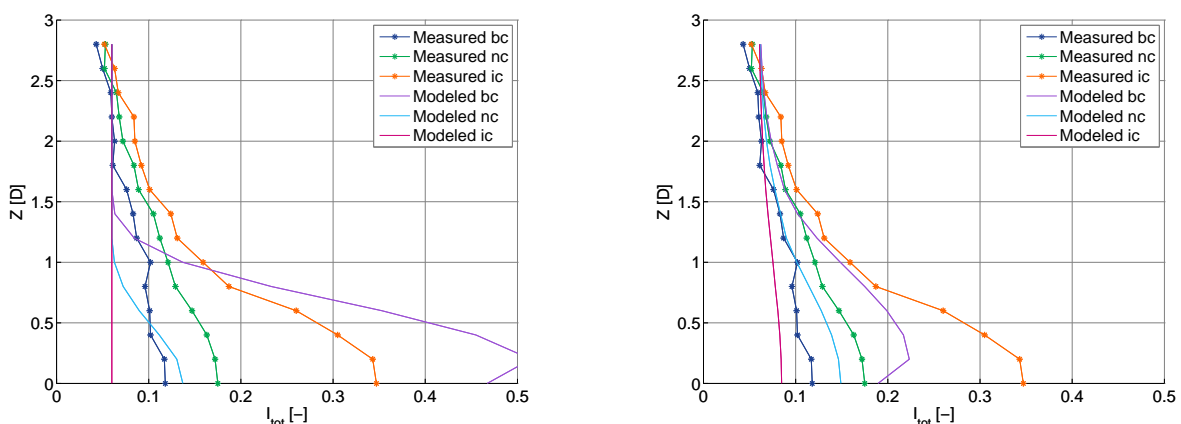


Figure K-6: Total turbulence intensity after the seventh row of turbines using ambient turbulence (left) and rotor averaged turbulence (right).